UNIVERSITY
OF MICHIGAN
APR 21 1955
CHEMISTRY
LIBRARY

Journal of Research

of the

National Bureau of Standards

MARCH 1955

VOLUME 54 NUMBER 3

U. S. DEPARTMENT OF COMMERCE
Sinclair Weeks, Secretary
NATIONAL BUREAU OF STANDARDS
A. V. Astin, Director

MARCH • 1955
VOLUME • 54
NUMBER • 3

JOURNAL OF RESEARCH

of the

NATIONAL BUREAU OF STANDARDS

PERIODICALS OF THE NATIONAL BUREAU OF STANDARDS

(Published monthly)

The National Bureau of Standards is engaged in fundamental and applied research in physics, chemistry, mathematics, and engineering. Projects are conducted in fifteen fields: electricity and electronics, optics and metrology, heat and power, atomic and radiation physics, chemistry, mechanics, organic and fibrous materials, metallurgy, mineral products, building technology, applied mathematics, data processing systems, cryogenic engineering, radio propagation, and radio standards. The Bureau has custody of the national standards of measurement and conducts research leading to the improvement of scientific and engineering standards and of techniques and methods of measurement. Testing methods and instruments are developed, physical constants and properties of materials are determined, and technical processes are investigated.

JOURNAL OF RESEARCH

The Journal presents research papers by authorities in the specialized fields of physics, mathematics, chemistry, and engineering. Complete details of the work are presented, including laboratory data, experimental procedures, and theoretical and mathematical analyses. Annual subscription: domestic, $4.00; foreign, $5.25.

TECHNICAL NEWS BULLETIN

Summaries of current research at the National Bureau of Standards are published each month in the Technical News Bulletin. The articles are brief, with emphasis on the results of research, chosen on the basis of their scientific or technologic importance. Lists of all Bureau publications during the preceding month are given, including Research Papers, Handbooks, Applied Mathematics Series, Building Materials and Structures Reports, Miscellaneous Publications, and Circulars. Each issue contains 12 or more two-column pages; illustrated. Annual subscription: domestic, $1.00; foreign, $1.35.

BASIC RADIO PROPAGATION PREDICTIONS

The Predictions provide the information necessary for calculating the best frequencies for communication between any two points in the world at any time during the given month. The data are important to all users of long-range radio communications and navigation, including broadcasting, airline, steamship, and wireless services, as well as to investigators of radio propagation and ionosphere. Each issue, covering a period of one month, is released three months in advance and contains 16 large pages, including pertinent charts, drawings, and tables. Annual subscription: domestic, $1.00; foreign, $1.25.

Order all publications from the Superintendent of Documents
U. S. Government Printing Office, Washington 25, D. C.

The printing of this publication has been approved by the Director of the Bureau of the Budget, May 12, 1953.

Journal of Research of the National Bureau of Standards Vol. 54, No. 3, March 1955 Research Paper 2572

A Method for the Numerical Integration of Differential Equations of Second Order Without Explicit First Derivatives [1]

Rene de Vogelaere [2]

This is a fourth-order step-by-step method based on difference formulas. The case of a single equation is discussed in detail. The use of this method for automatic computer is considered.

1. Introduction

This is a fourth-order step-by-step method based on difference formulas. The start of the computation is easy. Only the case of a single differential equation

$$\frac{d^2y}{dx^2}=f(x,y) \tag{1}$$

will be considered. The generalization to a system of differential equations

$$\frac{d^2y_i}{dx^2}=f_i(x,y_k) \qquad i,k=1,2,\ldots,n$$

is immediate. Application to electronic computing is discussed.

2. General Formulas

We first note some general formulas that may be deduced, for instance, from the expressions (1.32), (1.38), (1.39), and (4.15) of L. Collatz [1]:[3]

$$\int_0^x\int_0^x f(x)dx^2={}^{(2)}f(x)-{}^{(2)}f(0)-{}^{(1)}f(0)x$$

$$=h^2\sum_{p=0}P_{2,p}(u)\Delta^p f_{-p} \tag{2}$$

$$=h^2\sum_{p=0}(-1)^pP_{2,p}(-u)\Delta^p f_0 \tag{3}$$

where $x=uh$,

$$P_{2,0}(u)=u^2/2;\quad P_{2,1}(u)=u^3/6;\quad P_{2,2}(u)=(2u^3+u^4)/24;\quad P_{2,3}(u)=(20u^3+15u^4+3u^5)/360;\quad \ldots \tag{4}$$

and

$${}^{(n)}f=\int_a^x {}^{(n-1)}f dx \qquad {}^{(0)}f=f, \quad n=1,2.$$

Finally,

$${}^{(1)}f_2-{}^{(1)}f_0=h(2f_1+\frac{1}{3}\Delta^2 f_0-\frac{1}{90}\Delta^4 f_{-1}+\ldots). \tag{5}$$

---

[1] Work performed in part when the author was a guest worker at the National Bureau of Standards, November 1953, and in part at the University of Louvain, Belgium, 1948, toward the author's Dissertation.

[2] Department of Mathematics, University of Notre Dame, Ind.

[3] Figures in brackets indicate the literature references at the end of this paper.

The degree of approximation of the formulas given below is written in terms of the interval h: the symbol $\{n\}$ is equivalent to the usual $o(h^n)$. The following remarks are needed:

(1) f, computed from its definition, is of the same order of approximation as that of the y used;

(2) if $\Delta^{p+1}f$ is neglected in (2) or (3), these expressions are correct to the $(p+2)$nd order;

(3) if $\Delta^4 f_{-1}$ is neglected in (5), this formula is correct to the fourth order. In the notation introduced, the differential equation under consideration can be written as

$$y = {}^{(2)}f;$$

we shall also write

$$\frac{dy}{dx} = {}^{(1)}f = z.$$

3. Particular Formulas

When $x=h$, and if $\Delta^2 f_{-2}$ is neglected, (2) becomes

$$y_1 = y_0 + hz_0 + h^2(-f_{-1}+4f_0)/6, \qquad \{3\} \tag{6}$$

provided $y_0\{3\}$, $z_0\{2\}$, and $f_0\{1\}, f_{-1}\{1\}$.

If Δf_{-1} is neglected in the same formula (2), we have

$$\tilde{y}_1 = y_0 + hz_0 + h^2 f_0/2. \qquad \{2\} \tag{7}$$

When $x=h$, and if $\Delta^2 f_0$ is neglected, (3) becomes

$$y_1 = y_0 + hz_0 + h^2(2f_0+f_1)/6, \qquad \{3\} \tag{8}$$

provided $y_0\{3\}$, $z_0\{2\}$, and $f_0\{1\}, f_1\{1\}$.

The same formula yields, for $x=2h$, and with $\Delta^3 f_0$ neglected, since $P_{2,2}(-2)=0$,

$$y_2 = y_0 + 2hz_0 + h^2(2f_0+4f_1+0f_2)/3, \qquad \{4\} \tag{9}$$

and provided $y_0\{4\}$, $z_0\{3\}$, and $f_0\{2\}, f_1\{2\}$.

Neglecting $\Delta^4 f_{-1}$, (5) gives the Simpson formula

$$z_2 = z_0 + h(f_0+4f_1+f_2)/3 \qquad \{4\} \tag{10}$$

if $z_0\{4\}$ and $f_0\{3\}, f_1\{3\}, f_2\{3\}$.

Finally, when $x=2ht$, and if $\Delta^3 f_0$ is neglected, (3) becomes

$$y = y_0 + 2hz_0 t + 2h^2 f_0 t^2 + \tfrac{2}{3}h^2(-3f_0+4f_1-f_2)t^3 + \tfrac{2}{3}h^2(f_0-2f_1+f_2)t^4. \qquad \{4\} \tag{11}$$

4. Integration Method

We are now ready to explain our method for solving differential equations of second order that do not contain the first derivatives explicitly. The starting value of the independent variable will be taken as zero. Each step is subdivided into two intervals of length h.

The general step will be considered first. Therefore, we will suppose that $f=f_{-1}\{3\}$ is known for $x=(2n-1)h$, and that $y=y_0\{4\}$, $f=f_0\{4\}$, $z=z_0\{4\}$, are known for $x=2nh$.

Then for $x=(2n+1)h$, $y=y_1\{3\}$ is given by (6) and $f=f_1\{3\}$ is given by (1), whereas for $x=(2n+2)h$, $y=y_2\{4\}$ is given by (9), $f=f_2\{4\}$ by (1) and $z=z_2\{4\}$ by (10).

These values will then serve for the next step. The process is of fourth order for the function as well as for its first derivative.

Two equivalent methods may be used to compute the first step. For $x=0$, and with initial conditions $y=y_0$ and $z=z_0$, $f=f_0$ is computed by means of the differential equation.

Then

(a). A preliminary calculation may be done with (7) and (1) so as to give

$$y=\tilde{y}_1\{2\} \text{ and } f=\tilde{f}_1\{2\}, \text{ for } x=h.$$

Then formula (8) may be used with $f_1=\tilde{f}_1$; this gives

$$y=y_1\{3\} \text{ and } f=f_1\{3\}, \text{ for } x=h.$$

The computation of the values for $x=2h$ is the same as for the general step $(2n+2)h$.

(b). Or, alternatively, it is also possible first to go backwards with the formula equivalent to (7),

$$y_{-1}=y_0-hz_0+h^2f_0/2. \quad \{2\}$$

The process for the general step may then be used for $x=h$ and $x=2h$ because (6) requires only a knowledge of f_{-1} to the first order and this function is known to the second.

Table 1 gives the coefficients of the z and f functions, (the coefficient of y is always one) for certain intervals between 0.50 and 0.06; if the interval to be chosen is outside this range, it is preferable, especially with the use of desk machines, to change the independent variable; this will prevent rounding off errors or the need of computation with an excess of decimal places.

TABLE 1.

For the users' convenience, certain entries have been repeated.

Intervals	Coefficients in formulas—														
	(6)			(9)			(10)	(7)		(8)			(7)		
	z_0	$-f_{-1}$	f_0	z_0	f_0	f_1	$f_0+4f_1+f_2$	z_0	f_0	z_0	f_0	f_1	$-z_0$	f_0	
h	h	$h^2/6$	$2h^2/3$	$2h$	$2h^2/3$	$4h^2/3$	$h/3$	h	$h^2/2$	h	$h^2/3$	$h^2/6$	h	$h^2/2$	
0.060000	0.060000	0.000600	0.002400	0.120000	0.002400	0.004800	0.020000	0.060000	0.001800	0.060000	0.001200	0.000600	0.060000	0.001800	
.075000	.075000	.000938	.003750	.150000	.003750	.007500	.025000	.075000	.002813	.075000	.001875	.000938	.075000	.002813	
.080000	.080000	.001350	.005400	.180000	.005400	.010800	.030000	.080000	.003750	.080000	.002700	.001350	.080000	.003750	
.100000	.100000	.001667	.006667	.200000	.006667	.013333	.033333	.100000	.005000	.100000	.003333	.001667	.100000	.005000	
.120000	.120000	.002400	.009600	.240000	.009600	.019200	.040000	.120000	.007200	.120000	.004800	.002400	.120000	.007200	
.125000	.125000	.002604	.010417	.250000	.010417	.020833	.041667	.125000	.007813	.125000	.005208	.002604	.125000	.007813	
.150000	.150000	.003750	.015000	.300000	.015000	.030000	.050000	.150000	.011250	.150000	.007500	.003750	.150000	.011250	
.180000	.180000	.005400	.021600	.360000	.021600	.043200	.060000	.180000	.016200	.180000	.010800	.005400	.180000	.016200	
.200000	.200000	.006667	.026667	.400000	.026667	.053333	.066667	.200000	.020000	.200000	.013333	.006667	.200000	.020000	
.240000	.240000	.009600	.038400	.480000	.038400	.076800	.080000	.240000	.028800	.240000	.019200	.009600	.240000	.028800	
.250000	.250000	.010417	.041667	.500000	.041667	.083333	.083333	.250000	.031250	.250000	.020833	.010417	.250000	.031250	
.300000	.300000	.015000	.060000	.600000	.060000	.120000	.100000	.300000	.045000	.300000	.030000	.015000	.300000	.045000	
.360000	.360000	.021600	.086400	.720000	.086400	.172800	.120000	.360000	.064800	.360000	.043200	.021600	.360000	.064800	
.400000	.400000	.026667	.106667	.800000	.106667	.213333	.133333	.400000	.080000	.400000	.053333	.026667	.400000	.080000	
.420000	.420000	.029400	.117600	.840000	.117600	.235200	.140000	.420000	.088200	.420000	.058800	.029400	.420000	.088200	
.480000	.480000	.038400	.153600	.960000	.153600	.307200	.160000	.480000	.115200	.480000	.076800	.038400	.480000	.115200	
.500000	.500000	.041667	.166667	1.000000	.166667	.333333	.166667	.500000	.125000	.500000	.083333	.041667	.500000	.125000	

5. Application to High-Speed Computors

For this application, it is more convenient to introduce the quantities

$$hz_{2n}=Z_{2n}, \qquad \frac{1}{3}h^2f_{2n}=F_{2n}, \qquad \frac{4}{3}h^2f_{2n+1}=F_{2n+1}.$$

From our formulas it is easy to deduce that only four cells are needed to store the values of y, Z, and F. We shall give here a possible arrangement of the calculation so as to have only one multiplication when the F's are computed.

Thus for the general step, if in the memory cells, P, Q, R, S, we have at a certain moment the following situation [4]

$$(P)=y_0, \qquad (Q)=Z_0, \qquad (R)=F_0, \qquad (S)=F_{-1},$$

the following five orders

$$(Q)+(R)\rightarrow Q, \quad (P)+(Q)\rightarrow P, \quad \frac{1}{8}(S)\rightarrow S, \quad (R)-(S)\rightarrow S, \quad (P)+(S)\rightarrow S,$$

put y_1 in S or in the y cell of the subroutine corresponding to (1). This subroutine produces F_1, which is stored in S. The two orders

$$(Q)+(S)\rightarrow Q, \qquad (P)+(Q)\rightarrow P,$$

then put y_2 in P, and the subroutine corresponding to (1) computes F_2, which is then stored in R. Finally, the order

$$(Q)+(R)\rightarrow Q,$$

puts Z_2 in Q.

To start the computation the method (b) is preferable because once the backward step

$$y_{-1}=y_0-Z_0+\frac{3}{2}F_0$$

has been made, we immediately enter the general routine.

6. Change of Interval

Because f_{-1} needs only to be of first order in (6), there is no difficulty in changing the interval from h_1 to h_2 for the value x_0 of the independent variable. For, if $\overline{f_{-1}}$ denotes the value of f for the last step ($x=x_0-h_1$) and f_{-1}, the value of f which is needed ($x=x_0-h_2$), we have

$$\frac{\overline{f_{-1}}-f_0}{h_1}=\frac{f_{-1}-f_0}{h_2}. \qquad \{1\}$$

Inserting this in (6) we have

$$y_1=y_0+h_2z_0-\frac{h_2^2}{6}\left(\frac{h_2}{h_1}\right)\overline{f_{-1}}+\frac{2}{3}h_2^2\left(\frac{3}{4}+\frac{1}{4}\frac{h_2}{h_1}\right)f_0. \qquad \{3\} \qquad (12)$$

In this form, the quantities in the parenthesis are multipliers of the coefficients of (6) for a new interval h_2.

The formula (8) may be deduced from (12) with the particular value $h_1=-h_2$ and with $\overline{f_{-1}}$ replaced by f_1.

7. Error of the Process

Only the error of one general step will be considered. Moreover, since the first derivative has been calculated to the same order as the function itself, i. e., the fourth, only the fifth-order term of the function is of interest. If y_0, z_0, and f_0 are correct, this term is given by the first term neglected when (9) is derived, namely,

$$\frac{2}{45}h^2\Delta^3 f_0, \qquad (13)$$

since f_1 is known to the third order in h, regardless of which of the formulas, (6) or (8) is used

[4] (X) means contents of cell X.

to compute y_1. An estimate of the error is thus given by

$$\frac{2}{45}h^5\left(\frac{d^3f}{dx^3}\right)_0=\frac{2}{45}h^5\left(\frac{d^5y}{dx^5}\right)_0. \tag{14}$$

However, it is (13) that provides a practical method of estimating the total error.

To check the computation, two methods may be used.

(a) When a first integral of the equation or of the set of equations is known, this may be used at each step as a check because z has been computed. But confidence in this as a check should not be too great. Although, if the integration is part of a larger program, this check will be in general sufficient.

(b) If an isolated integration has to be done, greater care may be needed. The following procedure is then proposed. Recompute y_1 (which is known with third-order accuracy) by means of the interpolation formula (11) considered backward, so as to use y_2, z_2, and f_2:

$$y_1^*=y_2-hz_2+\frac{1}{24}h^2(-f_0+6f_1+7f_2). \tag{15}$$

The difference is, for the general step, approximately the first neglected term in (6),

$$y_1^*-y_1=\frac{1}{8}h^2\Delta^2f_{-2}=\frac{1}{8}h^4\left(\frac{d^4y}{dx^4}\right)_0 \tag{16}$$

and should be small and vary slowly.

The accuracy of the calculation may also be deduced from the comparison of the differences of $y_1^*-y_1$ for two consecutive steps,

$$(y_1^*-y_1)_{2n+2}-(y_1^*-y_1)_{2n}=\frac{1}{8}h^4\cdot 2h\left(\frac{d^5y}{dx^5}\right)_0 \qquad n>0, \tag{17}$$

which is 8/45, the allowed error. The variation of $y_1^*-y_1$ from one step to the other must therefore remain smaller than the 45/8 of the allowed error for each step.

8. Comparison With Other Methods

It is not our intention to make a detailed comparison here with similar methods—ordinary step by step method, Gauss-Jackson method, Runge-Kutta method. This task is very delicate, and it is necessary to take care of the higher order terms neglected, the precision needed, and the purpose of the integration.

But we should like to draw attention to the fact, that in most of the other step-by-step methods, predictor and corrector formulas are used for the same value of the independent variable; here, a formula of the corrector type (9) permits us to advance. Moreover, the advantages are evident—it is easy to start the integration, and there is no problem in changing the interval.

However, since it is possible to make a comparison with the Runge-Kutta method, we should like to develop this point a little more. It will be seen that the proposed method possesses some of the advantages of the Runge-Kutta method without having some of its inconveniences (see, for instance, Milne [4]). The Runge-Kutta method may be characterized by the fact that each step is independent and that functions and derivatives are calculated in general four times for the fourth-order process. Also, in contrast to the step-by-step processes. a maximum accuracy is not sought for each computation, the process being based on compensation, at the end, of all errors made during the step. But for the case of differential equations of second order of the type at present under consideration, there is one set of formulas for which only three calculations are needed (see Collatz, p. 33–34), and for which, by accident, the function but not the first derivative is calculated each time with maximum accuracy. In this case the error obtained by comparison with the value y_2 of the Taylor expansion may be written

in the form

$$y_2^* - y_2 = \tfrac{2}{15} h^5 \left[F + 6 \left(\frac{\partial f}{\partial y} \right)_0 D \right] f, \tag{18}$$

as may be deduced from the two formulas following (3.13) of reference [1]. In these formulas we set with $n=2$, $\nu=0$, $q=2$, and replace h by $2h$.

In the case of a single differential equation of type (1) the operators F and D are defined by

$$D = \left(\frac{\partial}{\partial x} \right)_0 + z_0 \left(\frac{\partial}{\partial y} \right)_0,$$

$$F = \left(\frac{\partial}{\partial x} + z \frac{\partial}{\partial y} \right)_0^3 + 3 f_0 D \left(\frac{\partial}{\partial y} \right)_0.$$

For the proposed method, (14) may be written with the same notation

$$y_2^* - y_2 = \tfrac{2}{15} h^5 \left[F + \left(\frac{\partial f}{\partial y} \right)_0 D \right] f. \tag{19}$$

Having made this remark, we may now point out that the new method also subdivides the process in steps. These steps are not independent, but the dependence is small (first order only on the second derivative), and because of this small dependence, only two computations are needed instead of three without making the change of interval difficult.

It appears also from a comparison of (18) and (19) that the function is better approximated in general, than with the Runge-Kutta method. This is not the case for the first derivative, which is determined in the Runge-Kutta method with fifth-order accuracy; however, this fifth-order accuracy may be completely illusory.

Finally, we should like to point out that the fourth-order interpolation formula (11) bears a great resemblance, to an analogous formula developed by Lemaitre for the Runge-Kutta methods [3].

9. Example

This method has been used principally for differential equations arising in dynamical problems with two degrees of freedom. Therefore, we shall give an example of this kind that is taken from the problem of primary cosmic rays (cf. references of [2]).

The equations written with the above notations are

$$\frac{d^2 y_1}{dx^2} = a e^{2y_1} - e^{-y_1} + e^{-2y_1} \cos^2 y_2$$

$$\frac{d^2 y_2}{dx^2} = (e^{-2y_1} \cos^2 y_2 - 1 - \tan^2 y_2) \tan y_2,$$

and the first integral is

$$\left(\frac{dy_1}{dx} \right)^2 + \left(\frac{dy_2}{dx} \right)^2 = a e^{2y_1} - 1 - \tan^2 y_2 + 2e^{-y_1} - e^{-2y_1} \cos^2 y_2.$$

Table 2 presents the computation for the initial conditions

$$y_{1,0} = \quad .448080, \quad y_{2,0} = 0.000000, \quad y'_{1,0} = 0.000000, \quad y'_{2,0} = 0.206279,$$

The value $a = 0.070598$ is deduced from the first integral.

The method (a) of section 4 was used for starting. The results in A were obtained by using $h=0.2$ and retaining six decimal places. The results in B were obtained by using $h=0.4$ and retaining five decimal places.

TABLE 2.

Case A

x	y_1	y_2	f_1	f_2	z_1	z_2	C_1	C_2	E_1	E_2	S
0.0	0.448080$_5$	0.000000$_0$	−0.057742	−0.000000	0.000000$_0$	0.206279$_1$					0
.2	.446925	.041256	−.058631	−.024492							
.2	.446919	.041093	−.058627	−.024394			3	0			
.4	.443413$_3$	.081210$_8$	−.061221	−.048620	−.023564$_7$	.196332$_7$			0	0	0
.6	.437469	.119383	−.065349	−.072382			−14	2			
.8	.428869$_7$	.154966$_8$	−.070734	−.095146	−.049788$_2$	.167646$_3$			1	1	0
1.0	.417462	.186141	−.076969	−.116085			−6	8			
1.2	.402863$_2$	.212906$_6$	−.083571	−.134105	−.080600$_4$	.121406$_7$			1	2	0
1.4	.385128	.234476	−.089941	−.147896			0	19			
1.6	.363697$_6$	.250065$_7$	−.095417	−.156251	−.116517$_4$	.062610$_4$			1	2	0

Case B

x	y_1	y_2	f_1	f_2	z_1	z_2	C_1	C_2	E_1	E_2	S
0.0	0.44808$_5$	0.00000$_0$	−0.05774	−0.00000	0.00000$_0$	0.20627$_9$					0
.4	.44346	.08251	−.06130	−.04943							
.4	.44337	.08119	−.06123	−.04861			4	1			
.8	.42885$_9$	.15465$_1$	−.07073	−.09514	−.04978$_5$	.16767$_1$			1	2	0
1.2	.40303	.21287	−.08354	−.13402			−9	9			
1.6	.36366$_5$	.25005$_2$	−.09541	−.15621	−.11649$_6$	.06268$_2$			3	6	2
2.0	.30912	.26204	−.10036	−.15266			9	52			
2.4	.23888$_8$	.25086$_7$	−.09175	−.12404	−.19486$_9$	−.05610$_3$			5	0	4
2.8	.15379	.21937	−.06102	−.07788			41	46			
3.2	.06010$_6$	.17624$_0$	−.00258	−.03068	−.24009$_1$	−.11826$_8$			4	−12	13

C_1 and C_2 are the fourth-order verification terms $y^*_{1,1}-y_{1,1}$ and $y^*_{2,1}-y_{2,1}$, computed by (16). E_1 and E_2 are the estimates of error deduced from (13). S is the error in the first integral. The quantities C_1, C_2, E_1, E_2, and S are to be multiplied by 10^{-6} in case A and by 10^{-5} in case B.

10. Remarks

(1). It should be noted that (17) is not true for $n=0$, i. e., for the first two steps; for, instead of (6), (8) was used, for which

$$y_1^*-y_1=-\tfrac{1}{24}h^2\Delta^2 f_0.$$

By comparison with (16) it appears that the first C is about minus one-third times the second one.

(2). One extra figure is used for $y_{i,2n}$ and $z_{i,2n}$ $(i=1,2)$ to lessen the rounding-off error; this changes very little in the computation, except that the second term in (9) must be written

$$\left(\frac{2h}{10}\right)(10z_0).$$

11. References

[1] L. Collatz, Numerische Behandlung von Differentialgleichungen, ch. 1 (Springer, Berlin, 1951).
[2] R. de Vogelaere, Equation de Hill et problème de Stormer, Can. J. Math. **2**, 440 (1950).
[3] G. Lemaitre, Interpolation dans la méthode de Runge-Kutta, Ann. soc. sci. Bruxelles **61**, 106 (1947).
[4] W. E. Milne, Note on the Runge-Kutta method, J. Research NBS **44**, 549 (1950) RP2101.

WASHINGTON, April 15, 1954.

Journal of Research of the National Bureau of Standards Vol. 54, No. 3, March 1955 Research Paper 2573

Selected Positive and Negative Ions in the Mass Spectra of the Monohalomethanes[1]

Vernon H. Dibeler and Robert M. Reese

Ionization potentials of the molecule ions and appearance potentials of the methyl and halogen positive ions and of the halogen negative ions have been measured for CH_3F, CH_3Cl, CH_3Br, and CH_3I and compared with previously reported spectroscopic and electron-impact data. A value is obtained for the ionization potential of HF by graphical comparison of the ionization potentials of the hydrogen and methyl halides. Carbon-halogen bond-dissociation energies are computed from appearance potentials of the methyl ion and of the halogen ion. A simple relation between bond-dissociation energy and bond distance is observed for the methyl halides.

1. Introduction

Electron-impact studies, including the measurement of ionization potentials and appearance potentials of the principal positive ions of most of the monohalomethanes, have been reported by Bauer and Hogness [1] [2], Morrison and Nicholson [2], McDowell and Cox [3a, b], and Branson and Smith [4]. Spectroscopic ionization potentials have been calculated by Price [5] from Rydberg series in far ultraviolet absorption bands. Only one of these studies has included measurements on methyl fluoride [3b].

In addition to the usual electron-impact measurements of the minimum energy required to form dissociated positive ions of the methyl halides, information concerning possible negative-ion formation and kinetic energy of dissociation products is necessary in order to reduce ambiguities in calculating bond-dissociation energies. Negative-ion studies are deemed particularly important for molecules containing halogen atoms.

On the basis of measurements of half-widths of ion beams [6], McDowell and coworkers [3a, b, 7] conclude that CH_3^+ ions from methyl chloride, bromide, and iodide are formed without excess kinetic energy. On the other hand, no effort to obtain direct information on the possible role of negative ions in the dissociation of methyl halides has been reported. Accordingly, this paper presents a short study of the appearance potentials and kinetic energy of selected positive and negative ions formed by ionization and by dissociation of the carbon-halogen bond for the complete series of the monohalomethanes.

2. Experimental Details

2.1. Apparatus

Data were obtained by means of a Consolidated type 21–103 mass spectrometer and a second instrument utilizing type 21–102 components modified for appearance potential measurements and other research. The ionization-emission control of the modified instrument permitted manual control of the filament current supplied by a storage battery. Provision was made to connect the ion-repeller electrodes to a fixed fraction of the ion-accelerating voltage or alternatively to small battery voltages, either positive or negative with respect to the ionization chamber. A decade potentiometer was connected to the output of the ionizing-voltage power supply, permitting the selection of ionizing-voltage increments as small as 0.01 v in the range of 0 to 100 v.

The 21–103 instrument contains an energy filter at the collector end of the analyser tube that can be connected to the ion-accelerating potential in order to stop ions of zero initial kinetic energy and to allow those with excess energy to reach the collector. The filter can be used to measure kinetic energy, but it is more convenient to measure directly the energy distribution of an ion beam from a voltage scan of a selected ion by using a very low ion-accelerating voltage ($<$200 v). As the mass scale varies inversely as the ion-accelerating voltage, the resolution in volts is given by the ion-accelerating voltage divided by the mass resolving power. Thus, at an ion-accelerating potential of 200 v, a voltage resolution of 0.5 v or less is easily attained.

An improvement of the technique previously described by Mohler, Dibeler, and Reese [8] substitutes for the conventional ion-accelerating voltage power supply, a well-regulated low-voltage power supply shunted with a suitable voltage divider that includes a 10-turn helipot. With the proper mass resolution, manual and automatic adjustment of the scanning voltage by means of the helipot in the vicinity of 200 v permits a precise study and measurement of the CH_3^+ ion peak shape with an estimated best voltage resolution of about 0.4 v. Methane introduced simultaneously with the methyl halide provided a fiduciary of CH_3^+ ions, known to be formed without excess kinetic energy [6]. The voltage interval between the resolved zero energy and kinetic-energy components of the CH_3^+ ion peak was measured with a sensitive meter by manual adjustment of the scanning voltage divider.

[1] Presented at the Second Annual Meeting ASTM E-14 Committee on Mass Spectrometry, New Orleans, La., May 1954.

[2] Figures in brackets indicate the literature references at the end of this paper

330526—55——2

A separate negative high-voltage power supply and sweep circuit were used to measure negative ion spectra.

The chloro-, bromo-, and iodomethanes were commercial products of high purity, as indicated by mass spectrometric analysis. The fluoromethane was prepared by passing methyl iodide over potassium fluoride in a glass-tube furnace at about 400° C. The product was obtained in good purity by simple separation of unreacted CH_3I in cold traps.

2.2. Determination of Appearance Potentials

Of the several empirical methods used for determining the minimum energy required to produce positive ions in the mass spectrometer, the one most commonly used is the so-called "vanishing-current" method [9a,b,d]. An inherent disadvantage of this method is the frequent opportunity for latitude in judgment concerning the precise point at which the ion current becomes zero.

In describing an alternative, "critical-slope" method, Honig [9c] pointed out that the initial portion of typical ionization-efficiency curves is exponential in character. A semilog plot of ion current versus ionizing voltage obtained with the requisite sensitivity produced an ionization-efficiency curve with a straight-line portion for a range of ion current extending over several orders of magnitude.

A brief note [10] has previously indicated the feasibility of evaluating ionization and appearance potentials of ions without the uncertainty of the extrapolation procedure, merely by measuring the voltage interval between two parallel straight lines plotted on the same normalized scale, one of which corresponds to the ion of unknown critical potential and the other corresponding to an ion of known ionization potential, such as argon or krypton. Normalization of the two curves is accomplished by adjusting partial pressures of the gases so as to give approximately equal ion current for the two ions at electron energies of 70 v. It is an experimental fact that for positive ions produced by ionization and dissociation processes of comparable probability and similar character, the conditions necessary to obtain parallel lines are not critical for molecule ions and many dissociative ions of a number of compounds studied so far. This method has been used for evaluating the appearance potentials of the positive ions in the present paper.

Ionization-efficiency curves of the negative halogen ions were plotted satisfactorily on the more conventional linear scale, although accurate calibration of the ionizing-voltage scale remained an acute problem, particularly for electron-capture processes. The O^- ion from CO (A.P.=9.6 ev) [11] provided a reasonably satisfactory calibration for the ion-pair processes. However, the appearance potential of the F^- ion from methyl fluoride apparently was more reproducible and served as a calibration for the measurement of the Cl^- ion in methyl chloride.

3. Results

The initial exponential portions of the ionization-efficiency curves of the CH_3I^+, CH_3^+, and I^+ ions, together with those of the calibrating gases, argon and krypton, are shown in the semilog plot of figure 1. The uncorrected ionizing voltage is plotted on the abscissa; the ion current in arbitrary units, on the ordinate. The curves are remarkably parallel, and the indicated voltage intervals between argon and krypton and between argon and CH_3I^+ are in good agreement with the intervals between the spectroscopic ionization potentials of these molecules. Thus, from the spectroscopic value, $I^z(A) = 15.76$ ev [12], the electron-impact ionization potential of krypton is 14.0_1 ev and that of CH_3I is 9.5_5 ev. The spectroscopic values for the first ionization potentials of krypton and methyl iodide are 13.996 [12] and 9.49 [5], respectively. The appearance potentials of the CH_3^+ and the I^+ ions are evaluated in the same way.

The curves in figure 1 are representative of the curves for the molecule ions and halogen positive ions of all of the methyl halides, except methyl fluorides and of the methyl ions of the iodo- and bromomethanes. A different type of curve is illustrated by the initial portion of the methyl ion curve from methyl chloride shown in figure 2, together with the calibrating gas, argon. The deviation in the

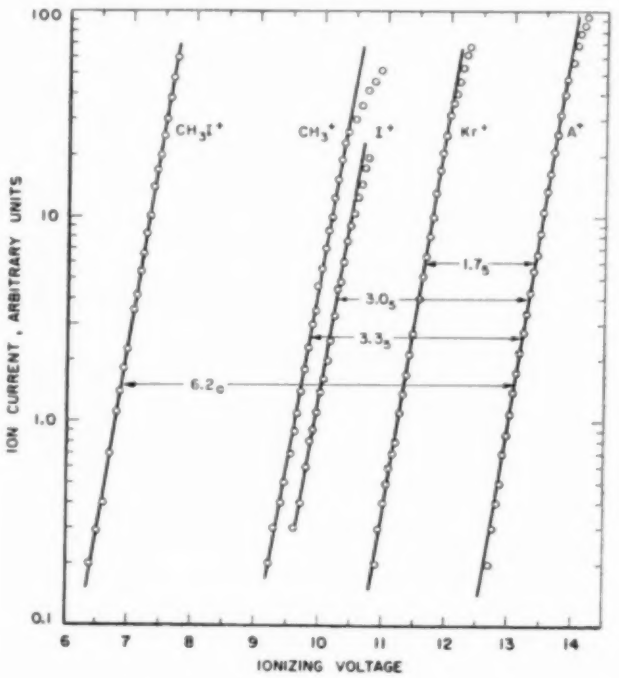

FIGURE 1. *Initial exponential portions of the ionization-efficiency curves for ions of methyl iodide and of the calibration gases, argon and krypton.*

The voltage scale is uncorrected.

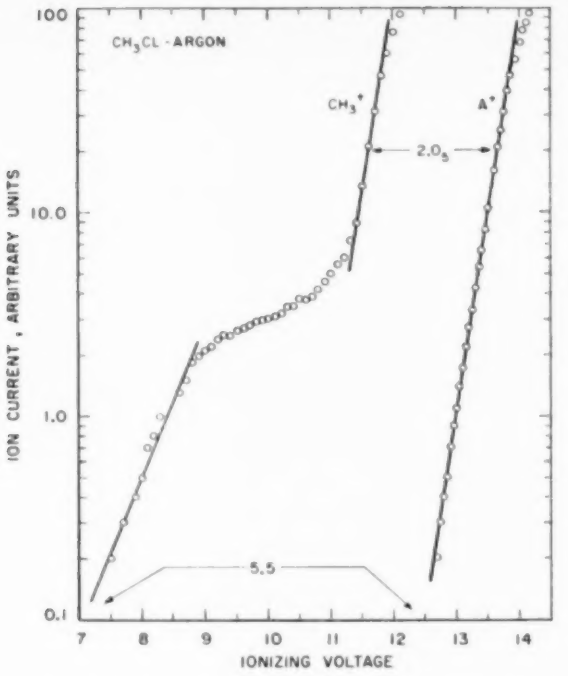

FIGURE 2. *Initial exponential portion of the CH_3^+ ion from methyl chloride compared with that of the calibrating gas, argon.*

The voltage scale is uncorrected.

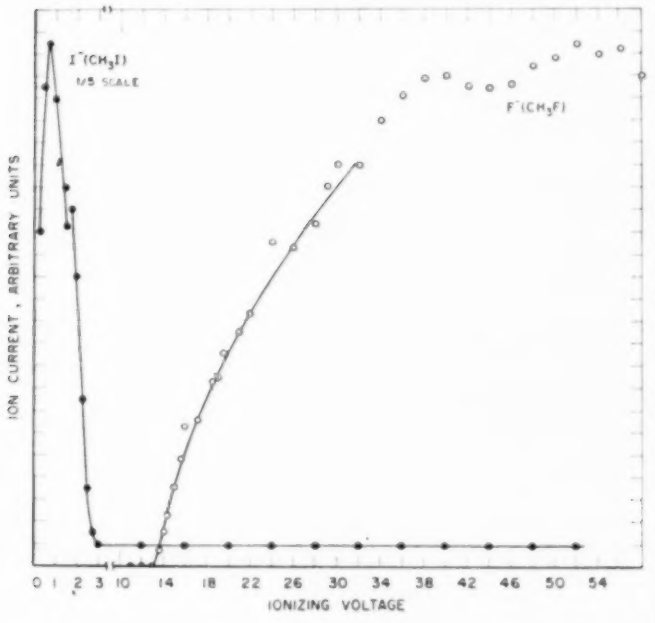

FIGURE 3. *Ionization-efficiency curves of the F^- and I^- ions from CH_3F and CH_3I, respectively.*

The voltage scale is uncorrected.

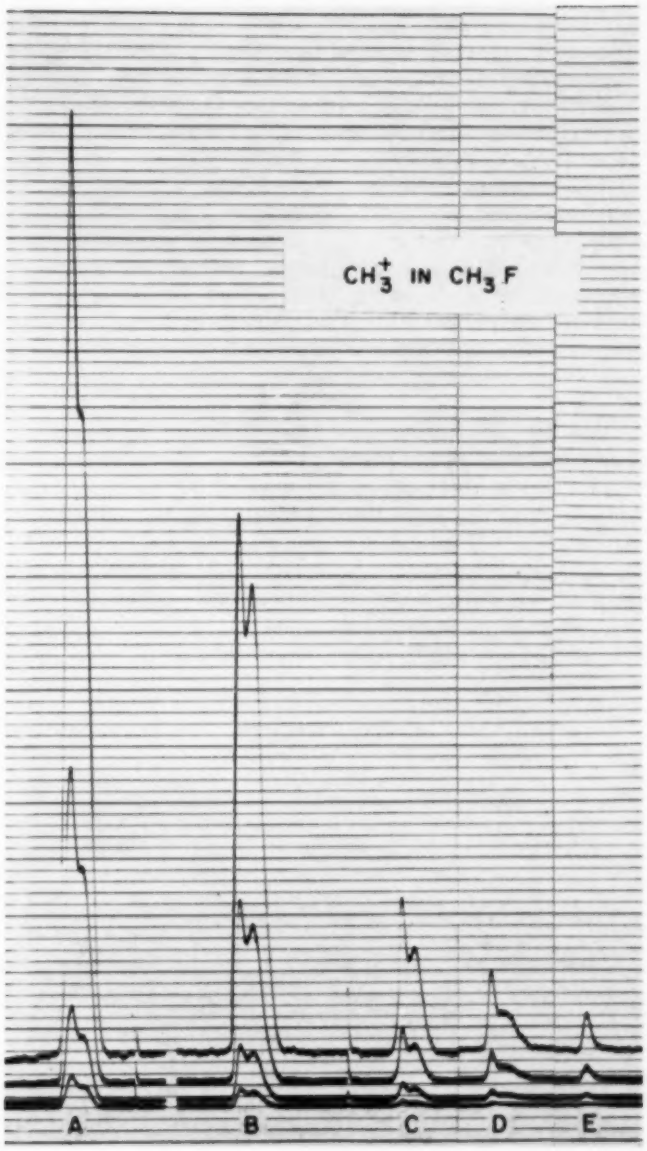

FIGURE 4. *Separation of the thermal- and kinetic-energy components of the CH_3^+ ion of methyl fluoride and the effect of ionizing voltage on the separate peaks.*

slope of the CH_3^+ curve is interpreted as indicating two ionization processes; i. e.,

$$CH_3Cl + e \rightarrow CH_3^+ + Cl + 2e \quad (1)$$

$$CH_3Cl + e \rightarrow CH_3^+ + Cl^- + e \quad (2)$$

This is supported by the fact that the difference in the two voltage intervals between the CH_3^+ and A^+ curves corresponding to processes (1) and (2) (3.5 v) approximates the electron affinity of the chlorine atom (3.7_5 v) [13].

The ionization efficiency curve for the CH_3^+ ion of methyl fluoride resembles that of the methyl ion from CH_3Cl. One appearance potential is about 1 v above the ionization potential of argon and one about 2.5 v below, with evidence of an intermediate appearance potential. The voltage interval between the extreme appearance potentials is roughly 3.5 v, and the electron affinity of the fluorine atom is 3.6 v [13].

The F^+ ion curve was very difficult to evaluate. The observed appearance potential was about 23 v.

The ionization-efficiency curves of the negative halogen ions are represented by the two curves shown in figure 3. The voltage scale is uncorrected. The I^- and Br^- ions are both formed by dissociative electron capture, with an appearance potential very near to zero volts, as illustrated in the figure. There was no evidence of other ionization processes with electron energies extending to 90 v. The very gradual increase in the small ion current observed at higher voltages is not deemed significant.

On the other hand, the Cl^- and F^- ions are formed by ion-pair processes only, with no evidence of an electron-capture process. As indicated, the appearance potential of the ion-pair process is a relatively simple one to evaluate compared to the capture process. The general features of the fine structure in the ionization-efficiency curves of the negative ions are quite reproducible, but are of unexplained origin at present.

Evidence of methyl ions formed with kinetic energy was found only in methyl fluoride. From the shape of the CH_3^+ peak recorded at low ion-accelerating voltage, the excess kinetic energy of methyl ions in CH_3Cl is estimated to be less than 0.5 v, and in the other methyl halides is estimated to be less than 0.2 v. Figure 4 is a composite record of the CH_3^+ ion peak of methyl fluoride partially separated into a narrow and a wide portion when measured at 200-v ion-accelerating voltage. Four galvanometers with different sensitivities record each peak, resulting in the four traces shown. From figure 4, A, the apparent abundance of ions with excess kinetic energy is about 71 percent of the abundance of ions with thermal energy. It is well known, however, that ions with initial kinetic energy are collected with low efficiency, and the apparent relative abundance of the ions having excess kinetic energy will decrease rapidly as the ion-accelerating voltage is decreased.

TABLE 1. *Relative abundances and appearance potentials of selected methyl halide ions*

Ion	Abundance	Appearance potential	Remarks	Comparison values
			CH_3F	
	C_r	eV		
CH_3F^+	100	$12.6_1 \pm 0.1$	Ionization potential	12.84 ±0.03 [3b].
CH_3^+	98	16.5 ± 0.5	"Second" appearance potential, $V_{IA} = 2,500$ v.	
		16.3 ± 0.3	"Kinetic-energy" ion, $V_{IA} = 200$ v.	
		14.7 ± 0.3	"Thermal-energy" ion, $V_{IA} = 200$ v	14.6 [19].
		12.7 ± 0.5	Ion-pair process. "First" appearance potential, $V_{IA} = 2,500$ v.	
F^+	1.5	23.0 ± 0.5	Principal process for F^+ ion.	
F^-	~0.6	12.4 ± 0.5	Ion-pair process.	
			CH_3Cl	
CH_3Cl^+	100	$11.3_4 \pm 0.1$	Ionization potential	11.17 [5], 11.25 [5], 11.3 [4].
CH_3^+	85	13.7 ± 0.2	Kinetic energy <0.5 v	13.44 [19], 13.5 [4].
		10.2 ± 0.5	Ion-pair process.	
Cl^+	4	16.5 ± 0.5		16.6 [4].
Cl^-	~0.1	10 ± 1	Ion-pair process.	
			CH_3Br	
CH_3Br^+	96	10.5 ± 0.1	Ionization potential	10.49 [5], 10.80 [5], 10.5 [4].
CH_3^+	100	12.9 ± 0.1	Kinetic energy <0.2 v	12.83 [19], 13.2 [4].
Br^+	8	14.8 ± 0.3		15.0 [4].
Br^-	~1	0	Electron capture.	
			CH_3I	
CH_3I^+	100	$9.5_5 \pm 0.1$	Ionization potential	9.49 [5], 10.11 [5], 9.6 [4].
CH_3^+	13	12.4 ± 0.2	Kinetic energy <0.2 v	12.15 [19], 12.4 [4], 12.36 [3a].
I^+	38	12.7 ± 0.2		12.88 [19], 12.9 [4].
I^-	~2	0	Electron capture.	

In figure 4, A, the energy filter is grounded, and ions with thermal and excess kinetic energy reach the collector; in figure 4, B, the energy filter is connected to the ion-accelerating voltage supply and adjusted to give nearly equal abundances of thermal-kinetic-energy peaks. Under the same filter conditions, figures 4, C, D, and E, show the effect on the separate peaks of lowering the uncorrected ionizing voltage to 20, 17, and 15 v, respectively. A plot of peak height versus ionizing voltage taken at 1-v intervals indicates the appearance potential of the ions with excess kinetic energy to be about 16.3 v, whereas that of the ions with thermal energy is about 14.7 v.

With the energy filter connected to high voltage and adjusted to give nearly equal heights of the thermal- and kinetic-energy peaks (fig. 4, B), the ion-accelerating voltage interval between the maxima of the two peaks was found to be approximately 0.7 v. Thus, the total kinetic energy of the dissociation process, calculated from the voltage interval between the maxima of the kinetic and thermal-energy peaks and consideration of the conservation of momentum, is 1.3 v. The difference of 1.6 v between the appearance potentials is equal to this within the experimental uncertainty.

There was no evidence of the heterogeneous nature of the CH_3^+ ion peak with an ion-accelerating voltage of 2,500 v. The observed "second" appearance potential of the CH_3^+ ion, measured at an ion-accelerating voltage of 2,500 v, apparently corresponds to that of the methyl ion formed with excess kinetic energy.

A summary of the appearance potentials and related data for selected ions of the methyl halides is given in table 1. Columns 1 and 2 list, respectively, the selected methyl halide ions, and the abundance relative to the most abundant ion (equals 100) at a nominal electron energy of 70 v. There are two exceptions: The abundances of the Br^- and the I^- ions are measured at electron energies of about 0.5 v (uncorrected), but are relative to the most abundant positive ion measured at 70 v. Column 3 gives the observed appearance potentials and the experimental errors estimated from the reproducibility of the measurements. The absolute value of an appearance potential less than 2 v is uncertain to the extent of at least 1 v. Explanatory remarks appear in column 4. Column 5 gives comparison values from the literature.

4. Calculation of Bond-Dissociation Energies

The minimum energy (appearance potential) required to form positive methyl ions and halogen atoms from the methyl halides is given by the relation

$$A(CH_3^+)=D(CH_3-X)+I(CH_3)+E_k,$$

where $D(CH_3-X)$ is the carbon-halogen bond-dissociation energy, $I(CH_3)$ is the ionization potential of the methyl radical, and E_k is the total kinetic energy of the dissociation products. Thus, in the case of methyl fluoride, from table 1, $A(CH_3^+)=16.5$ v. Substituting into the above relation this value and the values for the ionization potential of the methyl radical (9.95 v) [14] and the total kinetic energy (1.6 v) from the observed difference in appearance potentials of the resolved methyl ions gives a bond-dissociation energy of 4.9 ev. In the case of the thermal-energy ions measured, as illustrated in figure 4, $A(CH_3^+)=14.7$ v. Subtracting the ionization potential of the methyl radical gives directly the C—F bond-dissociation energy of 4.7 ev. For reasons apparent in the following pages, this value is preferred among those appearing in column 2, table 2.

TABLE 2. *Bond-dissociation energies of methyl halides*

Bond	Dissociation energy (ev) from observed values of—		Literature references—		
	$A(CH_3^+)$	$A(X^+)$	[19]	[4]	[22]
CH_3-F	4.7±0.2 [a]4.9±0.2 [b]4.7±0.3	5.6±0.5	4.6	...	...
CH_3-Cl	3.7±0.2 [a]4.0±0.5	3.5±0.5	3.5	3.4	3.5
CH_3-Br	2.9±0.1	3.0±0.3	2.9	3.2	2.9
CH_3-I	2.4±0.2	2.3±0.2	2.2	2.3	2.4

[a] Dissociation process in which kinetic energy equals 1.6 v.
[b] Ion-pair process in which kinetic energy equals 1.6 v.
[c] Ion-pair process.

When negative halogen and positive methyl ions are formed simultaneously, the appearance potential of either ion is given by the relation

$$A(CH_3^+, X^-)=D(CH_3-X)+I(CH_3)-E_a(X)+E_k,$$

where $E_a(X)$ is the electron affinity of the halogen atom. The observed appearance potentials of the ion-pair process, $A(CH_3^+)=12.7$ v and $A(F^-)=12.4$ v, again indicate a C—F bond-dissociation energy of about 4.7 ev.

The bond-dissociation energy in methyl chloride can be calculated similarly by using the ion-pair appearance potential. However, the higher value obtained by the simple formation of CH_3^+, Cl, and a free electron is considered the more precise. Therefore, as excess kinetic energy of the methyl ion is apparently negligible, the carbon-halogen bond-dissociation energy in the chloride, bromide, and iodide molecules is computed simply by subtracting the ionization potential of the methyl radical from the appearance potential of the methyl ion. Table 2, column 2, summarizes the bond-dissociation energies thus obtained. Similar calculations from the appearance potentials of the halogen ions (column 3, table 2) give satisfactory agreement within the estimated uncertainties.

5. Discussion

5.1. Molecule Ions

The ionization potentials of chloro-, bromo-, and iodomethane given in table 1 are in good agreement with the electron-impact values reported by Branson and Smith [4] and, except for methyl chloride, with the lower of the doublet spectroscopic values reported by Price [5]. No spectroscopic ionization potential of CH_3F has been published. The disagreement between the ionization potential of methyl fluoride reported here and that reported by McDowell and Cox [3b] is slightly greater than the sum of the estimated experimental errors in both researches.

The existence in the spectra of the methyl halides of two electronic series of absorption bands in the far ultraviolet corresponding to two ionization potentials was predicted by Mulliken [15] and independently observed by Price [5]. Although the voltage interval between the doublet spectroscopic ionization potentials is greater than 0.6 v for methyl iodide (and less for the others), no indication of a break was observed in the ionization-efficiency curve of the CH_3I^+ ion.

If the ionization potentials of the methyl halides from table 1 and of methane [4] are plotted against a scale proportional to the total quantum number of H, and the halogen atoms, the empirical linear relation shown in the lower curve of figure 5 is obtained. As the ionization of the methyl halides (with the exception of CH_3F [3b]) occurs by the removal of one of the nonbonding "$p\pi$" electrons localized on the halogen atom [15], it is somewhat interesting that the ionization potential of methane also falls on the same curve. A similar linear relation is expected to hold for the ionization potentials of the hydrogen halides.[3] That this is apparently the case, is shown by the spectroscopic data [17] plotted as the upper curve of figure 5. The assumption that the ionization potential of HF falls in line with the hydrogen halides and hydrogen, as CH_3F does with the methyl halides and methane, supports the indicated interpolation and the resultant value of I^z (HF) = 14.2 v. This is in agreement with the lowest of several values of the ionization potential; namely, 14.02, 15.7, and 18.04 v, estimated at various times by means of quantum mechanical and thermodyamic calculation [18]. A higher value of about 18 v is estimated from figure 1 of the paper by Teegan and Walsh [16].

[3] Teegan and Walsh [16] note empirical linear relationships between the ionization potentials of inert gases and of a number of isoelectronic atoms, ions, and diatomic molecules, including the hydrogen halides.

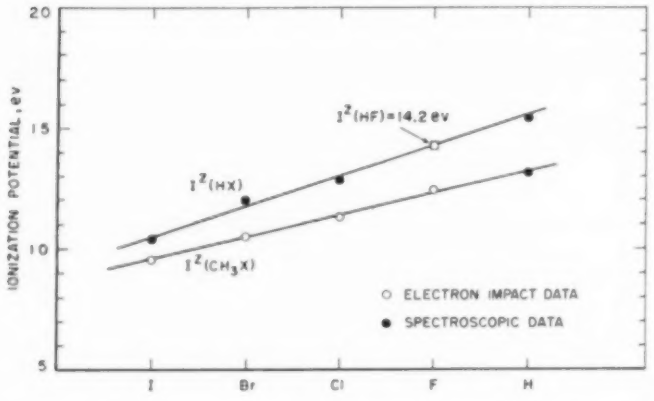

FIGURE 5. *Spectroscopic and electron-impact values for the ionization potentials of the hydrogen and methyl halides plotted against a scale proportional to the total quantum numbers of the hydrogen and halogen atoms.*

5.2. Dissociative Ions

The methyl ions are relatively abundant in all of the spectra, except that of methyl iodide, and the reproducibility of the appearance potential measurements is comparable with that of the ionization potential. As indicated in table 1, there is good agreement with previously published values for the chloro-, bromo-, and iodocompounds, although the second appearance potential associated with the ion-pair formation of the methyl ion in methyl chloride is previously unreported. Branson and Smith [4] did not search for negative ions, and their use of the linear extrapolation method for correcting the voltage scale evidently did not reveal the ion-pair process in methyl chloride. This is not surprising in view of the relative abundance of the Cl^- ion shown in table 1. However, this fact, together with the existence of Br^- and I^- ions formed by electron capture, does not affect their conclusions concerning the carbon-halogen bond-dissociation energies.

The production of CH_3^+ ions in methyl fluoride is complicated not only by the simultaneous formation of F^- ions, but also by the apparent existence of dissociation processes resulting in methyl ions with thermal energy and methyl ions with excess kinetic energy. An accurate measure of the relative probabilities of thermal- and kinetic-energy processes is very difficult in view of the magnitude of the effect of the ion-accelerating voltage on the efficiency of collecting ions with excess kinetic energy. That the ions with excess kinetic energy are in great abundance at 2,500 v, however, is suggested by the fact that a several-fold increase in the apparent abundance of such ions relative to thermal-energy ions has been observed by increasing the ion-accelerating voltage from 150 to 500 v [8]. This indicates a high probability for the process producing fragments with kinetic energy.

In agreement with previous research [3,7], no evidence was found for methyl ions with excess kinetic energy in the chloro-, bromo-, or iodomethanes.

For methyl fluoride, Lossing [19] has reported a measurement of $A(CH_3^+) = 14.6$ v. In the present research, measurements made at an ion-accelerating voltage of 2,500 v gave no clearly defined break in the exponential portion of the CH_3^+ ionization-efficiency curve corresponding to ions with this critical potential. However, good agreement with the value was obtained for the appearance potential of the thermal-

energy ions (14.7 v) when these were resolved from the ions with excess kinetic energy (A.P.=16.3 v). Unfortunately, the sensitivity of the measurement was considerably reduced at the necessarily low ion-accelerating voltage (200 v). Failure to observe the lowest appearance potential associated with ion-pair formation in this experiment was purely a matter of sensitivity. (The observed abundance of F^- relative to CH_3^+ is 0.6%.) The experiments give no direct evidence as to whether there is excess kinetic energy associated with ion-pair production.

The agreement of the C—F bond-dissociation energy obtained in this research (see table 2) with that reported by Lossing [19] is interesting, but may be fortuitous. Although the existence of three dissociation processes seems fairly well established, the evaluation of three appearance potentials in the range of a few volts is very difficult.

As the relative abundance of the halogen ions decreases markedly from the iodide to the fluoride, the precision of measurement of the appearance potential of these ions also decreases. The observation of the appearance potential of 23 v for the F^+ ion is not very precise, but apparently is well established by several measurements. An additional experimental uncertainty results from the undesirably large ($\sim$7 v) voltage interval between the appearance potential of F^+ and the ionization potential of the calibrating gas (argon). A more detailed study of these observations is included in research currently in progress on the ionization and dissociation of the complete series of fluoromethanes.

As demonstrated in table 2 of this research and as previously observed by Branson and Smith [4], satisfactory agreement is obtained for the chloro-, bromo-, and iodomethanes between the carbon-halogen bond-dissociation energy calculated from the appearance potential of the methyl ions and that calculated from the halogen ion. In disagreement with Branson and Smith, however, the present authors conclude that within the experimental uncertainties for these molecules, there is no evidence for the applicability of a rule proposed by Stevenson [4] and so successfully applied by him to the energetics of the dissociation of hydrocarbons by electron impact [20].

The concept of the relation between bond distance and bond-dissociation energy is well known and often demonstrated to be other than a simple one. However, a simple relation between bond distance and carbon-halogen bond-dissociation energy computed from the methyl ion appearance potential is indicated in figure 6. The dissociation energy for the first *C—H* bond in methane [20] is included for comparison. Its position on the energy scale relative to the methyl halides is consistent with the fact that hydrogen atoms will not react with CH_3F, but do react with increasing ease from CH_3Cl to CH_3I [21].

The uncertainty in the measurement of the appearance potentials of the dissociative electron-capture ions, Br^- and I^-, is much greater than that for the ion-pair process ions, F^- and Cl^-. The very low energy required for electron capture is considerably below the ionizing-voltage calibration range. Furthermore, the rapid change in ionizing current with ionizing voltage makes difficult the measurement of relative abundances of these ions near the threshold potential. It is evident, however, that in the case of methyl bromide and methyl iodide, the C—*X* dissociation energies are equal to or less than the electron affinities of the bromine and iodine atoms.

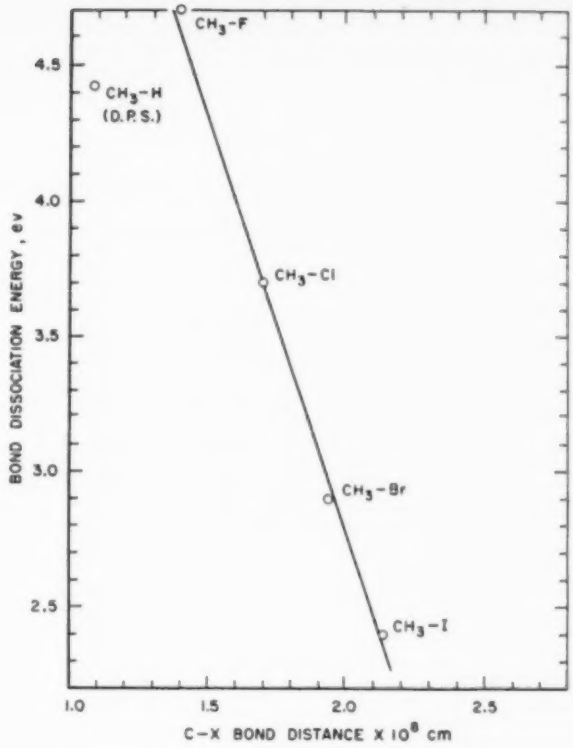

FIGURE 6. *Plot of the carbon-halogen bond distance versus the observed values for the C—X bond-dissociation energy of the methyl halides.*

In spite of the qualitative nature of the information of the dissociative electron-capture ions, the negative-ion studies give additional information on the electrical properties of the methyl halides. As a sharp distinction appears between the compounds in the matter of the electron-capture process, the behavior of the bromide and iodide molecules is expected to differ from that of the fluoride and chloride molecules when subjected to electric discharge or ionizing radiations.

The authors are indebted to Fred L. Mohler for helpful and stimulating discussions throughout the course of this work. The assistance of J. H. Lengel in the preparation of the methyl fluoride is also gratefully acknowledged.

[4] Stevenson has shown that in the process $R_1{-}R_2{+}e{\rightarrow}R_1^+{+}R_2{+}2e$ in *n*-and *i*soalkanes, for the equality $A(R_1^+){=}D(R_1{-}R_2){+}I(R_1)$ to hold, $I(R_1){\geq}I(R_2)$.

6. References

[1] S. Bauer and T. R. Hogness, J. Chem. Phys. **3**, 687 (1935).
[2] J. D. Morrison and A. J. C. Nicholson, J. Chem. Phys. **20,** 1021 (1952).
[3a] C. A. McDowell and B. G. Cox, J. Chem. Phys. **20,** 1496 (1952).
[3b] C. A. McDowell and B. G. Cox, J. Chem. Phys. **22,** 946 (1954).
[4] H. Branson and C. Smith, J. Am. Chem. Soc. **75,** 4133 (1953).
[5] W. C. Price, Phys. Rev. **47,** 419 (1935); J. Chem. Phys. **4,** 539 (1936).
[6] C. A. McDowell and J. W. Warren, Discussions Faraday Soc. No. **10,** 53 (1951).
[7] C. A. McDowell and J. W. Warren, Trans. Faraday Soc. **48,** 1084 (1952).
[8] F. L. Mohler, V. H. Dibeler, and R. M. Reese, J. Chem. Phys. **22,** 394 (1954).
[9a] D. P. Stevenson and J. A. Hipple, J. Am. Chem. Soc. **64,** 1588 (1942).
[9b] T. Mariner and W. Bleakney, Phys. Rev. **72,** 807 (1947).
[9c] R. E. Honig, J. Chem. Phys. **16,** 105 (1948).
[9d] J. J. Mitchell and F. F. Coleman, J. Chem. Phys. **17,** 44 (1949).
[10] V. H. Dibeler, R. M. Reese, and F. L. Mohler, J. Chem Phys. **20,** 761 (1952).
[11] H. D. Hagstrum, Rev. Mod. Phys. **23,** 185 (1951).
[12] C. E. Moore, NBS Circular 467.
[13] H. O. Pritchard, Chem. Rev. **52,** 529 (1953).
[14] F. P. Lossing, K. U. Ingold, and I. H. S. Henderson, J. Chem. Phys. **22,** 621 (1954).
[15] R. S. Mulliken, Phys. Rev. **47,** 413 (1935).
[16] J. P. Teegan and A. D. Walsh, J. Chem. Phys. **19,** 1070 (1951).
[17] W. C. Price, Chem. Rev. **41,** 257 (1947).
[18] G. Glockler, Fluorine chemistry, J. Simons, ed., p. 232, (Academic Press, Inc., New York, N. Y. 1950).
[19] F. P. Lossing, (private communication).[5]
[20] D. P. Stevenson, Trans. Faraday Soc. **49,** 867 (1953).
[21] E. W. R. Steacie, Atomic and free radical reactions, (Reinhold Publishing Corp. N. Y. 1946).
[22] J. S. Roberts and H. A. Skinner, Trans. Faraday Soc. **45,** 229 (1949).

[5] After the present paper was written, F. P. Lossing, K. U. Ingold, and I. H. S. Henderson [J. Chem. Phys. 22, 1489 (1954)] published the results of a study of the methyl halides, including the results referred to above.

Washington, October 15, 1954.

Journal of Research of the National Bureau of Standards Vol. 54, No. 3, March 1955 Research Paper 2574

Variation in Distortion with Magnification

Arthur A. Magill

The distortion introduced in the image by a lens for a given axial inclination of the chief ray is a linear function of the magnification. Specifically, if D_0 represents the distortion with parallel light incident on one side of the lens (zero magnification) and D_∞ the distortion with parallel light incident on the other, then the distortion D_m at any magnification m is given by $D_m = D_0 - {}^m D_\infty$. This equation has been experimentally verified for examples of three types of symmetrical lenses.

1. Introduction

The growth of photogrammetry with its high-precision imaging systems has necessitated accurate determination of the distortion introduced by a lens. Because the distortion varies with the magnification, it has been customary heretofore to have the distortion measured for each object-to-image ratio employed. To avoid making such a series of measurements, a simple linear equation for a lens with a single effective stop has been developed, from which the distortion at any magnification may be computed from the measured values obtained at two magnifications. The two distortions that would normally be used are those obtained with parallel light incident, in turn, on the front and on the back of the lens. These not only require the simplest experimental setup, but also have special significance as the limits of real image formation. Virtual images (i. e., negative magnifications) will be excluded as having little practical value.

2. Theoretical Development

In 1907 E. Wandersleb [1] developed a hyperbolic relation between magnification and the ratio of the lateral displacement of the image from its distortionless position to the height of the distortionless image. By defining the distortion as the later displacement of the image, the relationship may be reduced to a linear function, fully expressible by the introduction of the two values obtained with parallel light.

In figure 1, a lens of focal length f with surface 1 and final surface k has the paraxial foci F and F'. It is equipped with a single effective stop. The paraxial pupils are located at E_0 and E'_0 at distances p_0 and p'_0 from the foci. The spherical aberration of the lens elements preceding and following the stop changes the positions of the pupils for nonparaxial rays. For the chief ray with a slope angle of u to the optic axis in the object space and u' in the image space, the pupils are shifted by amounts δ and δ' to E and E' at distances p and p' from the foci.

Now consider the object point O with this same chief ray located at a height y from the optic axis, as shown in figure 2. The sign convention is that of taking figure 2 as an all-positive diagram. The intersection of the emergent chief ray with the Gaussian image plane at O′, a height y' from the axis, will be taken as the image of O. For low-aperture lenses with negligible zonal aberrations, this is certainly a legitimate definition of the image position. Because most precision projection is done

[1] E. Wandersleb, Uber die Verzeichnungsfehler Photographischer Objectiv, Z. Instrumentenk. **27,** 33-37, 75-85 (1907). The equation is also used in many optical texts.

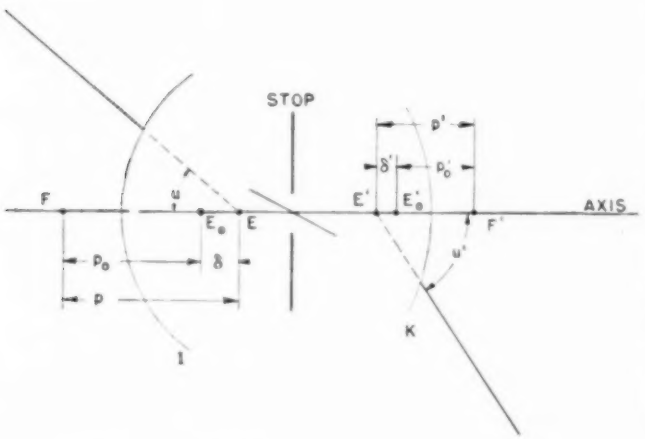

FIGURE 1. *Diagram of a lens and a given chief ray.*

The lens elements preceding and following the stop image is at E_0 and E'_0, respectively. For the indicated nonparaxial chief ray the spherical aberration of the elements relocates these images at E and E'.

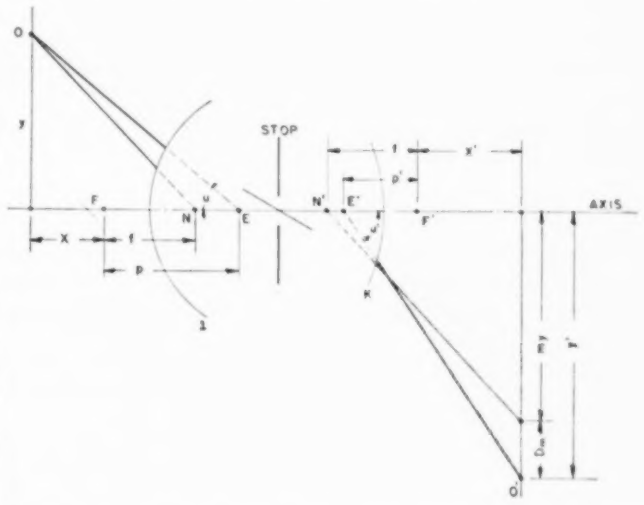

FIGURE 2. *Same lens as figure 1 with object and image planes included.*

The object O is imaged at O′ in the Gaussian image plane. The distortion D_m is the lateral displacement of O′ from its Gaussian position, $D_m = y' - my$. All distances and angles are to be considered positive, as shown.

at f-numbers of 22 or larger, the definition is also in accord with photogrammetric practice. Thus, the magnification m, can be defined in terms of Gaussian optics as

$$m=\lim_{y\to\infty}\frac{y'}{y}=\frac{x'}{f}=\frac{f}{x}, \tag{1}$$

where x and x' are the distances of the object and image planes from their respective foci. A ray in the object space directed toward the first nodal point N, will emerge at the same slope angle in the image space as though emanating from the second nodal point, N'. This ray intersects the Gaussian image plane at the distortionless image position, a height my from the optic axis.

The linear distortion for any magnification D_m is defined as the difference between the actual image position and this distortionless image position, that is,

$$D_m=y'-my. \tag{2}$$

From figure 2 it is apparent that the values of y and y' referred to the chief ray are

$$y=(x+p)\tan u, \tag{3}$$

$$y'=(x'+p')\tan u'. \tag{4}$$

By substituting the values of x and x' from eq (1) and multiplying y through by m, the following equations are obtained:

$$my=(f+mp)\tan u, \tag{5}$$

$$y'=(mf+p')\tan u'. \tag{6}$$

Substitution of eq (5) and (6) in eq (2) yields

$$D_m=(p'\tan u'-f\tan u)-(p\tan u-f\tan u')m. \tag{7}$$

For any given chief ray, all values in eq (7) are constants with the exception of the magnification, and D_m is a linear function of m.

The magnification for an object located an infinite distance to the left is zero and eq (7) reduces to

$$D_0=p'\tan u'-f\tan u. \tag{8}$$

This is geometrically illustrated in figure 3 where parallel light incident on the left at the slope angle u forms an image in the paraxial focal plane on the right at a height of $p'\tan u'$. The distortionless image position is given as the limiting value of my as m approaches zero and y approaches infinity, which from eq (5) is $f\tan u$.

For an object in the focal plane at the left, the magnification and the linear distortion are both infinite. However, if an object point is considered to be located at the position of the infinite image, it would in turn be imaged at the intersection of the chief ray with the focal plane on the left. The linear distortion D_∞, is here defined as that obtained

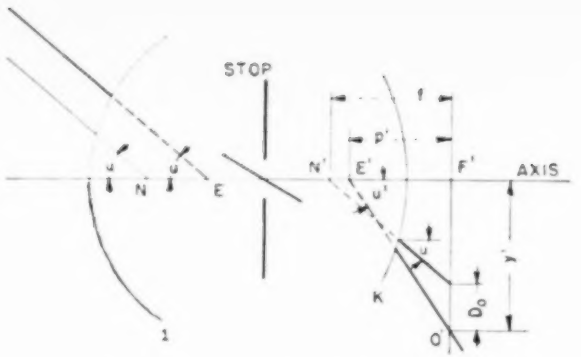

FIGURE 3. *Same lens as figure 1 at a magnification of zero.* An infinite point object on the left is imaged in the focal plane at the right at O'. For this magnification of zero the distortion is given by $D_0=y'-f\tan u$.

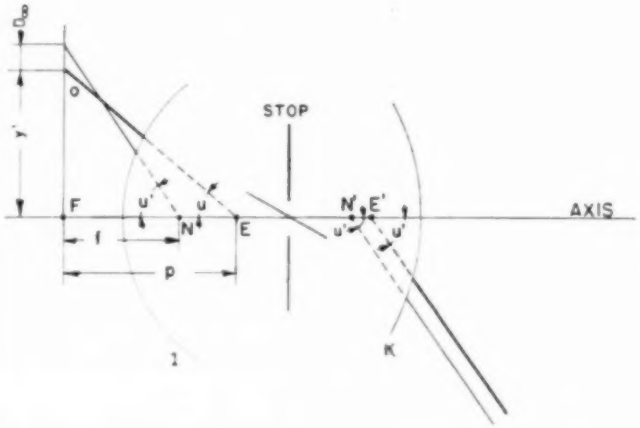

FIGURE 4. *Same lens as figure 1 at a magnification of infinity.* An object O in the focal plane at the left is imaged at infinity on the right. If the infinite image were replaced by an object, it would in turn be imaged at O'. The resulting distortion is designated D_∞ and in this case is negative.

when parallel light is incident on the right at a slope angle of u'. Referring to figure 4, it is clear that

$$D_\infty=p\tan u-f\tan u'. \tag{9}$$

By dividing eq (7) by m, it is also true that

$$D_\infty=-\lim_{m\to\infty}\frac{D_m}{m}=p\tan u-f\tan u', \tag{10}$$

where the negative sign indicates that D_∞ is measured with the light going backward through the lens. From eq (7), (8), and (9),

$$D_m=D_0-mD_\infty. \tag{11}$$

This equation gives the linear distortion at any magnification in terms of the two distortions obtained with parallel light for any given chief ray. The only restrictions are that there be a single effective stop and a requirement that the chief ray adequately determine the center of gravity of the image or that, if it does not, the discrepancy be a linear function of the magnification.

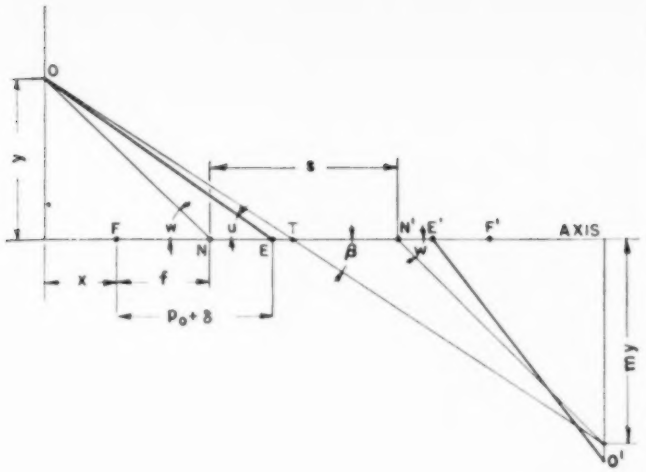

FIGURE 5. *Same lens as figure 1 illustrating other reference angles.*

It is often more convenient to refer the distortion to the slope angles w or β than it is to the slope angle, u. For a symmetrical lens, u, w, and β may be used interchangeably with little error.

3. Experimental Method

The equation has been verified for three types of commonly used symmetrical objectives at relative apertures of $f/22$. The experimental method is the same as that described by Bennett,[2] using a nodal slide and optical bench. The probable error of measurement varies with the slope angle, ranging from approximately 1 to 5 μ at 45° with parallel incident light. For finite object distances the probable error is greater by the nominal factor of $(m+1)$.

For the measurement of D_∞, the value of u' that corresponds to any given u may be found from eq (8), providing the distance $p'=(p_0'+\delta')$ is known. Furthermore, for the user of the lens to be able to refer distortion to the chief ray requires that he know either $(p_0+\delta)$ or $(p_0'+\delta')$. The measurement of the location of the paraxial pupils presents no particular problem. To determine the values of δ and δ', the stop could be equipped with a cross hair and the displacement of its image measured as the lens is rotated around each paraxial pupil in turn. The magnitude of δ could also be computed from eq (9) as a check on the measured values.

In practice it is often more convenient to refer the distortion to some other basis than the slope angle of the chief ray. In the nodal slide method the distortion is referred to the slope angle of the straight line joining the object and its Gaussian image, indicated as β in figure 5. The slope angle, w, of the ray in the object space directed toward the first nodal point might serve as a more convenient basis for the user of the lens, who normally computes the conjugate distances from the nodal points. The equations relating these two slope angles to that of the chief ray are

$$\tan w=\frac{p_0+\delta+x}{f+x}\tan u, \tag{12}$$

$$\tan \beta=\frac{p_0+\delta+x}{f+x+\dfrac{s}{m+1}}\tan u, \tag{13}$$

where s is the separation of the nodal points.

For the ideal symmetrical lens, the pupils coincide with the corresponding nodal points and $p_0=p_0'=f$, $u=u'$, and $\delta=\delta'$. Also from eq (8) and (9), $D_0=D_\infty=\delta\tan u$. Remembering that $x=f/m$, eq (12) and (13) may be rewritten

$$\tan w=\tan u+\frac{D_0}{f}\left(\frac{m}{m+1}\right), \tag{14}$$

$$\tan \beta=\frac{1}{1+\dfrac{s}{f}\dfrac{m}{(m+1)^2}}\tan w. \tag{15}$$

That u, w, and β may be used interchangeably with little error is superficially apparent because D_0 is normally a very small percentage of f and the discrepancy between β and w maximizes for $m=1$, for which magnification the distortion is zero. Although nominally symmetrical lenses are actually slightly asymmetric resulting in obvious differences between D_0 and D_∞, the effect on the reference slope angle has been ignored in obtaining the data for this paper; that is, the assumption has been made that u, u', and β are all equal. A detailed defense of this assumption for each lens tested would appear to be trivial in view of the good experimental agreement that was obtained. It should be pointed out, however, that if u' is not equal to u, the assumption of equality will in itself tend to minimize the errors introduced by employing a constant β for finite object distances.

4. Experimental Verification

The experimentally determined distortions are given for examples of the three types of symmetrical lenses in tables 1, 2, and 3. In all cases the value of the distortion at a slope angle of 5° is assumed to be zero. The errors in magnification are so small with respect to the other errors involved that all magnifications are considered exact. The measurements were made with a tungsten light source and a narrow-band filter having a dominant wavelength of 575 mμ.

The italicized digits represent the differences between the computed and observed values, and give a measure of the error involved in predicting distortion from D_0 and D_∞. In general these differences are what would be expected from the probable error of measurement. The greatest discrep-

[2] A. H. Bennett, The distortion of some typical photographic objectives, J. Opt. Soc. Am. and Rev. Sci. Instr. **14**, 235 (March 1927).

TABLE 1. *Distortion of two Hypergon-type lenses*

The measured values of the linear distortion D_m in millimeters for two Hypergon-type lenses are given for the indicated magnifications m and slope angles. The italicized digits beneath each distortion give the differences in microns between the values computed from D_0 and D_∞ and the measured values.

m	Slope angle							
	10°	15°	20°	25°	30°	35°	40°	45°
Lens A1, *f*/22, 127 mm								
0	0.000	0.001	0.005	0.012	0.024	0.041	0.067	(a)
∞	.001	.002	.004	.003	.000	−.007	−.013	(a)
	0		*0*	*−2*	*+3*	*−2*	*−4*	
0.2	.000	.001	.004	.013	.021	.044	.074	(a)
	0	*0*	*0*	*−2*	*+3*	*−2*	*−4*	
0.5	−.001	−.001	.003	.010	.025	.044	.074	(a)
	+1	*+1*	*0*	*0*	*−1*	*0*	*0*	
1	−.001	.000	.003	.014	.029	.054	.087	(a)
	0	*−1*	*−2*	*−5*	*−5*	*−6*	*−7*	
2	−.002	−.005	−.006	.003	.022	.044	.085	(a)
	0	*+2*	*+3*	*+3*	*+2*	*+11*	*+8*	
5	−.001	−.014	−.013	.001	.025	.068	.138	(a)
	−4	*+5*	*−2*	*−4*	*−1*	*+8*	*−6*	
Lens A2, *f*/22, 127 mm								
0	0.001	0.002	0.003	0.003	0.002	−0.001	−0.004	−0.008
∞	.001	.002	.007	.013	.031	.048	.064	.093
0.2	.000	.000	.000	.000	−.004	−.009	−.019	−.025
	+1	*+2*	*+2*	*0*	*0*	*−2*	*+2*	*−2*
0.5	.000	−.001	−.003	−.006	−.011	−.020	−.036	−.054
	0	*+2*	*+2*	*+2*	*−3*	*−5*	*0*	*0*
1	.000	.000	−.002	−.007	−.020	−.040	−.062	−.096
	0	*0*	*−2*	*−3*	*−9*	*−9*	*−6*	*−5*
2	−.002	−.004	−.012	−.028	−.049	−.090	−.146	−.209
	+1	*+2*	*+1*	*+5*	*−11*	*−7*	*+14*	*+15*
5	−.002	−.003	−.017	−.046	−.092	−.160	−.262	−.375
	−2	*−5*	*−15*	*−16*	*−61*	*−81*	*−62*	*−98*

[a] The special barrel in which this lens was mounted limited the effective total field to about 84°.

[b] The differences obtained at this magnification are an example of the systematic error introduced by a poor setting of the transverse axis over the center of rotation of the nodal slide. The differences could be materially reduced by employing a calibrating procedure such as that illustrated in figure 10.

TABLE 2. *Distortion of three Dagor-type lenses*

The measured values of the linear distortion D_m in millimeters for three Dagor-type lenses are given for the indicated magnifications m and slope angles. The italicized digits beneath each distortion give the differences in microns between values computed from D_0 and D_∞ and the measured values.

m	Slope angle						
	10°	15°	20°	25°	30°	35°	40°
Lens B, *f*/22, 6½ in.							
0	0.004	0.018	0.048	0.110	0.232	0.462	0.919
∞	.005	.017	.041	.101	.212	.413	.838
0.25	.002	.011	.032	.081	.173	.355	.702
	+1	*+3*	*+6*	*+4*	*+6*	*+4*	*+7*
1	.001	.001	.004	.010	.020	.052	.095
	−2	*0*	*+3*	*−1*	*0*	*−3*	*−14*
4	−.009	−.048	−.120	−.280	−.603	−1.194	−2.380
	−7	*−2*	*+4*	*−14*	*−13*	*+4*	*−53*

TABLE 2. *Distortion of three Dagor-type lenses*—Continued

The measured values of the linear distortion D_m in millimeters for three Dagor-type lenses are given for the indicated magnifications m and slope angles.[a] The italicized digits beneath each distortion give the differences in microns between values computed from D_0 and D_∞ and the measured values.

m	Slope angle						
	10°	15°	20°	25°	30°	35°	40°
Lens B3, *f*/22, 6½ in.							
0	0.004	0.017	0.049	0.116	0.244	0.488	0.967
∞	.002	.011	.032	.077	.171	.346	.796
0.25	.005	.013	.043	.100	.208	.412	.787
	−1	*+1*	*−2*	*−3*	*−7*	*−19*	*+3*
1	.001	.005	.016	.038	.073	.144	.265
	+1	*+1*	*+1*	*+1*	*0*	*−2*	*−4*
4	−.004	−.021	−.072	−.188	−.439	−.883	−1.884
	0	*−6*	*−7*	*−4*	*−1*	*−13*	*+27*
Lens B4, *f*/22, 6½ in.							
0	0.004	0.018	0.049	0.111	0.232	0.464	0.914
∞	.002	.012	.038	.086	.185	.372	.745
0.25	.005	.015	.039	.089	.191	.379	.739
	−1	*0*	*0*	*0*	*−5*	*−8*	*−11*
1	.002	.005	.013	.026	.047	.089	.163
	0	*+1*	*−2*	*−1*	*0*	*+3*	*+6*
4	−.009	−.033	−.100	−.216	−.526	−1.042	−2.098
	+5	*+1*	*−3*	*−17*	*+18*	*+18*	*+32*

TABLE 3. *Distortion of two Artar-type lenses*

The measured values of the linear distortion D_m in millimeters for two Artar-type lenses are given for the indicated magnifications m and slope angles. The italicized digits beneath each distortion give the differences in microns between the values computed from D_0 and $D\infty$ and the measured values.

m	Slope angle				
	10°	15°	20°	25°	30°
Lens, C1, *f*/22, 12 in.					
0	0.010	0.033	0.088	0.196	0.392
∞	.005	.024	.051	.121	.222
0.25	.008	.026	.073	.163	.331
	+1	*+1*	*+2*	*+3*	*+5*
0.5	.008	.023	.064	.137	.287
	0	*−2*	*−2*	*−1*	*−6*
1	.004	.008	.034	.073	.154
	+1	*+1*	*+3*	*+2*	*+10*
2	.000	−.006	−.016	−.054	−.061
	0	*−9*	*−2*	*+8*	*+2*
4	−.008	−.056	−.120	−.281	−.509
	−2	*−7*	*+4*	*−7*	*+13*
Lens C2, *f*/22, 16½ in.					
0	0.014	0.043	0.106	0.214	0.354
∞	.011	.040	.098	.215	.386
.5	.008	.022	.054	.115	[a]
	6	*+1*	*+3*	*−9*	
1	.001	.000	−.001	−.004	−.036
	+2	*+3*	*+9*	*+3*	*+4*
2	−.006	−.031	−.090	−.232	[a]
	−2	*−6*	*0*	*+16*	

[a] The conjugate distances were too great for the range of the optical bench.

TABLE 4. *Distortion of twenty Hypergon-type lenses*

The measured values of the linear distortion D_m in microns for 20 Hypergon-type lenses are given for parallel light and the indicated slope angles. These lenses have a nominal focal length of 127 mm and a nominal aperture of $f/22$.

Lens	m	Slope angle							
		10°	15°	20°	25°	30°	35°	40°	45°
A_1	0	2	3	3	7	12	19	29	54
	∞	2	4	6	7	12	17	21	27
A_4	0	−1	−2	−6	−11	−19	−24	−42	−63
	∞	1	5	10	18	32	52	82	124
A_5	0	2	3	8	13	20	29	41	64
	∞	0	1	3	3	2	0	−2	1
A_6	0	1	1	0	1	3	4	6	12
	∞	2	5	9	15	23	34	47	64
A_7	0	0	1	−5	−7	−6	−5	−4	6
	∞	0	4	6	15	23	33	49	67
A_8	0	3	7	12	19	28	42	65	91
	∞	−2	−4	−7	−9	−12	−16	−19	−19
A_9	0	0	2	3	6	11	14	20	26
	∞	0	2	4	6	11	16	27	45
A_{10}	0	6	2	6	10	16	25	38	56
	∞	1	3	5	5	2	1	1	1
A_{11}	0	0	1	3	6	8	12	12	12
	∞	0	1	2	6	11	17	30	52
A_{12}	0	0	0	3	6	13	20	32	54
	∞	0	1	3	7	10	14	16	22
A_{13}	0	0	0	1	3	5	7	11	22
	∞	1	3	5	9	17	27	39	56
A_{14}	0	0	2	3	6	11	19	30	53
	∞	0	0	0	2	6	12	18	23
A_{15}	0	1	3	5	6	9	12	14	22
	∞	0	−2	−2	4	11	22	39	55
A_{16}	0	−2	−4	−5	−6	−6	−3	1	14
	∞	1	3	7	12	25	32	40	58
A_{17}	0	0	1	2	5	9	13	18	25
	∞	0	0	1	5	10	17	26	42
A_{18}	0	1	3	4	6	7	7	9	10
	∞	−1	−2	−1	6	13	24	40	65
A_{19}	0	0	0	0	5	8	13	18	29
	∞	1	2	3	8	17	24	36	60
A_{20}	0	1	0	1	5	9	17	23	42
	∞	1	4	6	11	15	21	35	49
A_{21}	0	3	7	9	14	17	28	32	48
	∞	1	1	1	4	9	18	26	47
A_{22}	0	0	1	3	5	8	13	22	38
	∞	2	6	9	16	22	34	44	57

ancy occurs for lens A_2 at a magnification of 5, representing about three times the nominal probable error. The good agreement at other magnifications for this lens indicates that the greatest part of the discrepancy is a result of errors in the observed values. That the differences have the same algebraic sign is evidence of a systematic error, which can be attributed to the method of measurement. This consisted of making a run at 5° intervals of the slope angle without resorting to the time-consuming process of resetting the lens on the nodal slide for each angle measured. Thus, any longitudinal displacement of the transverse axis (located at T in fig. 5) from the center of rotation of the nodal slide for a given run results in a systematic error in the distortion. The magnitude of this error is very closely proportional to the tangent of the slope angle. With the exception of B_2 and B_5, all of the lenses were submitted to the Bureau for routine tests and were not available for sufficient time to allow more than 2, and in some cases 3, such runs to be made at each magnification.

The data obtained on four other lenses are presented graphically in figures 6, 7, 8, and 9. For convenience in plotting, the equation has been defined in two regions around unit magnification. D_m is plotted against m for $0 \leq m \leq 1$ and D_m/m against $1/m$ for $1 \leq m \leq \infty$. This allows the point $-D_\infty$ to be included as the $\lim_{m \to \infty} D_m/m$. The points give the experimental distortions and the straight lines the computed values from D_0 and D_∞. For the perfectly symmetrical lens, all the lines would intersect at zero distortion and unit magnification; only in this case would there be no discontinuity. For the lenses measured, minimum distortion occurs at some other magnification than unity, indicating slight asymmetries introduced in manufacture. For very low distortion lenses, these slight asymmetries can result in pronounced differences in distortion between lenses of the same type. This is clearly illustrated in table 4, where the measured values of D_0 and D_∞ in microns are given for 20 Hypergon-type lenses of the same nominal focal length submitted to the Bureau for test.

Equation (11) may also be applied to minimized distortions that have been calibrated by a given cri-

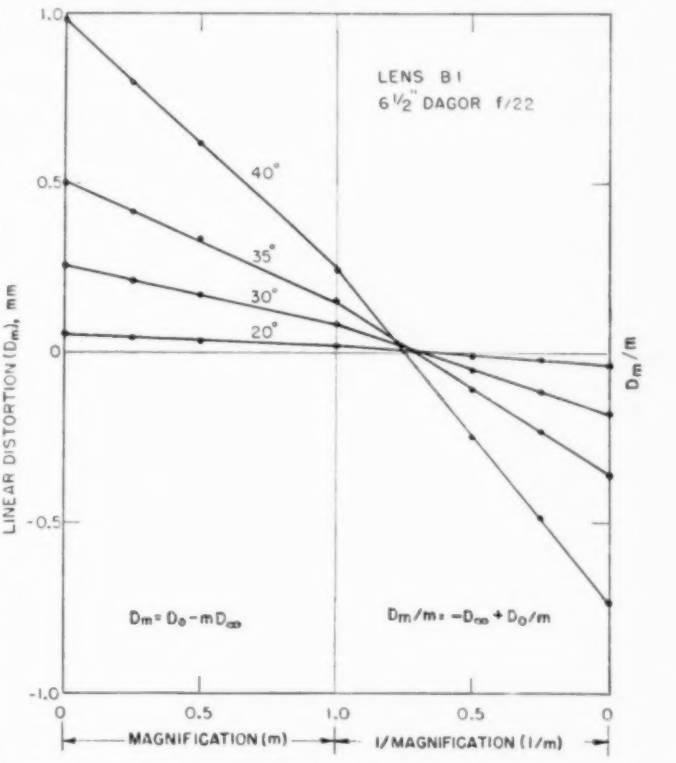

FIGURE 6. *Distortion plotted against magnification for the indicated slope angles.*

In order to include infinite magnifications, the graph has been split as shown into two regions at unit magnification. The straight lines represent the values computed from the two equations shown in their respective regions. The points indicate the experimentally determined values. The same graphical form has been employed in figures 7, 8, 9, 10, and 11.

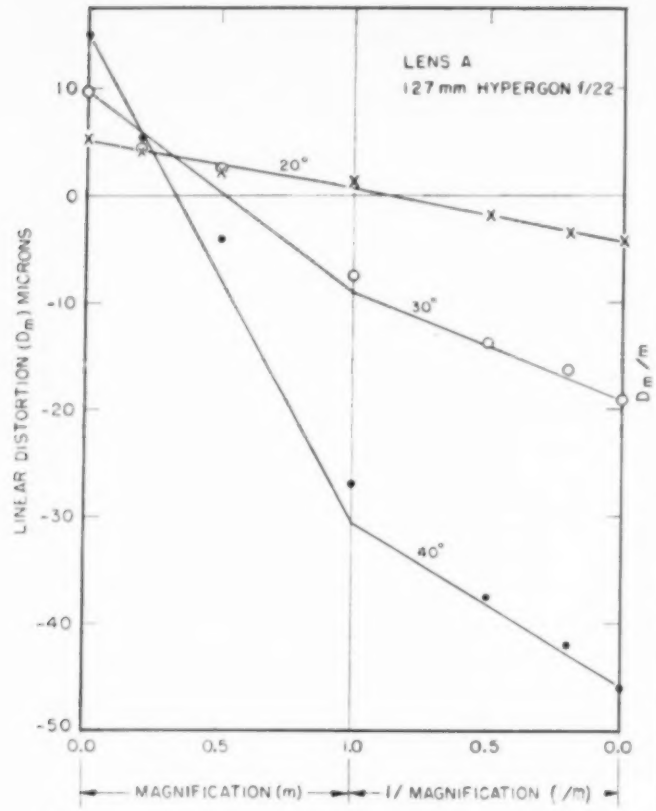

FIGURE 7. *Distortion plotted against magnification for the indicated slope angles.*

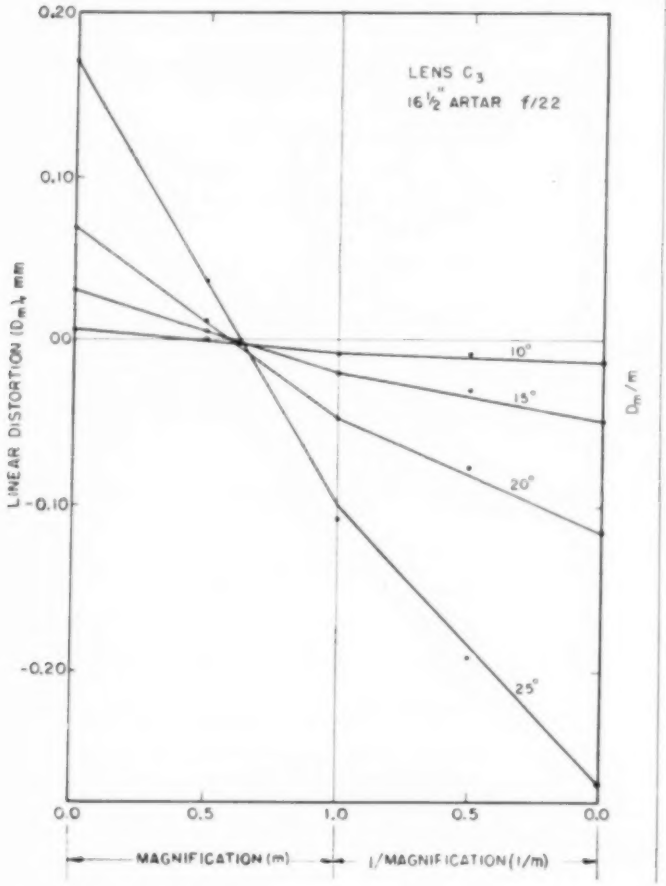

FIGURE 8. *Distortion plotted against magnification for the indicated slope angles.*

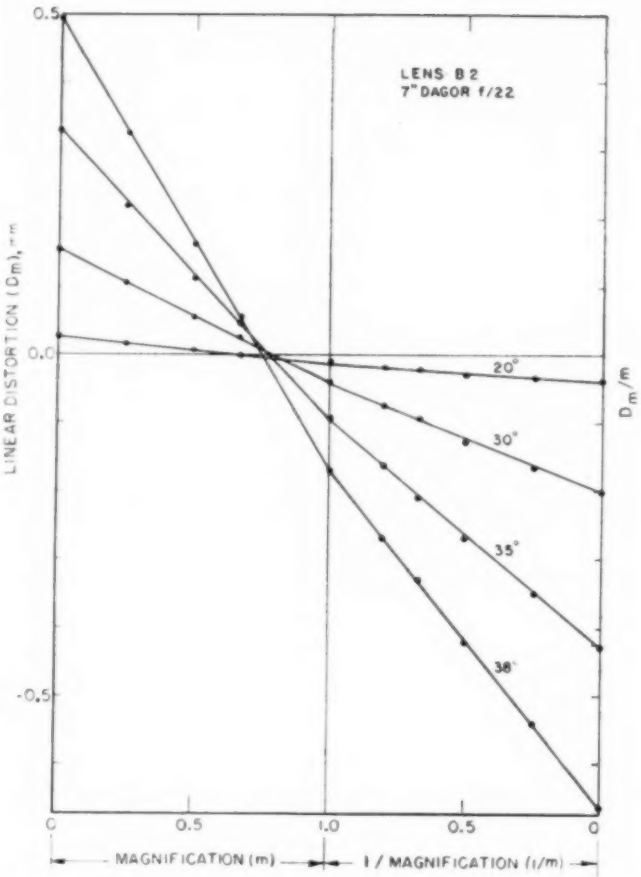

FIGURE 9. *Distortion plotted against magnification for the indicated slope angles.*

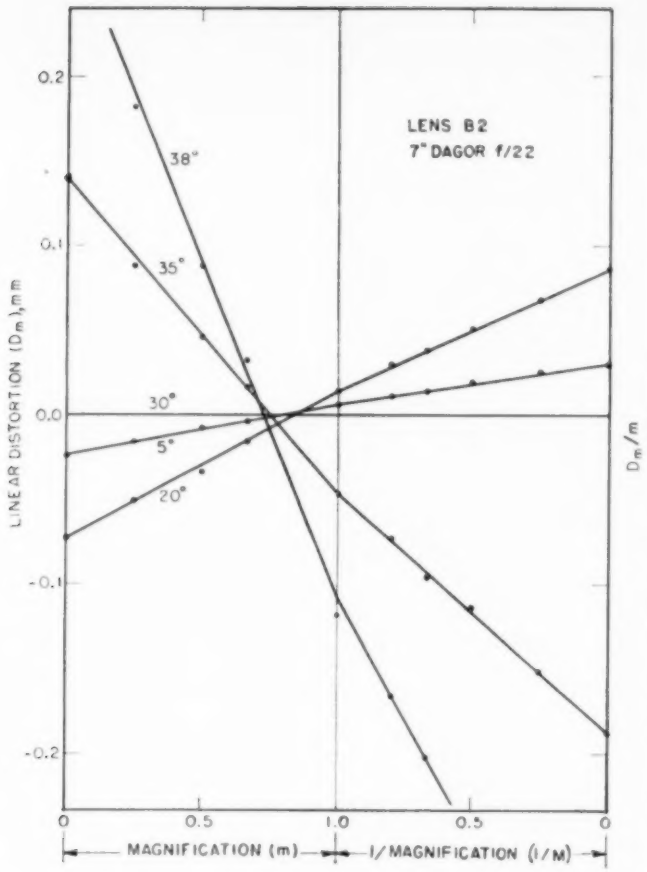

FIGURE 10. *Calibrated distortion plotted against magnification for the indicated slope angles.*

The data for the same lens as presented in figure 8 has been calibrated to give zero distortion at a slope angle of 30°. The magnitude of the change in distortion for any given magnification is proportional to the tangent of the slope angle.

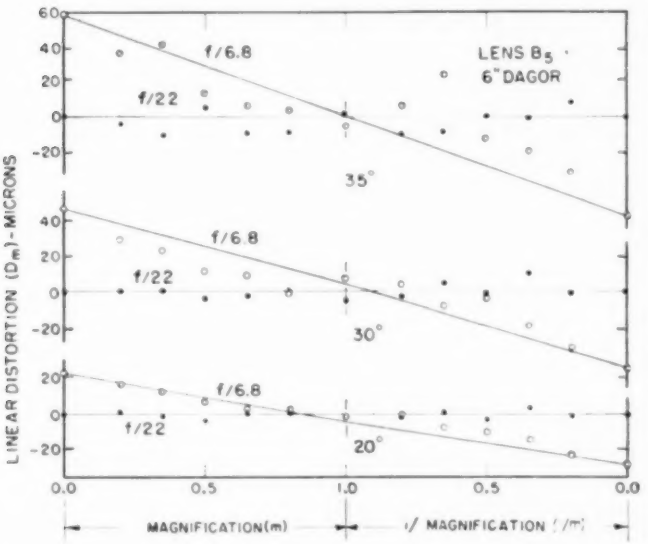

FIGURE 11. *Difference between the experimentally determined distortions for the indicated slope angles and those computed from the measured values of D_0 and D_∞ at f/22.*

The open circles represent data obtained at an aperture of f/6.8, and the solid circles at an aperture of f/22.

terion. At any given magnification, the magnitude of the change in distortion introduced by this calibration is proportional to the tangent of the slope angle, representing an effective shift in the position of the nodal points. For parallel incident light this results in calibrated focal lengths, which are equal only for a perfectly symmetrical lens. At finite object distances this results in a calibrated image distance or, more conveniently, a calibrated magnification. The calibrated focal lengths and magnifications are applied solely as scale factors and are not used in the determination of conjugate distances. Figure 10 shows the distortion presented in figure 8 calibrated to zero at a slope angle of 30°.

A detailed discussion of the effects on distortion of zonal aberrations introduced at apertures larger than f/22 is beyond the scope of this paper. However, their net effect can only result in a shift of the center of gravity of the nonparaxial image and a change in the plane of best focus. If the center of gravity shift is a linear function of the magnification and if the Gaussian identities expressed in eq (1) adequately determine the image plane of best focus when the higher aperture focal length is used, then eq (11) will still be valid.

In figure 11 the experimental distortions of a symmetrical-type lens at f/22 and the maximum aperture of f/6.8 have been plotted as the difference from the values computed from D_0 and D_∞ at f/22. The focal lengths and the values of D_0 and D_∞ for both apertures are given in table 5. No attempt was made to determine whether the image planes computed from the measured focal lengths were actually the planes of best over-all definition. At maximum aperture the effective stops were the outer lens retaining rings.

For this lens the experimental points for f/6.8 seem to lie along an S-shaped curve rather than being distributed about the straight line given by eq (11). The probable error of measurement is certainly higher at f/6.8 than at f/22, particularly for the larger slope angles. More data would have to be taken to determine if figure 11 is typical of all lenses of the same type, so at the present time the results must be considered as applying only to this particular lens. It is of interest that the difference between the distortion at f/22 and f/6.8 minimizes in the region about unit magnification, and elsewhere is generally greater than the deviation of the experimental distortions at f/22 from the computed values.

TABLE 5. *Change in focal length and distortion with aperature*

The change in focal length and distortion with aperature for two apertures of the Dagor-type lens B_5, with a nominal focal length of 6 in. The distortion is given in millimeters at the indicated slope angles.

Aperture	Focal length	m	Distortion		
			20°	30°	35°
	mm				
f/22	150.52	0	0.028	0.152	0.302
		∞	.047	.224	.435
f/6.8	150.12	0	.052	.199	.360
		∞	.075	.267	.492

5. Conclusion

The findings reported show that for low-aperture symmetrical lenses, the distortion at finite object distances can be simply computed from the two values obtained with parallel incident light with about the same accuracy as the direct experimental measurement. The necessary modifications required in carrying out this computation on other types of lenses have been indicated, and it is hoped that experimental verification of these procedures will soon be available.

Acknowledgment is made to F. E. Washer, who suggested the project and to W. R. Darling, who made many of the calculations and experimental measurements.

WASHINGTON, October 5, 1953.

Journal of Research of the National Bureau of Standards Vol. 54, No. 3, March 1955 Research Paper 2575

Heats of Combustion and Isomerization of Six Pentadienes and Spiropentane

Frances Maron Fraser and Edward J. Prosen

The heats of combustion of six pentadienes and spiropentane were measured by combustion of the hydrocarbon vapors, carried by helium gas, in a flame at constant pressure; the reaction was carried out in a glass reaction vessel contained in a calorimeter. The calorimeter system was calibrated by means of electric energy.

The experimental data yielded the following values for the standard heat of combustion, $-\Delta Hc°$, at 25° C and constant pressure, of the gaseous hydrocarbon in gaseous oxygen to form gaseous carbon dioxide and liquid water, with all the reactants and products in their thermodynamic standard reference states, in kilocalories per mole, where 1 kcal=4.1840 kj: 1,2-pentadiene, 777.14 ±0.15; 1,*cis*-3-pentadiene, 763.30 ±0.21; 1,*trans*-3-pentadiene, 761.64 ±0.15; 1,4-pentadiene, 768.94 ±0.30; 2,3-pentadiene, 775.32 ±0.16; 2-methyl-1,3-butadiene (isoprene), 761.62 ±0.23; spiropentane, 787.77 ±0.17.

From the above data the heats of isomerization to isoprene in kilocalories per mole were calculated to be 2-methyl-1,3-butadiene (isoprene)=0; 1,2-pentadiene=−15.52 ±0.23; 1,*cis*-3-pentadiene=−1.68 ±0.27; 1,*trans*-3-pentadiene=−0.02 ±0.22; 1,4-pentadiene=−7.32 ±0.34; 2,3-pentadiene=−13.70 ±0.23; spiropentane=−26.14 ±0.24.

Values of the heats of formation and hydrogenation were also derived from these data.

1. Introduction

This investigation is a continuation of the program on thermochemistry of monomers and related compounds [1,2,3,4] [1] sponsored by the Office of Synthetic Rubber of the Federal Facilities Corporation. It also forms a part of the work of the Thermochemical Laboratory of the National Bureau of Standards on the determination of heats of formation of compounds of importance to industry and science [5].

Calorimetric measurements have been made of the heats of combustion at constant pressure of isoprene and six of its isomers of empirical formula C_5H_8. Values of heats of isomerization, formation, and hydrogenation are derived from these data.

These data are useful in the calculation of heats of other reactions involving these compounds and, in addition, the data are precise and accurate enough to yield valuable information on relations between energy content and structure of molecules and, together with thermodynamic functions, yield equilibrium constants of important reactions, such as isomerization, hydrogenation, etc.

2. Method and Apparatus

The unit of energy is the absolute joule. For conversion to the conventional thermochemical calorie, the following relation was used: 1 cal=4.1840 abs j.

The molecular weight of carbon dioxide upon which the amounts of reaction in these experiments were based was taken as 44.010 from the 1952 table of international atomic weights [6].

The heats of combustion of the seven compounds reported in this investigation were determined by the method described previously [1,2] for gaseous hydrocarbons. As the present compounds are normally liquids at room temperature, the vapors were passed into the calorimeter by use of helium gas as a carrier.

Briefly, the method consists in determining in one set of experiments the energy equivalent, E_s, of the calorimeter system by measuring the electric energy supplied to the calorimeter heater to produce a 4-deg C rise in the temperature of the calorimeter. In another set of experiments, roughly the same 4-deg C rise in the temperature of the calorimeter is produced by the chemical energy of combustion of the hydrocarbon in oxygen in a flame; the reaction is carried out in the glass reaction vessel contained in the calorimeter. Thus, the calorimeter is simply used as a comparator of the two types of energy.

The calorimeter assembly, thermometric system, reaction vessel, sparking system, and electric-energy measuring apparatus have been described previously [1,2]. However, several improvements have been made in the apparatus and procedure.

In the sparking system [1], the four dry cells previously used as a source of energy were replaced during the course of these experiments by a 6-v storage battery. This produced a more constant sparking energy over long periods of time.

The present compounds are liquids at room temperature, 25° C, with boiling points ranging from 26° to 48° C. To introduce the vapors into the calorimeter, helium was bubbled through the liquid hydrocarbon with the bubbler and liquid maintained at some constant temperature below room temperature in the range 19° to 24° C. A very steady and efficient flame was easily produced, even though, in some cases, a fairly large percentage of helium was passed in with the hydrocarbon.

An improvement was made in the method of

[1] Figures in brackets indicate the literature references at the end of this paper.

switching the hydrocarbon gas or hydrocarbon-helium gas mixture into the calorimeter from the bypass line. Previously [1,2] the hydrocarbon rate was set through a bypass line, and the pressure in this line was somewhat lower than the pressure inside the reaction vessel with oxygen flowing through it. In order to avoid backflow of oxygen into the hydrocarbon line when the hydrocarbon was turned into the vessel, it was necessary to hold back the hydrocarbon for a few seconds to build up a back pressure slightly larger than the pressure in the vessel. This was also desirable because the slightly higher pressure thus built up in the hydrocarbon line made the hydrocarbon reach the burner tip more rapidly, and thus the time required for sparking was shorter than it would otherwise be. This method proved to be irreproducible and tended to produce a large initial flame, which then decreased in size until a steady flow established itself. When hydrocarbon-helium mixtures were used, this method was particularly cumbersome. These difficulties were avoided by installing a differential mercury manometer between the hydrocarbon bypass line and the hydrocarbon line leading into the reaction vessel. With a needle valve at the end of the bypass line, it was then a simple matter to produce a steady pressure in the bypass line about 1 mm of mercury higher than the pressure in the vessel. When the hydrocarbon or hydrocarbon-helium mixture was then turned into the reaction vessel, the rate was steady, and the hydrocarbon reached the burner tip in the same number of seconds in each experiment.

3. Materials and Procedure

The pentadienes used in the present experiments were NBS Standard Samples with the following amounts of impurities in mole percent: 1,2-pentadiene, 0.34 ±0.15; 1,*cis*-3-pentadiene, 0.08 ±0.04; 1,*trans*-3-pentadiene, 0.08 ±0.03; 1,4-pentadiene, 0.07 ±0.05; 2,3-pentediene, 0.15 ±0.07; and 2-methyl-1,3-butadiene (isoprene), 0.04 ±0.03. The purification and determination of purities of these pentadienes, by the freezing-point method, are described by Streiff, Soule, Kennedy, Janes, Sedlak, Willingham, and Rossini [7] for their API-Standard lots.

The spiropentane was obtained from G. Waddington of the Thermodynamics Laboratory, Petroleum Experiment Station, Bureau of Mines. The purification and determination of purity, by the calorimetric freezing-point method, are described by Scott, Finke, Hubbard, McCullough, Gross, Williamson, Waddington, and Huffman [8] for their sample C. The purity was 99.87 mole percent.

It is believed that in each case the impurity was predominately isomeric and present in such small amount that the heat of combustion was not affected in the worst case by more than one-half the estimated uncertainty of the final results listed in tables 3, 4, and 5.

The oxygen used for combustion and the helium used as a carrier gas were freed of combustible impurities by passage through copper oxide at about 550° C. They were then freed of carbon dioxide and water before entering the calorimeter or bubbler by passage through tubes containing successively ascarite, magnesium perchlorate, and phosphorus pentoxide.

Samples of the products of combustion were analyzed, by means of indicator tubes [9] for carbon monoxide, the most likely product of incomplete combustion, and mass spectrometrically for other products of incomplete combustion by the Gas Chemistry Section of the Bureau. In no case was the total amount of carbon monoxide greater than 0.005 percent of the amount of carbon dioxide formed in the combustion. No other products of incomplete combustion were found by mass spectrometer analysis; hence no corrections were applied for incomplete combustion.

For each calorimetric combustion experiment, the amount of reaction was determined from the mass of carbon dioxide formed; 1 mole, or 44.010 g,[2] of carbon dioxide was taken as equivalent to one-fifth mole of these C_5 hydrocarbons.

In these experiments, as in the experiments on the C_4 hydrocarbons [1,2], in addition to the determination of the mass of water vaporized during the experiment, a determination was usually made of the total mass of water formed during the combustion by flushing the reaction vessel with dry oxygen overnight. From the total masses of water and carbon dioxide, the stoichiometric ratio, r, of the number of moles of carbon dioxide to the number of moles of water collected multiplied by the factor $b/2a$ or 8/10 (where C_aH_b is the empirical formula of the hydrocarbon) was calculated as described in [2]. The number of experiments, the mean value of r, and the standard deviation of the mean for these compounds (except for 1,*trans*-3-pentadiene) were: 1,2-pentadiene (4), 0.99988 ±0.00021; 1,*cis*-3-pentadiene (4), 1.00003 ±0.00013; 1,4-pentadiene (5), 0.99952 ±0.00027; 2,3-pentadiene (4), 1.00007 ±0.00019; 2-methyl-1,3-butadiene (4), 0.99963 ±0.00008; spiropentane (3), 0.99957 ±0.00007. These ratios give additional evidence of complete combustion. In the above calculation, the molecular weights of carbon dioxide and water were taken as 44.010 and 18.0160, respectively.

Because it is possible that a strong drying agent in the hydrocarbon line might cause isomerization or partial polymerization of these hydrocarbons, most experiments were performed without any drying agent in the line. However, in some of the calorimetric combustion experiments the hydrocarbon vapors were passed through a short length of tubing containing magnesium perchlorate before entering the calorimeter. The results of these experiments did not differ significantly from those run without the drying agent except in the case of 2,3-pentadiene

[2] The international atomic weight of carbon has recently been changed from 12.010 [6] to 12.011 [22]. The molecular weight of carbon dioxide was taken as 44.010 in this paper to retain consistency with values previously determined in the Thermochemical Laboratory for the heats of formation of other hydrocarbons and of carbon dioxide. The values of the heats of combustion per mole of hydrocarbon reported here can be corrected for the effect of the change to the new atomic weight of carbon by multiplication, using the factor 44.011/44.010.

and of 1,*trans*-3-pentadiene. In these cases the higher results, obtained with the drying agent in the line and the discoloration of the drying agent in the case of 2,3-pentadiene, indicated that some alteration of the hydrocarbon took place over the drying agent. In these two compounds only the results without drying agent were used in obtaining the mean value.

In none of the compounds, except 1,*trans*-3-pentadiene, was a significant amount of water vapor carried into the calorimeter with the hydrocarbon vapors, even in those cases where no drying agent was used. This is indicated by the values of the stoichiometric ratios, r, given above. In the case of 1,*trans*-3-pentadiene, the sample was allowed to stand in the bubbler tube in the refrigerator for 2 weeks before use, and some moisture got into the bubbler lines. The stoichiometric ratios, r, indicated that in the calorimetric combustion experiments, the following amounts of water vapor were carried into the reaction vessel with the hydrocarbon: 9.20, 12.61, 7.81, 3.55, and 0.48 mg in the experiments 1 to 5, respectively. The values of the water vaporization corrections, q_v, were decreased in absolute magnitude by the appropriate amounts, so that, in effect, this water entered and left the calorimeter in the vapor state.

In the course of these experiments, it was discovered that there was an error in the gas correction, q_g. Several experiments were run when the room air conditioner was not operating and the room temperature was about 30° C instead of near 25° C. In these experiments it was discovered from the erratic result that q_g overcorrected for the gas energies introduced into the calorimeter. It was presumed that this was due to the fact that the inlet gas temperatures were taken as that of the room, whereas in reality, the inlet tubes pass through a region in which they are affected somewhat by the jacket temperature. By running calorimetric experiments in which only the gases were passed into the calorimeter with different room temperatures, it was found that the proper q_g was obtained when the difference between the room temperature and the calorimeter temperature was multiplied by the factor 0.44. This correction was applied to all of the experiments reported here and was an appreciable correction, even though in only one of the experiments was the air conditioner not operating. In this experiment (No. 5 on 1,*cis*-3-pentadiene), the correction was 0.09 percent. The usual magnitude of this correction was about 0.01 percent or less. This indicates that it might be desirable to equilibrate the inlet gases in a coil in the jacket of the calorimeter before leading them into the reaction vessel in the calorimeter.

In the electrical calibration experiments the usual corrections [2] were made for the potentiometer ratio, the loss in the heater leads between the calorimeter and jacket, and the difference in power during the temporary settings of the automatic switch during the first and last (approximately) 3 sec of the heating period. This latter correction, amounting to only about 3 ppm, was made more accurately by actually determining the change in current and voltage from the temporary to the permanent settings in separate experiments, rather than calculating it from the different resistances of the paths. This correction could be made completely negligible by making the resistances of the paths through the switch low and equal.

4. Results

The results of the electrical calibration experiments are given in table 1. The ground glass joint on the reaction vessel cracked after the experiments on 1,*cis*-3-pentadiene. Because of necessary repairs, two calorimeter systems were used. System I was used in the experiments on 2-methyl-1,3-butadiene, 1,4-pentadiene, spiropentane, 2,3-pentadiene, and 1,*cis*-3-pentadiene, and system II on 1,*trans*-3-pentadiene and 1,2-pentadiene. The difference in energy equivalent of the systems agreed satisfactorily with that calculated from the change in mass of the calorimeter parts. System I differed from that last used on the C_4 hydrocarbons [2] in that it contained an entirely new calorimeter can; hence, the difference in energy equivalent could not be calculated.

TABLE 1. *Electrical calibration experiments*

Experiment	ΔR_c	Electric energy, E	E_s	Mean value of E_s with its standard deviation
		Calorimeter system I		
	Ohms	*j*	*j/ohm*	*j/ohm*
1	0.393128	58890.1	149798.8	149792.2 ±2.5
2	.405814	60785.7	149787.1	
3	.400331	59967.5	149794.8	
4	.370683	55522.9	149785.4	
5	.395052	59176.7	149794.7	
		Calorimeter system II		
1	0.395990	58937.7	148836.3	148839.3 ±4.9
2	.397879	59211.4	148817.6	
3	.396393	58999.4	148840.7	
4	.394910	58782.8	148851.1	
5	.412187	61350.5	148841.4	
6	.393411	58558.8	148848.9	

In table 1 are listed: the experiment number; ΔR_c, the temperature rise of the calorimeter system corrected for heat transfer to the surroundings and for heat of stirring, expressed as an increase in resistance of the given platinum resistance thermometer on the given resistance bridge; the electric energy, E, added to the calorimeter system; and $E_s = E/\Delta R_c$, the energy equivalent of the system expressed in absolute joules per ohm. The temperature rise was approximately 4 deg C, the initial temperature 23° C, and the final temperature 27° C. The jacket temperature was maintained constant at approximately 27.01° C.

As a further check on the energy equivalent and the stability of the system, another set of electrical calibration experiments on system II was made a year later. A series of six electrical calibration experiments yielded the mean value 148837.4 ±7.5, which is in excellent agreement with the value in the table, 148839.3 ±4.9.

The results of the calorimetric combustion experiments are given in table 2, in which are included: the experiment number; the mass of carbon dioxide collected, upon which the amount of reaction was based; ΔR_c in ohms; q_g, the gas correction; q_v, the correction for vaporization of water from the calorimeter, which in the case of 1,*trans*-3-pentadiene includes a reduction in this correction for the water vapor carried into the calorimeter with the hydrocarbon; q_i, the ignition-energy correction; and $-\Delta H$, the heat of combustion at 25° C expressed in absolute joules per gram of carbon dioxide formed where

$$-\Delta H=[E_s\Delta R_c-q_g-q_v-q_i]/(\mathrm{gCO_2}).$$

As in the electric-energy experiments, the total energy involved was usually about 59,000 j, the temperature rise about 4 deg C, the initial temperature 23° C, the final temperature usually 27° C, and the jacket maintained constant at about 27.01° C.

The ignition energy was determined in separate short-time experiments [2]. The mean ignition energies as determined by such experiments were: 2-methyl-1,3-butadiene, 54.8; 1,4-pentadiene, 45.7; spiropentane, 46.4; 2,3-pentadiene, 49.6; 1,*cis*-3-pentadiene, 44.1; 1,*trans*-3-pentadiene, 58.3; 1,2-pentadiene, 47.9 j, all computed to 20 sec of sparking. In separate experiments in which only sparking occurred, the energy was found to be 49.85 j for 20 sec of sparking. The values of q_i given in table 2 were computed from the ignition energies given above on the basis of 20 sec of sparking; 49.85/20 j were added for each second of sparking beyond 20 sec, because the sparking was continued for longer periods in many cases to be sure the reaction had started. The values of the ignition energies given above are all close to the sparking energy, 49.85 j for 20 sec of sparking, indicating that the departures of the flame from steady conditions during ignition and extinction and the "blank" corrections to the absorption tubes were small.

TABLE 2. *Calorimetric combustion experiments*

Compound	Experiment [d]	Mass CO_2	ΔR_c	q_g	q_v	q_i	$-\Delta H$ at 25° C	Mean value of $-\Delta H$ with its standard deviation
		g	*Ohm*	*j*	*j*	*j*	*j/(gCO₂)*	*j/(gCO₂)*
2-Methyl-1, 3-butadiene [a] (isoprene)	1[d]	1.86586	0.178616	+10.0	−432.4	154.5	14483.0	14481.1 ±1.9
	2[d]	4.12649	.396816	−11.2	−363.4	54.8	14482.0	
	3[d]	4.11258	.395225	−12.0	−389.6	54.8	14479.6	
	4[d]	2.46925	.234347	+10.2	−774.1	104.7	14483.2	
	5	3.86149	.370867	−4.4	−433.3	104.7	14472.7	
	6	3.14389	.303870	+4.3	−482.7	453.6	14485.9	
1,4-Pentadiene [a]	1	3.22788	0.313945	+2.9	−297.0	108.0	14626.5	14620.3 ±2.6
	2	4.06198	.394023	−11.3	−427.9	95.6	14614.8	
	3	3.98273	.385675	−14.7	−496.8	70.6	14616.1	
	4	4.00762	.388295	−16.3	−596.3	195.3	14617.4	
	5[d]	2.07938	.201465	+7.2	−426.9	182.8	14626.9	
Spiropentane [a]	1	3.95927	0.392446	−11.5	−576.9	58.9	14981.2	14978.4 ±1.2
	2	3.94549	.391151	−15.2	−541.1	58.9	14976.3	
	3[d]	3.96727	.393204	−15.1	−574.0	58.9	14979.8	
	4[d]	3.90147	.386683	−16.5	−550.0	58.9	14976.3	
2,3-Pentadiene [a]	1	3.98516	0.387589	−10.7	−748.3	62.1	14743.4	14741.6 ±1.0
	2	3.99631	.388957	−13.4	−700.8	62.1	14742.3	
	3	3.82431	.372353	−16.7	−655.0	62.1	14743.9	
	4[d]	3.98980	.388529	−19.3	−699.3	59.6	(14752.0)	
	5	3.95789	.385356	−9.3	−698.4	62.1	14739.9	
	6	2.82274	.274297	−2.9	−574.5	62.1	14738.5	
1,*cis*-3-Pentadiene [a]	1	4.10073	0.393807	−11.2	−584.0	56.6	14516.4	14513.1 ±1.7
	2	4.09427	.393134	+9.0	−578.6	56.6	14508.4	
	3	3.93324	.377592	+3.4	−596.0	56.6	14516.4	
	4[d]	4.06982	.390855	+3.7	−584.0	56.6	14514.3	
	5[d]	4.10997	.394952	+33.1	−564.5	56.6	14510.0	
1,*trans*-3-Pentadiene [b]	1	4.09662	0.395830	−8.4	[c] −475.4	70.8	14482.2	14481.6 ±0.9
	2	4.11379	.397232	−12.7	[c] −501.4	70.8	14479.8	
	3	4.07907	.393948	−12.4	[c] −499.6	70.8	14482.7	
	4[d]	4.06799	.393365	−8.1	[c] −525.0	70.8	(14506.1)	
	5[d]	2.96571	.286520	+6.4	[c] −422.2	70.8	(14495.8)	
1,2-Pentadiene [b]	1	3.99848	0.393699	+1.2	−533.4	60.4	14773.0	14776.2 ±0.8
	2	3.98300	.392098	−3.3	−560.3	60.4	14776.3	
	3[d]	3.96142	.389955	−2.9	−557.2	60.4	14777.6	
	4[d]	3.98687	.392396	−3.2	−567.7	60.4	14777.1	
	5[d]	3.97958	.391668	−2.2	−569.7	60.4	14777.2	

[a] E_s=149792.2 j/ohm.
[b] E_s=148839.3 j/ohm.
[c] Corrected for the effect of 9.20, 12.61, 7.81, 3.55, and 0.48 mg of water vapor carried into the calorimeter with the hydrocarbon in the five experiments.
[d] Experiments marked d were run with magnesium perchlorate in the hydrocarbon vapor line. These experiments were included in obtaining the mean for all compounds except 2,3-pentadiene and 1,*trans*-3-pentadiene (see text).

TABLE 3. *Heats of combustion*

Compound (gas)	$-\Delta H$ at 25° C		
	j/(gCO_2)	*kj/m*	*kcal/m*
1,2-Pentadiene	14776.2 ±2.8	3251.50 ±0.62	777.13 ±0.15
1,*cis*-3-Pentadiene	14513.1 ±3.9	3193.61 ±0.86	763.29 ±0.21
1,*trans*-3-Pentadiene	14481.6 ±2.9	3186.68 ±0.64	761.63 ±0.15
1,4-Pentadiene	14620.3 ±5.7	3217.20 ±1.25	768.93 ±0.30
2,3-Pentadiene	14741.6 ±2.9	3243.89 ±0.65	775.31 ±0.16
2-Methyl-1,3-butadiene (isoprene)	14481.1 ±4.3	3186.57 ±0.96	761.61 ±0.23
Spiropentane	14978.4 ±3.3	3296.00 ±0.73	787.76 ±0.17

In table 3 are listed for the seven compounds the values of the heat of combustion, $-\Delta H$, at 25° C, expressed in joules per gram of carbon dioxide, kilojoules per mole of hydrocarbon (1 mole of hydrocarbon is considered equivalent to 5 moles of carbon dioxide), and kilocalories per mole of hydrocarbon. These values refer to the heat of combustion in the standard calorimetric process. In these experiments, in which approximately three times as much oxygen was used as was needed, the process may be defined by the equation

$$C_5H_8 \text{ (gas, 1 atm, 25° C)} + 21\ O_2 \text{ (gas, 1 atm, 25° C)} =$$

$$[5CO_2 + 14\ O_2] \text{ (gas, 1 atm, 25° C)} + 4H_2O \text{(lig, 1 atm, 25° C)}.$$

The estimated over-all uncertainties assigned to the values given in table 3 were arrived at by the combination of twice the standard deviations of the means of the calorimetric combustion experiments and the electrical calibration experiments, together with an estimated 0.01 percent for uncertainty in electrical measurements and 0.01 percent for uncertainty in the determination of the absolute amount of reaction.

In table 4 are given the values of the heats of combustion, formation, and hydrogenation of these compounds. The standard heat of combustion, $-\Delta Hc°$, was derived [2] from $-\Delta H$ by taking into account the change in heat content for each gas from its given pressure to zero pressure, so that each substance will have the heat content of the thermodynamic standard state. These heats of combustion refer to the reaction:

$$C_5H_8(\text{gas}) + 7\ O_2(\text{gas}) = 5CO_2(\text{gas}) + 4H_2O(\text{liq}).$$

The heats of formation were calculated from the heats of combustion, utilizing the values 68.317 ± 0.010 kcal/mole [10] and 94.052 ±0.011 kcal/mole [11] for the heats of formation of liquid water and gaseous carbon dioxide, respectively.

The heats of hydrogenation are the heats of hydrogenation to the parent saturated hydrocarbon, *n*-pentane or 2-methylbutane. They were derived by utilizing the values previously reported for the heats of formation of gaseous *n*-pentane and 2-methylbutane, −35.00 ±0.16 and −36.92 ±0.20 kcal/m, respectively [12].

In table 5 are given the heats of isomerization of the various isomers to form 2-methyl-1,3-butadiene (isoprene).

TABLE 4. *Heats of combustion, formation, and hydrogenation in the gaseous state at 25° C*

Compound (gas)	$\Delta Hc°$	$\Delta Hf°$	$\Delta H°$ hydrogenation
	kcal/mole	*kcal/mole*	*kcal/mole*
1,2-Pentadiene	−777.14 ±0.15	+33.61 ±0.16	−68.61 ±0.21
1,*cis*-3-Pentadiene	−763.30 ±0.21	+19.77 ±0.22	−54.77 ±0.25
1,*trans*-3-Pentadiene	−761.64 ±0.15	+18.11 ±0.16	−53.11 ±0.21
1,4-Pentadiene	−768.94 ±0.30	+25.41 ±0.31	−60.41 ±0.33
2,3-Pentadiene	−775.32 ±0.16	+31.79 ±0.17	−66.79 ±0.21
2-Methyl-1, 3 butadiene (isoprene)	−761.62 ±0.23	+18.09 ±0.24	−55.01 ±0.29
Spiropentane	−787.77 ±0.17	+44.23 ±0.18	

TABLE 5. *Heats of isomerization to 2-methyl-1,3-butadiene (isoprene)*

Compound (gas)	$\Delta H°$ isomerization to isoprene (gas) at 25° C
	kcal/mole
2-Methyl-1,3-butadiene (isoprene)	0
1,2-Pentadiene	−15.52 ±0.23
1,*cis*-3-Pentadiene	−1.68 ±0.27
1,*trans*-3-Pentadiene	−0.02 ±0.22
1,4-Pentadiene	−7.32 ±0.34
2,3-Pentadiene	−13.70 ±0.23
Spiropentane	−26.14 ±0.24

5. Comparison with Previous Investigations

Lebedev, Chochlovkin, and Kalacheva [13] determined the heat of combustion of isoprene with an uncertainty of about 1 percent. Their value agrees with the value from the present investigation within this uncertainty.

Jessup [14] determined the heat of combustion of liquid isoprene in a bomb calorimeter. Correction of his value for the new value for the standard heat of combustion of NBS Standard Benzoic Acid, with which he calibrated his calorimeter {Q_B (25° C) = 26433.8 abs j/g [15,16,17]}, together with the use of slightly better values for ΔC_p and $p\Delta V$ for the reaction, yields $-\Delta Hc°$ (25° C) = 754.9 ± 0.4 kcal/mole for liquid isoprene. Taking the heat of vaporization of isoprene as 6.3 kcal/mole [23] yields $-\Delta Hc°$ (25° C (= 761.2 ± 0.4 kcal/mole for gaseous isoprene. This is in good agreement with the value 761.62 ± 0.23 kcal/mole from the present investigation.

Kistiakowsky et al. [18,19] determined the heats of hydrogenation of 1,4-pentadiene and of a mixture of 1,*cis*-3-pentadiene and 1,*trans*-3-pentadiene. These data were corrected to a molecular weight of carbon dioxide of 44.010 and from the experimental temperature of 355° K down to 298.16° K [20]. For 1,4-pentadiene, they obtained $\Delta Hh°$ (25° C) = −60.21 ±0.18 kcal/mole, which is in good agreement with the present value of −60.41 ±0.33 kcal/mole. For the mixture of 1,*cis*-3-pentadiene and 1,*trans*-3-pentadiene, they obtained $\Delta Hh°$ (25° C) = −53.63 ±0.18 kcal/mole, which lies between the present values of −54.77 ±0.25 kcal/mole and −53.11 ±0.21 kcal/mole for 1,*cis*-3-pentadiene and 1,*trans*-3-pentadiene, respectively.

Humphrey and Spitzer [21] determined the heat of combustion of liquid spiropentane in a bomb calorimeter. Their value corrected for the new value of the standard heat of combustion of benzoic acid

[15,16,17], with which they calibrated their calorimeter, is −778.8 kcal/mole. Taking the heat of vaporization as 6.6 kcal/mole [8], their value for the heat of combustion of spiropentane gas, at 25° C, becomes −785.4 kcal/mole. This value is not in agreement with the present value of −787.77 ±0.17 kcal/mole. However, they indicated that the uncertainty in their value was large and that the value should be considered as preliminary.

6. References

[1] E. J. Prosen, F. W. Maron, and F. D. Rossini, J. Research NBS **42,** 269 (1949) RP1968.
[2] E. J. Prosen, F. W. Maron, and F. D. Rossini, J. Research NBS **46,** 106 (1951) RP2181.
[3] F. W. Maron and E. J. Prosen, unpublished data on the heat of combustion of 4-vinyl-1-cyclohexene and the heat of dimerization of 1,3-butadiene.
[4] E. J. Prosen, W. H. Johnson, and F. D. Rossini, J. Am. Chem. Soc. **69,** 2068 (1947); **72,** 626 (1950).
[5] W. H. Johnson, E. J. Prosen, and F. D. Rossini, J. Research NBS **42,** 251 (1949) RP1966.
[6] E. Wichers, J. Am. Chem. Soc. **74,** 2447 (1952).
[7] A. J. Streiff, L. F. Soule, C. M. Kennedy, M. E. Janes, V. A. Sedlak, C. B. Willingham, and F. D. Rossini, J. Research NBS **45,** 173 (1950) RP2122.
[8] D. W. Scott, H. L. Finke, W. N. Hubbard, J. P. McCullough, M. E. Gross, K. D. Williamson, G. Waddington, and H. M. Huffman, J. Am. Chem. Soc. **72,** 4664 (1950).
[9] M. Shepherd, Anal. Chem. **19,** 77 (1947).
[10] D. D. Wagman, J. E. Kilpatrick, W. J. Taylor, K. S. Pitzer, and F. D. Rossini, J. Research NBS **34,** 143 (1945) RP1634.
[11] E. J. Prosen, R. S. Jessup, and F. D. Rossini, J. Research NBS **33,** 447 (1944) RP1620.
[12] E. J. Prosen and F. D. Rossini, J. Research NBS **34,** 263 (1945) RP1642.
[13] S. B. Lebedev, M. A. Chochlovkin, and A. V. Kalacheva, J. Appl. Chem. (USSR) **9,** 1605 (1936).
[14] R. S. Jessup, J. Research NBS **20,** 589 (1938) RP1093.
[15] R. S. Jessup, J. Research NBS **29,** 247 (1942) RP1499.
[16] R. S. Jessup, J. Research NBS **36,** 421 (1946) RP1711.
[17] Announcement of changes in electrical and photometric units, NBS Circular 459 (U. S. Government Printing Office, Washington 25, D. C., 1948) price 5c.
[18] G. B. Kistiakowsky, J. R. Ruhoff, H. A. Smith, and W. E. Vaughan, J. Am. Chem. Soc. **58,** 146 (1936).
[19] M. A. Dolliver, T. L. Gresham, G. B. Kistiakowsky, and W. E. Vaughan, J. Am. Chem. Soc. **59,** 831 (1937).
[20] J. E. Kilpatrick, C. W. Beckett, E. J. Prosen, K. S. Pitzer, and F. D. Rossini, J. Research NBS **42,** 225 (1949) RP1964.
[21] G. L. Humphrey and R. Spitzer, J. Chem. Phys. **18,** 902 (1950).
[22] E. Wichers, J. Am. Chem. Soc. **76,** 2033 (1954).
[23] N. Bekkedahl, L. A. Wood, and M. Wojciechowski, J. Research NBS **17,** 883 (1936) RP951.

WASHINGTON, December 7, 1954.

Journal of Research of the National Bureau of Standards Vol. 54, No. 3, March 1955 Research Paper 2576

Solid-State Reactions and Dielectric Properties in the System Magnesia-Lime-Tin Oxide-Titania[1]

L. W. Coughanour, R. S. Roth, S. Marzullo, and F. E. Sennett

A study has been made of solid-state reactions in the quaternary system MgO-CaO-SnO_2-TiO_2 and in its subordinate binary and ternary systems. Compatibility relations have been determined for each. Extensive solid-solution formation has been noted in the SnO_2-TiO_2, MgO-SnO_2-TiO_2, CaO-SnO_2-TiO_2, and MgO-CaO-SnO_2-TiO_2 systems. Little or no solid solution was observed in the other systems involved. One ternary compound, having the probable formula $2MgO{\cdot}SnO_2{\cdot}TiO_2$, has been observed. No quaternary compounds were detected.

A survey has been conducted of the effect of composition and temperature variations on the dielectric properties of specimens in some of these systems. Data are given for the values of K and Q at 50 kilocycles per second, and at 1 and 20 megacycles per second. The changes in these values with changes in temperature have been studied at 1 megacycle per second.

Indexed X-ray powder patterns are listed for the compounds $CaO{\cdot}TiO_2$, $CaO{\cdot}SnO_2$, and $2MgO{\cdot}SnO_2{\cdot}TiO_2$. An unindexed pattern is given for the compound $2CaO{\cdot}SnO_2$.

1. Introduction

A partial survey of the MgO-CaO-SnO_2-TiO_2 system has been conducted as a part of a program of fundamental research on ceramic dielectrics. Limited portions of a few of the subsystems involved have been studied by previous investigators. The MgO-TiO_2 system has been reported on by Rieke and Ungewiss [1][2] and by Shelton et al. [2]. The properties of dielectrics in the CaO-TiO_2 system have been reported by Bunting et al. [3]. Dielectrics in the SnO_2-TiO_2 system were studied by Schusterius [4] and by Verwey and Stevels [5]. Wainer [6] received a number of patents for dielectric bodies composed of alkaline-earth titanates and alkaline-earth stannates. Coffeen [7] has discussed the ceramic and dielectric properties of some individual stannates.

In the present work, the emphasis has been on the study of solid-state reactions occurring among the oxide components, and the effects of composition and temperature on dielectric properties, rather than on the development of ceramic dielectrics having specific properties or meeting any given set of specifications.

2. Materials and Methods

2.1. Materials

The following materials were used as sources of the component oxides in this study:

MgO.—Reagent-grade magnesium carbonate of purity represented as 99.5 percent was the usual source material. However, in the fabrication of a few of the dielectric test specimens, a sample of periclase of 96.4-percent purity was used.

CaO.—Reagent-grade calcium carbonate of purity represented as 99.5 percent.

TiO_2.—Spectrographic-grade titania of nominal purity over 99.9 percent was used in all specimens for the solid-state studies. In the preparation of some of the dielectric test specimens, a less highly purified grade of titania, designated TMO, was used. This grade of titania has a purity of about 98.7 percent. A commercial-grade calcium titanate was used in the preparation of a few dielectric test samples. This material has a nominal purity of 96.5 percent, the major impurities being MgO, SiO_2, and Al_2O_3.

SnO_2.—Precipitated tin oxide of purity over 98.5 percent. Hydrated, precipitated magnesium stannate and calcium stannate were used as source materials in some cases. The calcium stannate was used wherever possible in dielectric test specimens. These materials both have a nominal purity over 99.5 percent.

2.2. Sample Preparation

Compositions to be prepared were designated on a mole-ratio basis, and calculations of the weight compositions were made to ± 0.01 percent. No corrections were made for the percentage purity of the raw materials, although it is realized that dielectric properties may be affected by the presence of different kinds and amounts of impurities.

The raw materials in sufficient amounts to yield a 10-g sample were weighed to the nearest milligram and well mixed in the dry state. The samples were then mixed with about 5 percent of a 5-percent starch-solution binder, and 1-in.-diameter disks were formed at a pressure of 5,000 lb/in^2. The pressed disks were calcined for 4 hours at 1,000° to 1,200° C on platinum foil in an oxidizing atmosphere. The calcined disks were pulverized, using a mullite mortar and pestle, and the samples were ready to be used either for the solid-state studies or for pressing into dielectric specimens. No chemical analyses were made after the firing.

[1] This study was sponsored by the Office of Ordnance Research, Department of the Army.

[2] Figures in brackets indicate the literature references at the end of this paper.

2.3. Study of Solid-State Reactions

In the study of solid-state reactions, a conventional type platinum-wound quench furnace was used. The temperature in the furnace was measured with a Pt-Pt-10-percent-Rh thermocouple and was controlled by a modified Roberts-type controller. The quenching technique was used in order that high-temperature solid solutions could be observed. For quench tests, a small amount of the prepared sample was placed in a platinum envelope, which was then suspended in the furnace. The test temperature ranged from 1,400° to 1,550° C and was maintained constant for a given length of time. After this reaction time, the sample was quenched, usually in air. In some cases, water or carbon tetrachloride was used as the quenching medium.

Alternatively, samples were heated to temperatures as high as 1,750° C and were cooled relatively slowly. The quenched or slowly cooled specimens were then analyzed by X-ray diffraction means and by petrographic methods.

These procedures are, in general, similar to those discussed by Foster [8].

2.4. Preparation of Dielectric Test Specimens

The prepared samples were moistened with about 5 percent of starch-solution binder, and disks about ⅛ in. thick and ½ to 1½ in. in diameter were formed at a pressure of 10,000 to 15,000 lb/in.^{2} The pressed disks were fired for ½ to 1 hour on platinum foil in an oxidizing atmosphere. Maturing temperatures varied from 1,400° to 1,750° C, depending upon the composition and the raw materials used. For maturing temperatures up to 1,550° C, a platinum-wound resistance furnace was used. Temperatures were measured with a Pt-Pt-10-percent-Rh thermocouple and were controlled by an automatic commercial controller-recorder. For maturing temperatures higher than 1,550° C, an oxide-resistor furnace [9] was used. This furnace was manually controlled, and temperatures were measured with a calibrated optical pyrometer.

The fired specimens were then used to determine their absorption value, which is a convenient measure of the degree of maturity. The absorption was determined by placing the weighed disk in chemically pure carbon tetrachloride. The liquid was boiled for 5 hours and allowed to cool. The specimen was removed from the liquid, quickly surface dried, and weighed in a stoppered bottle. From the gain in weight, the equivalent water absorption was calculated. A specimen was considered to be properly matured when its equivalent water absorption was 0.1 percent or less of the dry weight.

Some compositions could not be fired to an impervious condition, and, in these cases, dielectric tests were performed on specimens having an absorption value greater than 0.1 percent.

2.5. Determination of Dielectric Properties

At frequencies between 50 kc/s and 20 Mc/s and at temperatures between 25° and 250° C, the dielectric constant (K) and the Q-value (when greater than 10, the Q-value is very nearly equal to the reciprocal of the power factor) were determined by measurements on a Q-meter. The test specimens were coated on each side with a silver paste and fired to 750° C to form silver electrodes 3 to 5 mils thick. The specimen was then cooled overnight. Preliminary determinations were made at a temperature of 25° ±0.5° C, and at a controlled relative humidity of 40 percent or less.

For measurements at temperatures greater than 25° C, the specimens were placed on an electric hotplate and were connected to the Q-meter by 10-in. leads. The temperature was controlled by means of an adjustable autotransformer and was measured by means of a thermocouple inserted into a silvered ceramic disk adjacent to the specimen. Correction factors for the capacitance and inductance of the lead wires were applied.

For measurements in the temperature range between −50° and 25° C, the specimens were placed in an insulated chamber cooled by dry ice. The temperature was controlled by a thermostat and was measured by means of a liquid-in-glass thermometer. The measurements were made at a frequency of 1 Mc/s and were obtained by using a type 820A twin-T impedance circuit combined with a model HRO–50T radio receiver. Corrections for the capacitance and inductance of the lead wires were applied.

For a given specimen, the reproducibility of measurements of dielectric constant is about ±3 percent, depending upon the dimensions and capacitance of the sample. For different specimens of the same gross composition, additional variations of K-values result from factors such as differences in firing schedules, purity of raw materials, etc.

3. Results of Solid-State Reaction Studies

3.1. Binary Systems

a. MgO-TiO_2

Three binary compounds are known to exist in the MgO-TiO_2 system [10]. They are $2MgO{\cdot}TiO_2$, $MgO{\cdot}TiO_2$, and $MgO{\cdot}2TiO_2$. There is no solid-solution development in this system.

b. CaO-TiO_2

There are two binary compounds in this system [11]. They are $CaO{\cdot}TiO_2$ and $3CaO{\cdot}2TiO_2$. The X-ray pattern for $3CaO{\cdot}2TiO_2$ has been given in a previous publication [11].The indexed powder pattern for $CaO{\cdot}TiO_2$ is listed in table 1. This compound is an orthorhombic perovskite with the following pseudocubic-type parameters, as suggested by Megaw [12].

$$a \simeq \sqrt{2} \times \text{basic pseudocell} = 5.381 \text{ A},$$
$$b \simeq 2 \times \text{basic pseudocell} = 7.645 \text{ A},$$
$$c \simeq \sqrt{2} \times \text{basic pseudocell} = 5.443 \text{ A}.$$

TABLE 1. *X-ray diffraction pattern for the compound* $CaO \cdot TiO_2$

hkl	$1/d^2$ obs.	$1/d^2$ calc.	R. I.[a]	*hkl*	$1/d^2$ obs.	$1/d^2$ calc.	R. I.[a]
101	0.068	0.068	30	333	.7681	.7686	7
111	.085	.085	7	162	.7840	.7855	2
002	.135	.135	51	044	.8134	.8138	18
121	.137	.137	100+	440	.8260	.8263	14
200	.138	.138	70	070	.8352	.8384	5
012	.152	.152	4	144	.8480	.8483	4
102	.169	.170	4	170	.8726	.8729	3
201	.172	.172	6	105	.8776	.8784	5
112	.186	.187	5	115	.8949	.8955	7
211	.189	.189	17	171	.9065	.9067	3
022	.203	.203	12	125	.9464	.9468	12
220	.206	.207	11	244	.9518	.9520	21
131	.222	.222	6	163	.9542	.9543	21
122	.238	.238	5	361	.9606	.9605	38
221	.240	.240	4	521	.9654	.9655	40
202	.273	.273	80	135	1.0321	1.0324	7
040	.274	.274	78	404	1.0925	1.0926	8
032	.289	.289	6	254	1.0855	1.0859	6
212	.290	.290	7	414	1.1092	1.1097	3
132	.323	.324	2	145	1.1520	1.1521	5
231	.325	.326	2	305	1.1540	1.1547	5
103	.338	.338	5	541	1.1705	1.1709	4
222	.341	.342	7	006	1.2146	1.2151	4
141	.342	.342	5	325	1.2229	1.2231	16
113	.355	.355	9	363 / 016	1.2310	(1.2306) / (1.2322)	29
311	.361	.362	4				
123	.407	.407	29	523	1.2357	1.2356	28
042	.409	.409	32	372	1.2840	1.2842	4
240	.412	.412	34	155	1.3059	1.3061	6
321	.413	.413	39	335	1.3084	1.3086	5
				206	1.3530	1.3533	6
241	.445	.446	3				
150	.462	.462	4	282 / 036	1.3668	1.3681	16
133	.492	.492	8				
004	.540	.540	6	216	1.3695	1.3691	22
242	.547	.547	29	090	1.3852	1.3859	4
				226	1.4218	1.4217	5
400	.552	.553	7	345	1.4284	1.4284	5
104	.574	.575	3				
401	.586	.586	4	191	1.4542	1.4542	4
152	.597	.597	7	046	1.4896	1.4889	4
332	.600	.600	6	165	1.4949	1.4943	9
				561	1.5143	1.5131	13
143	.611	.612	6	640	1.5179	1.5171	12
313	.631	.632	5				
204	.678	.678	7	355	1.5836	1.5824	2
323	.683	.683	12	326	1.5957	1.5944	3
161	.685	.684	15	246	1.6277	1.6270	9
402	.688	.688	10				
214	.6942	.6953	6				
252	.7002	.7009	5				
431	.7396	.7403	4				
153	.7660	.7661	7				

[a] R. I. is the intensity of diffraction peaks relative to the strongest peak.

c. MgO-CaO

This system has been shown to contain a simple eutectic, with no compounds or solid solutions [13].

d. $MgO-SnO_2$

Only a brief study of this system was made, in order to verify previously published data [14].

The $MgO-SnO_2$ compositions studied are listed in table 2, together with the results obtained. X-ray and petrographic examination of these fired specimens indicated the existence of two binary compounds. They are $2MgO \cdot SnO_2$, which is thermally stable at temperatures as high as 1,550° C, and $MgO \cdot SnO_2$, which decomposes into $2MgO \cdot SnO_2$ and SnO_2 between 800° and 1,000° C. The compound $2MgO \cdot SnO_2$ has a cubic spinel-type structure with $a=8.645$ A and with an index of refraction equal to approximately 1.82. These results are in agreement with the work of Tanaka [14], but are somewhat at variance with the results of Coffeen [7], who reported the compound $MgO \cdot SnO_2$ to be thermally stable.

TABLE 2. *Results of X-ray examination of specimens in the* $MgO-SnO_2$ *system*

Mole ratio		Composition by weight		Heat treatment[a]		Phases identified
MgO	SnO_2	MgO	SnO_2	Time	Temperature	
		%	%	*hr*	°C	
4	1	51.70	48.30	6	1,550	$MgO+2MgO \cdot SnO_2$.
2	1	34.86	65.14	19	1,550	$2MgO \cdot SnO_2$.
1	1	21.11	78.89	66	800	$MgO \cdot SnO_2$+trace SnO_2+trace $2MgO \cdot SnO_2$.
1	1	21.11	78.89	48	1,000	$2MgO \cdot SnO_2+SnO_2$.
1	1	21.11	78.89	1	1,550	$2MgO \cdot SnO_2+SnO_2$.
1	2	11.80	88.20	18	1,550	$2MgO \cdot SnO_2+SnO_2$.

[a] Each sample had been previously calcined for 4 hours at 1,100° C. The specimens were quenched in air from the temperature indicated.

e. $CaO-SnO_2$

Two compounds were noted in this system. They are $CaO \cdot SnO_2$, which has an orthorhombic perovskite structure, and $2CaO \cdot SnO_2$. These results agree with the findings of Tanaka [15]. An indexed powder pattern for the compound $CaO \cdot SnO_2$ is given in table 3. The parameters of $CaO \cdot SnO_2$ are:

$$a \cong \sqrt{2} \times \text{basic pseudocell} = 5.518 \text{ A},$$
$$b \cong 2 \times \text{basic pseudocell} = 7.884 \text{ A},$$
$$c \cong \sqrt{2} \times \text{basic pseudocell} = 5.664 \text{ A}.$$

TABLE 3. *X-ray diffraction pattern for the compound* $CaO \cdot SnO_2$

hkl	$1/d^2$ obs.	$1/d^2$ calc.	R. I.[a]	*hkl*	$1/d^2$ obs.	$1/d^2$ calc.	R. I.[a]
101	0.064	0.064	100+	153	.....	.7156	.....
111	.080	.080	7	044	.7561	.7562	6
002	.125	.125	63	440	.7829	.7830	5
121	.129	.128	100++	105	.8125	.8121	3
200	.131	.131	56				
				343	.8343	.8336	6
201	.163	.163	4	262	.....	.8352	7
211	.178	.179	7	125	.8774	.8765	4
022	.189	.189	8	244	.8878	.8875	7
220	.196	.196	8	163	.8925	.8926	9
131	.209	.209	4				
				361	.9065	.9060	9
122	.222	.222	2	442	.9079	.9077	12
202	.256	.256	61	521	.9168	.9167	8
040	.257	.257	66	404	1.0248	1.0243	3
212	.272	.272	4	080	1.0296	1.0296	4
103	.313	.313	17				
				145	1.0701	1.0695	4
141/222	.321	.321	37	305	1.0752	1.0749	5
301	.327	.327	9	424	1.0894	1.0887	4
123	.378	.378	37	181	1.0941	1.0937	5
042	.382	.382	26	325	1.1397	1.1393	5
240	.389	.389	25				
				363	1.1553	1.1553	8
321	.391	.391	46	280	1.1612	1.1610	9
133	.459	.458	2	523	1.1666	1.1661	8
004	.499	.499	7	182	1.1870	1.1872	6
242	.514	.513	22	264	1.2105	1.2090	5
400	.526	.526	6				
				155	1.2159	1.2143	5
024	.563	.563	6	444	1.2825	1.2817	5
143	.571	.571	10	282	1.2864	1.2857	5
060	.579	.579	4	226	1.3184	1.3179	4
341	.584	.584	5	345	1.3325	1.3323	3
420	.590	.590	4				
				143	1.3436	1.3430	3
204	.630	.630	5	471	.....	1.3450	.....
323	.641	.641	11	165	1.3919	1.3913	4
161	.643	.643	16	561	1.4325	1.4315	8
402	.650	.650	6	316	.....	1.4339	.....
224	.695	.694	6				
				246	1.5119	1.5110	3
422	.7151	.7146	6	642	1.5649	1.5646	5

[a] R.I. is the intensity of diffraction peaks relative to the strongest peak.

The structure of the 2:1 compound has not been determined. Its X-ray diffraction pattern is listed in table 4.

The compositions studied in the CaO-SnO_2 system and the results obtained are given in table 5.

TABLE 4. *X-ray diffraction pattern of the compound* $2CaO \cdot SnO_2$

2θ	d	R. I.[a]	2θ	d	R. I.[a]
17.93	4.9	100	87.09	1.118	1
18.29	4.8	18	88.18	1.107	.5
24.00	3.70	5	89.96	1.089	.5
27.31	3.26	2	90.50	1.085	1
31.08	2.88	25	91.06	1.079	2
			92.36	1.068	5
31.74	2.82	77			
32.87	2.72	80	92.80	1.064	7
33.04	2.71	32	92.91	1.063	6
36.29	2.47	7	93.19	1.060	6
37.04	2.42	10	93.48	1.058	6
			93.90	1.054	5
40.33	2.23	12			
41.81	2.16	10	94.71	1.047	2
42.88	2.11	16	95.61	1.039	3
45.97	1.97	45	96.90	1.029	5
46.62	1.95	11	97.92	1.021	3
			98.94	1.013	1
48.34	1.88	7			
49.09	1.85	10	99.67	1.008	1
49.36	1.84	2	101.18	0.9969	4
49.54	1.84	3	101.56	.9942	3
50.83	1.79	2	102.13	.9902	3
			102.66	.9865	3
51.17	1.78	7			
55.67	1.65	10	105.09	.9703	0.5
56.28	1.63	14	107.56	.9543	.5
56.39	1.63	21	108.74	.9477	1
56.89	1.62	7	109.59	.9427	2
			109.90	.9409	4
57.06	1.61	15	110.06	.9399	4
57.47	1.60	22	110.57	.9371	8
58.94	1.57	3	111.82	.9301	2
59.56	1.55	7	112.32	.9273	3
61.59	1.50	2	112.64	.9256	4
63.08	1.47	9	113.66	.9202	5
64.20	1.45	3	115.87	.9089	2
64.77	1.44	3	116.99	.9034	3
65.54	1.42	3	118.14	.8979	1
65.68	1.42	6	119.43	.8919	3
66.05	1.41	14	120.09	.8890	3
66.23	1.41	13	120.92	.8853	2
67.88	1.38	8	122.75	.8775	0.5
68.74	1.36	4	125.00	.8684	.5
69.23	1.36	4	127.09	.8603	2
69.70	1.35	4	128.65	.8546	4
71.01	1.33	3	129.59	.8513	2
71.11	1.32	3	130.95	.8466	4
72.33	1.31	2	132.24	.8424	5
73.00	1.29	2	134.82	.8343	2
74.36	1.27	4	138.10	.8248	0.5
75.43	1.26	5	140.26	.8190	2
76.36	1.25	3	141.10	.8169	3
76.98	1.24	3	142.02	.8146	5
77.24	1.23	4	143.86	.8102	2
77.83	1.23	3	145.11	.8074	3
78.10	1.22	3	148.10	.8011	3
79.47	1.21	2	148.82	.7997	4
82.64	1.167	2	151.69	.7944	2
83.10	1.161	5	155.42	.7883	1
83.44	1.157	5	157.37	.7855	1
84.13	1.149	4	158.23	.7844	3
84.74	1.143	4	160.07	.7821	2
85.25	1.137	4	162.00	.7799	3
86.53	1.124	3	163.58	.7782	4

[a] R. I. is the intensity of diffraction peaks relative to the strongest peak.

TABLE 5. *Results of X-ray examination of specimens in the* CaO-SnO_2 *system*

Mole ratio		Composition by weight		Heat treatment [a]		Phases identified
CaO	SnO_2	CaO	SnO_2	Time	Temperature	
		%	%	hr	°C	
4	1	59.82	40.18	18	1,400	$CaO+2CaO \cdot SnO_2$.
5	2	48.19	51.80	40	1,300	$CaO+2CaO \cdot SnO_2$.
2	1	42.67	57.33	3	1,550	$2CaO \cdot SnO_2$+small amount $CaO \cdot SnO_2$.
1	1	27.12	72.88	1	1,550	$CaO \cdot SnO_2$.
1	2	15.69	84.31	17	1,400	$CaO \cdot SnO_2+SnO_2$.
1	4	8.51	91.49	3	1,550	$CaO \cdot SnO_2+SnO_2$.

[a] Each sample had been previously calcined for 4 hours at 1,200° C. All samples were quenched in air from the temperature indicated.

f. SnO_2–TiO_2

This system was found to consist, at 1,550° C, of a continuous solid-solution series. These solid solutions may be effectively stabilized by quenching in air. Slow cooling, however, results in an unmixing reaction in the compositions in the central portion of the system. The results of the tests are given in table 6. These results are in general agreement with those of Schusterius [4].

TABLE 6. *X-ray data for the* SnO_2-TiO_2 *system* [a]

Mole ratio		Composition by weight		a	c	c/a ratio
SnO_2	TiO_2	SnO_2	TiO_2			
		%	%	A	A	
1	0	100	0	4.738	3.185	0.6772
4	1	88.30	11.70	4.710	3.143	.6673
2	[b]1	79.05	20.96	4.692	3.130	.6672
1	[b]1	65.35	34.65	4.664	3.065	.6572
1	[b]2	48.54	51.47	4.644	3.029	.6522
1	4	32.04	67.96	4.624	3.001	.6491
0	1	0	100	4.592	2.959	.6444

[a] Each sample had been fired to 1,550° C for at least 3 hours before cooling and conducting a petrographic and X-ray examination.

[b] An unmixing reaction occurred on slow cooling of these samples. The unmixing was prevented by quenching in air from the high temperature.

3.2. Ternary Systems

a. MgO-CaO-TiO_2

A total of 42 compositions were prepared in this system for studies of phase relations and of dielectric properties. Of these, 18 selected samples were used in the determination of the compatability relations. These samples were subjected to suitable heat treatment and subsequently analyzed by X-ray or petrographic methods. The results of these tests are given in table 7, and the composition triangles are shown in figure 1. Of the various possible binary joins in the ternary system, the following exist in the subsolidus diagram:[3]

MT_2-CT, MT-CT, M_2T-CT, MgO-CT, and MgO-C_3T_2.

[3] M=MgO, C=CaO, T=TiO_2, S=SnO_2. Thus the formula $3CaO \cdot 2TiO$ is shortened to C_3T_2.

It should be noted that the results (table 8) indicate little or no solid-solution formation in this system, with the probable exception of the areas adjacent to the compound C_3T_2. This compound was found to undergo marked changes in structure with only very small quantities of impurities entering its lattice. These changes are discussed in a later portion of this report.

TABLE 7. *Results of X-ray and petrographic study of selected compositions in the system* MgO-CaO-TiO_2

Mole ratio M:C:T	Binary join or ternary field	Heat treatment		Phases identified
		Time	Temperature	
		hr	*°C*	
4:1:9	MT_2-CT	1	[a]1,550	MT_2+CT.
1:4:6	do	1	1,550	Do.
4:1:5	MT-CT	1	1,550	MT+CT.
1:2:3	do	4	[b]1,475	Do.
1:5:6	do	1	1,550	Do.
6:1:4	M_2T-CT	1	1,550	M_2T+CT.
2:7:8	do	1	1,550	Do.
1:3:3	MgO-CT	1	1,740	MgO+CT.
18:3:2	MgO-C_3T_2	2.5	1,550	[c] MgO+C_3T_2.
1:3:2	do	1	1,645	Do.
2:27:18	do	2	>1,600	[c] C_3T_2+trace CaO.
1:1:5	MT_2-CT-TiO_2	1	[b] 1,450	MT_2+CT+TiO_2.
3:2:6	MT_2-MT-CT	1	[a] 1,550	MT_2+MT+CT.
4:1:4	MT-M_2T-CT	1	[a] 1,590	MT+M_2T+CT.
4:1:2	MgO-M_2T-CT		[a] 1,672	MgO+M_2T+CT.
1:5:4	MgO-CT-C_3T_2	1	1,645	[d] MgO+CT+C_3T_2.
2:2:1	MgO-CaO-C_3T_2	1	1,645	[c] MgO+CaO+C_3T_2.
2:3:1	do	1	1,645	Do.

[a] The sample had fused at the temperature indicated.
[b] The sample was quenched from the temperature indicated.
[c] The results indicate the possibility of a small amount of solid solution in the areas adjacent to the compound C_3T_2.
[d] Interpretation of powder patterns is difficult in this area due to the overlapping of some of the lines of CT and C_3T_2. The results indicate that there may be a small amount of solid solution in the areas adjacent to the compound C_3T_2.

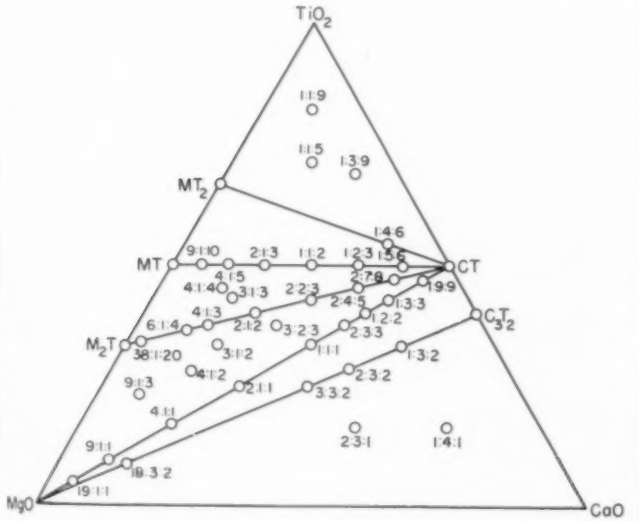

FIGURE 1. *Compatibility relations in the system* MgO-CaO-TiO_2.
The compositions are indicated by numbers and placed graphically according to mole ratios.

b. MgO-CaO-SnO_2

Sixteen compositions in this system have been prepared for study of solid-state reaction and dielectric properties. Nine of these compositions were selected for a preliminary study of compatibility relations in the system. The specimens were quenched from 1,550° C and analyzed by X-ray methods. The results obtained are listed in table 8. Because the results indicated that there is little or no solid-solution development, and that there are no ternary compounds, these nine tests were sufficient to establish the binary joins existing, which are: M_2S-CS, MgO-CS, and MgO-C_2S. The arrangement of compatibility triangles is shown in figure 2.

TABLE 8. *Results of X-ray diffraction studies of specimens in the* MgO-CaO-SnO_2 *system*

Mole ratio M:C:S	Binary join or ternary field	Heat treatment [a]		Phases identified
		Time	Temperature	
		hr	*°C*	
2:1:2	M_2S-CS	3	1,550	M_2S+CS.
1:1:1	MgO-CS	3	1,550	MgO+CS.
2:1:1	do	3	1,550	Do.
2:2:1	MgO-C_2S	3	1,550	MgO+C_2S.
1:1:2	M_2S-CS-SnO_2	3	1,550	M_2S+CS+SnO_2.
1:1:4	do	3	1,550	Do.
3:1:2	MgO-M_2S-CS	3	1,550	MgO+M_2S+CS.
1:3:2	MgO-C_2S-CS	3	1,550	MgO+C_2S+CS.
2:4:1	MgO-CaO-C_2S	3	1,550	MgO+CaO+C_2S.

[a] Each sample had been previously calcined for 4 hours at 1,100° C. Each specimen was quenched in air from the temperature indicated

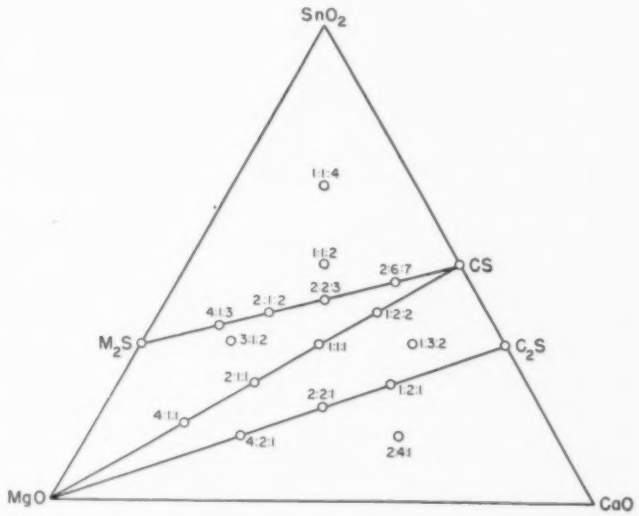

FIGURE 2. *Compatibility relations in the system* MgO-CaO-SnO_2.
The compositions are indicated by numbers and placed graphically according to mole ratios. The compound MgO-SnO_2 is not indicated as it decomposes between 800° and 1,000° C, and the specimens studied here were all heated to 1,550° C.

c. MgO-SnO_2-TiO_2

Twenty compositions in the ternary field were given suitable heat treatment and, after cooling or quenching, were analyzed by X-ray and petrographic methods. From the results of these tests, which are listed in table 9, the arrangement of composition triangles was determined. An estimate of the solid-solution areas in the system was also obtained from these results.

TABLE 9. *Results of X-ray diffraction study of specimens in the* MgO-SnO_2-TiO_2 *system*

Mole ratio M:S:T	Binary join or ternary field	Heat treatment[a]		Phases identified (ss=solid solution)
		Time	Temperature	
		Hr	°C	
2:1:1		3	1,550	M_2ST (single phase).
1:1:2	MT_2-SnO_2	3	1,550	MT_2 ss+SnO_2 ss.
1:4:2	do	3	1,550	Do.
3:1:3[b]	MT_2-M_2ST			Equilibrium conditions could not be obtained.
3:1:2	MT-M_2ST	3	1,550	(MT-M_2ST) ss.
5:1:4	do	3	1,550	(MT-M_2ST)ss+trace M_2S.
3:1:1	MT-M_2S	2.5	1,550	MT ss+M_2S ss.
6:1:4	do	16	1,300	Do.
4:1:2	do	15	1,400	None equilibrium.
4:1:1	M_2T-M_2S	3.5	1,550	(M_2T-M_2S)ss+trace MgO.
4:2:1	M_2S-M_2ST	3	1,550	M_2S ss+M_2ST ss.
2:3:1	M_2ST-SnO_2	3	[b]1,550	M_2ST+SnO_2 ss.
1:1:4	MT_2-SnO_2-TiO_2	15	1,400	MT_2ss+(SnO_2-TiO_2) ss.
6:1:6	MT_2-MT-M_2ST	1	1,550	MT_2ss+(MT-M_2ST) ss.
1:1:1	MT_2-M_2ST-SnO_2	2.5	1,550	MT_2 ss+M_2ST+SnO_2 ss.
2:1:2	do	3	1,550	Do.
3:2:1	M_2S-M_2ST-SnO_2	2.5	1,550	M_2S ss+M_2ST ss+SnO_2.
8:1:4	M_2T-MT-M_2S	2.5	1,550	(M_2S-M_2T) ss+MT ss.
6:2:3	M_2S-MT-M_2ST	3	1,550	M_2S ss+(MT-M_2ST) ss.
6:1:1	MgO-M_2S-M_2T	3	[b]1,550	MgO+(M_2S-M_2T) ss.

[a] Each sample had been previously calcined for 4 hours at 1,100° C.
[b] The specimen was slowly cooled. All others were quenched from the temperature indicated.

The compatibility relations and the location of the compositions studied are shown in figure 3. The estimated solid-solution limits are indicated in figure 4. Extensive solid-solution development is noted throughout the system. However, the solid-solution areas and limits shown are not considered located with a high degree of accuracy. In addition, it is highly probable that the limits would change with differing heat treatments.

There is indicated a ternary compound having the probable formula $2MgO{\cdot}SnO_2{\cdot}TiO_2$ or M_2ST. This compound is of the ilmenite type, is isostructural with the compound $MgO{\cdot}TiO_2$, and forms a continuous series of solid solutions with it. The fact that all compositions on the MT-M_2ST join consist of a single phase and show a regular variation in lattice parameters and indices of refraction makes it quite difficult to establish unambiguously the formula of the ternary compound. The lattice parameters of the ternary composition M_2ST are $a=5.533$ A, $\alpha=55.6°$. An indexed powder pattern for this composition is included as table 10. The optical properties of this composition are: uniaxial negative, $\epsilon=1.85$, $\omega=2.07$.

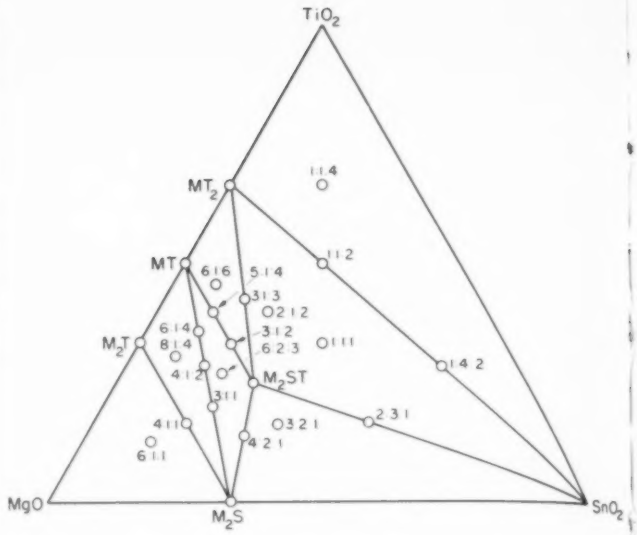

FIGURE 3. *Compatibility relations in the system* MgO-SnO_2-TiO_2.

The compositions are indicated by numbers and placed graphically according to mole ratios. All specimens were heated to 1,300° C or higher. Since the compound $MgO{\cdot}SnO_2$ decomposes at a much lower temperature, it is not indicated on the diagram.

TABLE 10. *X-ray diffraction pattern of the compound* $2MgO{\cdot}SnO_2{\cdot}TiO_2$

hkl	$1/d^2$ obs.	$1/d^2$ calc.	R. I.[a]	*hkl*	$1/d^2$ obs.	$1/d^2$ calc.	R. I.[a]
111	0.046	0.046	90	122	.657	.655	3
010	.055	.055	75	341	.677	.677	4
110	.071	.071	41	442	.7103	.7115	7
121	.132	.132	100+	231	.7329	.7322	4
011	.151	.150	100++	240	.7848	.7845	5
222	.184	.184	8	352	.8605	.8616	8
120	.196	.196	62	251	.9679	.9777	5
111	.206	.205	6	141	1.0338	1.0324	6
220	.282	.282	29	151	1.0519	1.0510	9
232	.300	.300	17	041	1.0983	1.0966	4
231	.334	.334	73	440	1.1283	1.1278	6
021	.356	.355	4	451	1.1609	1.1618	6
121	.376	.371	8	250	1.1991	1.2011	13
124	.432	.432	31	150	1.2358	1.2347	15
121	.451	.450	60	033	1.3497	1.3508	19
030	.497	.496	7	142	1.3994	1.3968	7
242	.526	.527	4	361	1.4631	1.4620	7
343	.559	.561	18	242	1.4851	1.4826	3
022	.600	.600	13	664	1.5132	1.5093	6
141	.636	.634	3				

[a] R. I. is the intensity of diffraction peaks relative to the strongest peak.

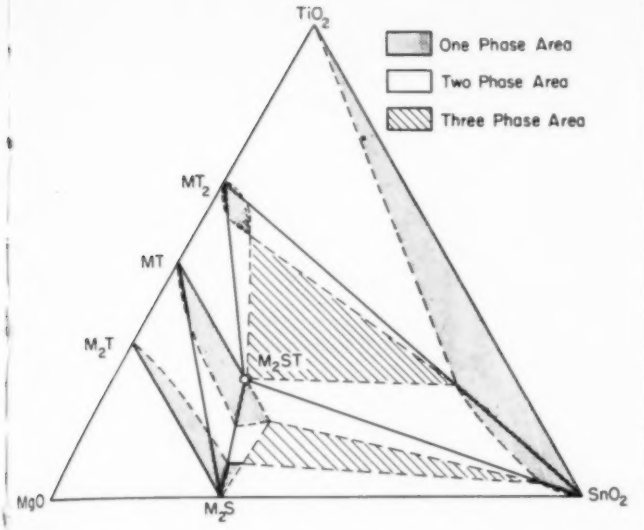

FIGURE 4. *Estimated solid-solution areas in the system* $MgO\text{-}SnO_2\text{-}TiO_2$.

The temperature range involved is between 1,300° and 1,550° C.

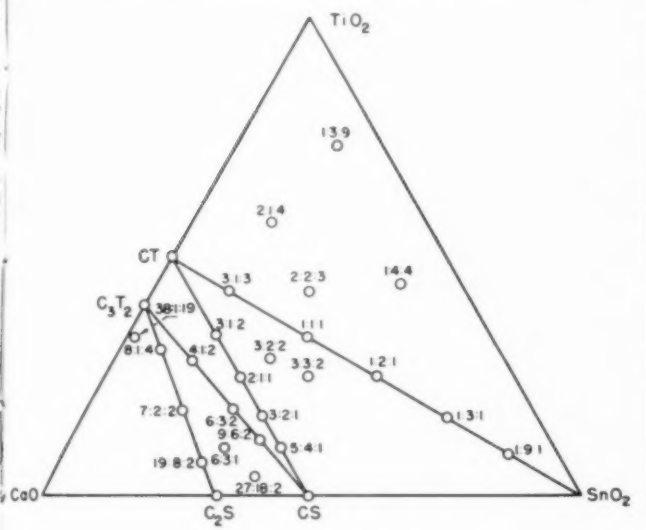

FIGURE 5. *Compatibility relations in the system* $CaO\text{-}SnO_2\text{-}TiO_2$.

The compositions are indicated by numbers and placed graphically according to mole ratios.

d. $CaO\text{-}SnO_2\text{-}TiO_2$

In this system, 22 selected ternary compositions were examined by X-ray methods after having been quenched from a temperature of 1,300° to 1,550° C. Figure 5, showing the compatibility relations, was constructed from data in table 11. The binary joins are CT-SnO_2, CT-CS, C_3T_2-CS, and C_3T_2-C_2S. Solid solutions were noted in all parts of the system. The estimated limits of the solid-solution areas are shown in figure 6.

In this case, as in that of the $MgO\text{-}SnO_2\text{-}TiO_2$ system, it is considered that the solid-solution limits are only approximate and that they would shift with heat treatments other than those used in this study.

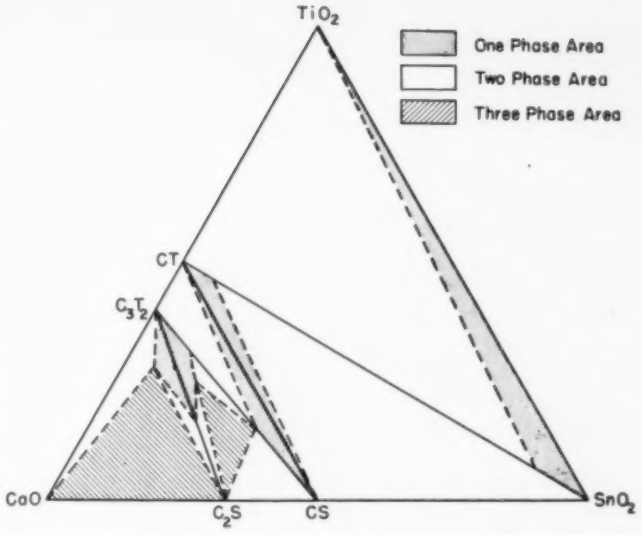

FIGURE 6. *Estimated solid-solution areas in the system* $CaO\text{-}SnO_2\text{-}TiO_2$.

The temperature range involved is between 1,300° and 1,550° C.

TABLE 11. *Results of X-ray study of selected compositions in the system* $CaO\text{-}SnO_2\text{-}TiO_2$

Mole ratio C:S:T	Binary join or ternary field	Heat treatment[a]		Phases identified (ss=solid solution)
		Time	Temperature	
		hr	*°C*	
3:1:3	CT-SnO_2	2.5	1,550	CT ss+SnO_2 ss.
1:1:1	do	3	1,550	Do.
1:3:1	do	2.5	1,550	Do.
1:9:1	do	3	1,550	Do.
3:1:2	CT-CS	3	1,550	(CT-CS) ss.
3:2:1	do	3	1,550	Do.
4:1:2	C_3T_2-CS	3	1,550	CS ss+small amount C_3T_2 ss.
6:3:2	do	3	1,550	CS ss+trace C_3T_2 ss.
9:6:2	do	3	1,550	CS ss.
8:1:4	C_3T_2-C_2S	3	1,550	C_3T_2 ss.
7:2:2	do	3	1,550	Do.
19:8:2	do	3	1,550	C_3T_2 ss+C_2S.
1:1:4	CT-TiO_2-SnO_2	16	1,315	CT ss+(TiO_2-SnO_2) ss.
1:3:9	do	3	1,400	Do.
3:2:2	CT-CS-SnO_2	3	1,550	(CT-CS) ss+SnO_2 ss.
4:4:1	do	3	1,550	Do.
7:2:4	C_3T_2-CT-CS	3	1,550	C_3T_2 ss+(CT-CS) ss.
3:1:1	C_3T_2-CS-C_2S	3	1,550	CS ss+C_2S+C_3T_2 ss.
9:6:1	do	3	1,550	CS ss+C_2S.
27:18:2	do	3	1,550	Do.
4:1:1	C_3T_2-C_2S-CaO	3	1,550	CaO+C_2S+C_3T_2 ss.
38:1:19	do	3	1,550	CaO+C_3T_2 ss.

[a] Each sample had been previously calcined for 4 hours at 1,000° to 1,100° C. Each specimen was quenched from the temperature indicated.

3.3. The System $MgO\text{-}CaO\text{-}SnO_2\text{-}TiO_2$

In addition to the 19 binary joins established in the four subsidiary ternary systems, there are 13 possible binary joins across the interior of the quaternary tetrahedron. Investigation of 10 selected quaternary compositions (with the preliminary assumption that there are no quaternary compounds present) indicated that only 2 of these binary joins

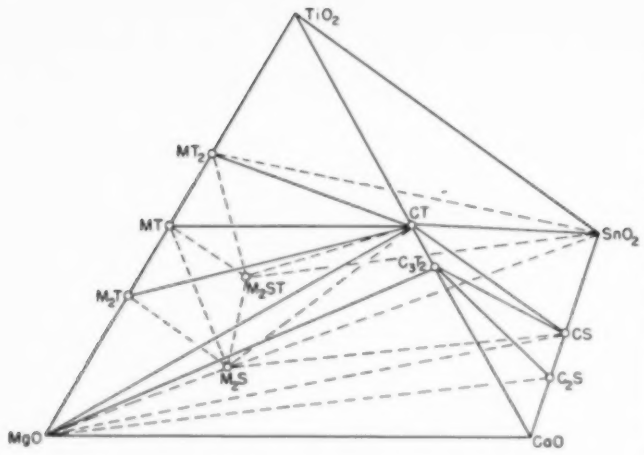

FIGURE 7. *Compatibility relations in the system* MgO-CaO-SnO_2-TiO_2.

No attempt has been made to indicate the extensive solid-solution development that occurs in this system.

are valid. They are the M_2S-CT and M_2ST-CT joins. The quaternary system could then be divided into 12 subsystems or tetrahedra. In order to verify the initial assumption as to the lack of quaternary compounds, at least one composition in the interior of each of the subtetrahedra was studied. In each case the expected phases were identified, and no indication of the presence of any quaternary compound was obtained. Solid-solution development was observed in all of the quaternary compositions. The results of the tests on quaternary samples are given in table 12. The arrangement of composition tetrahedra is illustrated in figures 7 and 8, in which no attempt has been made to indicate solid solutions.

TABLE 12. *Results of X-ray diffraction studies of specimens in the* MgO-CaO-SnO_2-TiO_2 *system*

Mole ratio M:C:S:T	Binary join, join plane, or quaternary volume	Heat treatment[a]		Phases identified (ss=solid solution)
		Time	Temperature	
		hr	*°C*	
2:1:1:1	M_2S-CT	3	1,550	M_2S ss+CT ss.
2:3:1:3	do	3	1,550	Do.
2:2:1:2	do	3	1,550	Do.
2:1:1:2	M_2ST-CT	3	1,550	M_2ST ss+CT.
3:4:3:1	MgO-CT-CS	6	1,550	MgO+(CT-CS) ss.
2:4:4:1	M_2S-CT-CS	3	1,550	M_2S ss+(CT-CS) ss.
2:2:2:1	do	3	1,550	Do.
3:1:1:2	M_2S-MT-CT	3	1,400	M_2S ss+MT ss+CT.
1:2:1:2	M_2S-CT-SnO_2	3	1,450	M_2S ss+CT ss+SnO_2 ss.
2:1:2:1	do	3	1,400	Do.
1:6:1:2	MgO-CaO-C_2S-C_3T_2.	3	1,550	C_3T_2 ss+CaO+MgO.
1:1:2:4	M_2S-M_2T-MT-CT	3	1,400	C_3T_2 ss+CaO.
1:15:4:4	do	3	1,400	Do.
1:6:2:2	MgO-C_2S-CS-C_3T_2	3	1,550	C_3T_2 ss+CS ss+MgO
5:1:1:2	MgO-M_2S-M_2T-CT.	3	1,550	(M_2T-M_2S) ss+CT+MgO.
1:5:1:3	MgO-CS-CT-C_3T_2	3	1,550	C_3T_2ss+(CT-CS) ss+MgO.
6:2:2:1	MgO-M_2S-CS-CT	3	1,550	MgO+M_2S+(CT-CS) ss.
5:1:1:3	M_2S-M_2T-MT-CT	3	1,400	(M_2S-M_2T)ss+MT ss+CT.
5:1:2:3	M_2S-M_2ST-MT CT.	3	1,400	M_2S ss+(M_2ST-MT) ss+CT.
4:1:3:2	M_2S-M_2ST-CT-SnO_2.	3	1,450	M_2S ss+M_2ST+CT ss+SnO_2.
2:2:3:1	M_2S-CS-CT-SnO_2	3	1,550	M_2Sss+(CT-CS) ss+SnO_2.
1:1:1:2	M_2ST-MT_2-CT-SnO_2.	3	1,550	MT_2 ss+M_2ST ss+CT+SnO_2 ss.
4:1:1:5	M_2ST-MT-MT_2-CT.	5	1,400	(M_2ST-MT)ss+MT_2 ss+CT.
1:1:1:4	MT_2-CT-TiO_2-SnO_2.	4	1,350	MT_2+CT+TiO_2 ss+SnO_2 ss.

[a] Each sample had been previously calcined for 4 hours at 1,000° to 1,100° C. Each specimen was quenched from the temperature indicated.

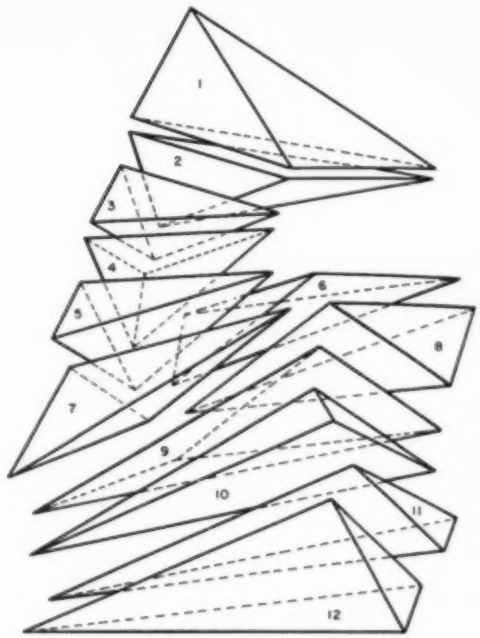

FIGURE 8. *An "expanded" version of figure 7.*

No.	End members of the 12 subtetrahedra of the system MgO-CaO-SnO_2-TiO_2
1	MT_2-CT-TiO_2-SnO_2.
2	MT_2-M_2ST-CT-SnO_2.
3	MT_2-MT-M_2ST-CT.
4	MT-M_2S-M_2ST-CT.
5	MT-M_2T-M_2S-CT.
6	M_2S-M_2ST-CT-SnO_2.
7	MgO-M_2T-M_2S-CT.
8	M_2S-CT-CS-SnO_2.
9	MgO-M_2S-CS-CT.
10	MgO-CS-CT-C_3T_2.
11	MgO-C_2S-CS-C_3T_2.
12	MgO-CaO-C_2S-C_3T_2.

4. Results of Dielectric Testing

4.1. The System MgO-CaO-TiO_2

The circles in figure 1 represent compositions which were formed into appropriate specimens and tested for their dielectric properties. The results of these tests are listed in tables 13, 14, and 15. The maturing temperatures were found to be high,

TABLE 13. *Results of dielectric testing*

Mole ratio	Binary join, ternary field, or quaternary volume	Heat treatment [a]		Shrinkage	Absorption	Dielectric constant, K, at 25° C and—			Reciprocal, Q, of power factor at 25° C and—		
		Time	Temperature			50 kc	1 Mc	20 Mc	50 kc	1 Mc	20 Mc
M:C:T	The system MgO-CaO-TiO_2										
		hr	°C	%	%						
4:1:5	MT-CT	1	1,500	14.5	0.00	35.1	35.1	35.0	1,100	3,000	3,000
2:1:3	do	1	1,500	11.4	.13	54.1	54.1	54.1	900	9,000	1,400
1:1:2	do	1	1,500	14.0	.06	78.6	78.5	78.1	10,000	10,000	700
1:2:3	do	2	1,500	12.6	.06	110	100	108	3,000	9,000	6,000
1:5:6	do	1	1,500	16.6	.02	144	143	145	10,000	10,000	3,000
38:1:20	M_2T-CT	1	1,550	14.3	.02	18.0	17.8	17.3	4,000	2,000	8,000
6:1:4	do	2	1,550	16.0	.01	31.6	31.6	31.6	10,000	10,000	2,000
4:1:3	do	1	1,540	13.8	.19	38.0	38.0	37.6	1,100	6,000	1,300
2:1:2	do	1	1,550	11.8	.00	60.6	60.6	60.6	10,000	10,000	2,000
2:2:3	do	1	1,550	12.7	.05	92.9	92.7	92.7	9,000	7,000	700
2:4:5	do	1	1,550	16.0	.00	122	121	122	4,000	10,000	7,000
2:7:8	do	1	1,550	17.9	.17	135	135	135	6,000	9,000	10,000
9:1:1	MgO-CT	1	1,725	15.1	.13	23.6	23.6	23.6	3,000	10,000	5,000
4:1:1	do	1	1,725	14.7	.07	43	43	43	3,000	10,000	1,500
2:1:1	do	1	1,725	15.4	.07	73	73	73	2,500	6,000	900
2:1:1 [b]	do	1	1,500	13.5	.00	69	69	69	3,000	4,000	510
1:1:1	do	1	1,725	14.0	.04	98	98	98	4,000	7,000	600
2:3:3	do	½	1,730	14.0	.00	119	118	118	4,000	8,000	3,000
2:3:3 [c]	do	1	1,500	12.2	.10	106	106	106	1,000	5,000	1,000
2:3:3 [b]	do	1	1,500	13.2	.00	109	109	109	1,000	4,000	2,000
1:2:2	do	1	1,725	14.7	.12	----	128	126	------	7,000	------
1:3:3	do	½	1,730	14.4	.02	153	153	152	2,400	3,600	5,000
1:3:3 [b]	do	1	1,500	13.4	.00	129	129	129	1,000	5,000	1,000
18:3:2	MgO-C_3T_2	½	1,625	15.8	.10	15.2	16.9	17.2	400	3,800	2,600
3:3:2	do	½	1,625	15.8	.05	40.5	39.4	----	900	1,700	1,000
2:3:2	do	½	1,650	16.0	.26	42.8	42.8	41.6	1,300	1,300	1,800
1:3:2	do	½	1,650	15.6	.22	47.0	47.2	45.9	1,100	2,100	1,700
1:1:5	MT_2-CT-TiO_2	1	1,350	16.0	.06	67	66	66	800	1,200	2,000
1:1:9	do	1	1,350	17.3	.20	94	92	90	44	126	440
1:3:9	do	1	1,350	17.3	.01	109	106	105	86	230	1,500
3:1:3	MT-M_2T-CT	2	1,500	12.2	.18	44	43	43	1,300	10,000	2,400
4:1:4	do	2	1,500	12.3	.06	37	37	37	10,000	1,000	2,000
9:1:3	M_2T-MgO-CT	1	1,540	10.2	.10	24	24	24	4,000	10,000	2,700
4:1:2	do	1	1,550	12.4	.10	41	40	40	1,500	10,000	2,600
3:1:2	do	2	1,550	11.9	.09	52	52	51	10,000	10,000	2,100
3:2:3	do	1	1,550	12.0	.13	77	77	76	6,000	10,000	700
2:3:1	MgO-C_3T_2-CaO	½	1,625	20.0	.06	26	28	28	300	1,600	1,400
1:4:1	do	½	1,650	21.0	.00	30	29	27	600	2,000	1,900
M:C:S	The system MgO-CaO-SnO_2										
2:1:2 [d]	M_2S-CS	1	1,550	18.0	0.15	11.0	10.8	10.7	1,100	770	410
2:6:7	do	1	1,550	19.5	.26	14.1	14.0	14.0	190	670	620
4:1:1	MgO-CS	1	1,550	19.5	.01	14.0	14.0	14.0	4,000	10,000	2,000
2:1:1	do	1	1,550	21.0	.03	13.2	13.2	13.2	2,000	10,000	2,000
1:1:1	do	1	1,550	21.0	.02	14.3	14.3	14.3	3,000	10,000	1,000
1:2:2	do	1	1,550	22.2	.02	14.4	14.4	14.4	3,000	10,000	4,000
4:2:1 [d]	MgO-C_2S	1	1,550	20.1	.00	11.2	11.0	11.0	300	230	360
2:2:1	do	1	1,550	19.0	.41	10.6	10.6	10.6	500	850	600
1:2:1 [d]	do	1	1,550	21.5	.00	13.4	13.4	13.4	200	760	760
C:S:T	The system CaO-SnO_2-TiO_2										
3:1:3	CT-SnO_2	1	1,500	16.8	0.01	106	106	106	600	2,000	1,500
1:3:1	do	1	1,550	19.7	.12	39	39	38	30	170	230
1:9:1 [d]	do	1	1,550	18.0	.16	27	25	----	40	30	------
3:1:2	CT-CS	1	1,500	17.9	.00	84	84	84	2,800	5,000	800
2:1:1	do	1	1,550	17.8	.15	62	61	61	850	5,000	2,100
3:2:1	do	1	1,550	16.8	.02	38	38	37	2,000	4,000	2,000
5:4:1	do	1	1,500	19.9	.00	24	24	24	1,500	2,000	2,000
4:1:2 [d]	C_3T_2-CS	1	1,550	21.0	.12	45.2	44.9	----	210	470	------
6:3:2 [d]	do	½	1,550	22.0	.02	37.8	37.6	37.4	200	600	380
9:6:2	do	1	1,500	21.5	.08	30.6	30.6	30.6	7,000	10,000	760
8:1:4 [d]	C_3T_2-C_2S	1	1,550	21.7	.05	42	42	----	90	400	------
7:2:2 [d]	do	1	1,550	23.7	.08	35	34	35	55	70	170
19:8:2 [d]	do	1	1,550	22.9	.02	18	18	18	70	230	460
1:3:9	CT-SnO_2-TiO_2	1	1,430	15.0	.02	76	76	76	200	1,300	680
2:1:4	do	1	1,500	16.8	.09	111	110	110	2,000	3,000	2,200
2:2:3	do	1	1,500	15.0	.00	82	81	81	1,700	2,300	2,400
3:3:2	CT-CS-SnO_2	1	1,500	17.0	.16	62	59	59	400	1,500	1,600
3:2:2 [d]	do	1	1,550	16.3	.04	67	67	67	1,000	2,000	440
27:18:2 [d]	C_3T_2-CS-C_2S	1	1,550	23.1	.00	17.5	17.3	17.3	150	320	340
6:3:1 [d]	do	1	1,550	23.5	.00	23.7	23.5	23.5	220	470	400

See footnotes at end of table.

TABLE 13. *Results of dielectric testing*—Continued

Mole ratio	Binary join, ternary field, or quaternary volume	Heat treatment [a]		Shrinkage	Absorption	Dielectric constant, K, at 25° C and—			Reciprocal, Q, of power factor at 25° C and—		
		Time	Temperature			50 kc	1 Mc	20 Mc	50 kc	1 Mc	20 Mc
M:C:S:T			The system MgO-CaO-SnO_2-TiO_2								
8:1:4:1 [b]	M_2S-CT	1	1,500		0.18	14.8	14.7	14.7	2,000	7,000	2,000
4:1:2:1 [b]	do	1	1,500	20.2	.43	17.4	17.4	17.4	2,000	4,000	3,000
2:1:1:1	do	1	1,550	16.4	.34	29.6	29.6	29.6	3,000	7,000	4,000
2:2:1:2	do	1	1,550	13.9	.23	53.1	53.0	52.9	5,000	5,000	2,000
2:3:1:3 [d]	do	1	1,550	15.0	.13	68.1	68.0	68.0	2,000	6,000	800
2:5:1:5 [b]	do	1	1,500	13.4	.16	102	102	102	1,000	4,000	2,000
2:9:1:9 [b]	do	1	1,500	12.8	.26	118	118	118	180	250	1,000
2:1:1:2	M_2ST-CT	1	1,450	14.0	.17	32.8	32.6	32.6	2,000	4,000	1,800
2:2:1:3	do	1	1,450	12.8	.05	56.0	56.0	56.0	3,000	1,700	560
2:9:1:10 [b]	do	1	1,500	11.8	.00	109	109	108	1,000	3,000	2,000
1:3:1:2 [b]	MgO-CT-CS	1	1,500	17.1	.05	72.7	72.7	72.7	7,000	4,000	500
2:2:1:1	do	1	1,550	16.8	.12	33.7	33.7	33.7	3,000	3,000	2,000
3:4:3:1	do	1	1,550	14.3	.23	22.1	22.1	22.1	3,000	6,000	1,000
2:5:4:1	do	1	1,550	19.3	.05	22.3	22.2	22.2	2,000	5,000	700
2:2:2:1	M_2S-CT-CS	1	1,550	19.4	.12	27.7	27.6	27.5	420	5,000	640
3:1:1:2	M_2S-MT-CT	1	1,400	11.5	.30	27.6	27.4	27.4	1,000	4,000	1,500
5:1:2:3	MT-M_2S-M_2ST-CT	1	1,450	11.6	.66	23.7	23.6	23.6	40	360	800
5:1:1:3	MT-M_2T-M_2S-CT	1	1,450	10.4	.10	24.0	23.9	23.9	3,000	4,000	5,000
5:1:1:2	MgO-M_2T-M_2S-CT	1	1,550	14.2	.40	27.2	27.1	27.0	4,000	7,000	580
4:3:2:2	MgO-M_2S-CS-CT	1	1,550	16.3	.44	41.5	41.4	41.4	3,000	4,500	1,300
1:5:1:3	MgO-CS-CT-C_3T_2	1	1,550	22.5	.35	45.8	45.8	45.3	140	280	500
1:6:2:2	MgO-C_2S-CS-C_3T_2	1	1,550	17.8	.29	34.4	34.2	34.1	500	500	330
1:6:1:2 [b]	MgO-CaO-C_2S-C_3T_2	1	1,500	22.2	.18	37.3	37.3	37.1	430	900	380
1:15:4:4	do	1	1,500	22.6	.04	30.6	30.2	29.7	90	130	280

[a] Each specimen had been calcined once prior to the recorded heat treatment.
[b] A commercial grade of CaO-TiO_2 was used in the preparation of this specimen.
[c] Periclase of 96-percent purity was used in the preparation of this specimen.
[d] One percent of Fe_2O_3 was added to the specimen.

TABLE 14. *Variation of dielectric constant with temperature*

Mole ratio	Binary join, ternary field, or quaternary volume	Value of K at 1 Mc and—											Average temperature coefficient of K over range indicated
		−50° C	0° C	25° C	50° C	75° C	100° C	125° C	150° C	175° C	200° C	225° C	250° C	
M:C:T						The system MgO-CaO-TiO_2								
														ppm/° C
9:1:10	MT-CT	24.1	23.9	23.7	23.5	23.4	23.4	23.3	23.3	23.2	23.2	23.2	23.2	−130
4:1:5	do	38.9	37.6	37.1	36.4	35.8	35.3	34.9	34.5	34.1	33.8	33.5	33.3	−520
2:1:3	do	58.5	55.3	54.1	52.7	51.5	50.3	49.4	48.6	47.8	47.0	46.4	45.9	−800
1:1:2	do	87.1	81.9	78.5	75.2	72.7	70.5	68.3	66.6	65.2	63.7	62.5	61.4	−1,080
38:1:20	M_2T-CT	.....	.....	17.7	17.7	17.7	17.7	17.7	17.7	17.8	17.8	17.8	18.2	+280
6:1:4	do	33.1	32.5	32.0	31.6	31.0	30.6	30.2	29.8	29.4	29.1	28.9	28.7	−480
2:1:2	do	66.8	62.4	60.6	58.2	56.4	54.7	53.2	52.0	50.9	49.8	48.9	48.2	−1,100
2:2:3	do	104	97.6	92.7	88.6	85.4	82.4	79.8	77.7	75.6	73.4	72.0	70.1	−1,300
2:7:8	do	151	141	135	128	123	119	114	111	107	104	102	100	−1,360
4:1:1	MgO-CT	46.1	44.3	43.1	42.0	41.0	40.2	39.4	38.8	38.2	37.8	37.3	37.1	−720
2:1:1	do	79.5	74.5	72.7	70.2	68.2	66.3	64.7	63.3	62.0	60.9	60.1	(a)	−1,010
2:1:1 [b]	do	77	72	69	67	65	64	62	61	60	59	58	57	−1,000
1:1:1	do	108	100	97.6	93.7	90.4	87.6	84.9	82.9	80.8	78.9	77.7	(a)	−1,090
2:3:3 [b]	do	123	113	109	106	103	100	97	95	92	91	89	88	−1,100
1:2:2	do	142	133	128	123	119	115	112	109	106	104	102	(a)	−1,190
1:3:3 [b]	do	146	135	129	125	121	117	114	111	108	106	103	102	−1,180
18:3:2	MgO-C_3T_2	18.4	17.4	17.4	17.3	17.3	17.3	17.3	17.4	17.5	17.6	17.7	(a)	.....
2:3:2	do	45.4	44.8	44.6	44.5	43.8	43.6	43.4	43.2	43.1	43.3	43.5	(a)	.....
1:3:9	MT_2-CT-TiO_2	122	114	111	108	105	103	100	97.6	95.5	93.4	91.6	89.6	−1,020
4:1:4	MT-M_2T-CT	38.8	37.7	36.9	36.2	35.7	35.1	34.6	34.3	33.9	33.5	33.2	33.0	−540
3:2:3	M_2T-MgO-CT	84.4	80.4	76.7	73.4	71.0	68.9	66.8	65.0	63.0	62.2	61.2	59.9	−1,130
2:3:1	MgO-C_3T_2-CaO	31.0	30.8	30.7	30.8	30.7	30.6	30.6	30.6	30.7	30.8	31.1	(a)	.....
1:4:1	do	29.3	29.2	29.1	29.0	28.9	28.9	28.9	29.0	29.2	29.4	(a)	.....	.....

See footnotes at end of table.

TABLE 14. *Variation of dielectric constant with temperature*—Continued

Mole ratio	Binary join, ternary field, or quaternary volume	Value of K at 1 Mc and—												Average temperature coefficient of K over range indicated
		−50° C	0° C	25° C	50° C	75° C	100° C	125° C	150° C	175° C	200° C	225° C	250° C	
M:C:S	The system MgO-CaO-SnO_2													
2:6:7	M_2S-CS	13.7	13.9	13.9	14.0	14.1	14.1	14.1	14.1	14.1	14.1	14.1	14.2	+120
4:1:1	MgO-CS	13.9	14.0	14.0	14.0	14.2	14.3	14.3	14.3	14.4	14.4	14.5	14.5	+140
2:1:1	do	13.2	13.2	13.3	13.3	13.3	13.3	13.3	13.4	13.4	13.5	13.5	13.6	+100
1:1:1	do	14.2	14.3	14.3	14.4	14.4	14.4	14.5	14.5	14.6	14.6	14.7	14.7	+120
1:1:1 [c]	do	14.2	14.3	14.3	14.4	14.4	14.4	14.4	14.5	14.5	14.5	14.6	14.7	+120
1:2:2	do	14.3	14.3	14.3	14.4	14.4	14.4	14.4	14.5	14.5	14.6	14.7	14.7	+90
4:2:1 [c]	MgO-C_2S	10.9	11.0	11.0	11.2	11.2	11.3	11.4	11.4	11.4	11.5	11.5	11.6	+210
2:2:1	do	9.9	10.5	10.5	10.5	10.6	10.6	10.6	10.6	10.7	10.7	10.7	10.8	+290
1:2:1 [c]	do	13.3	13.4	13.4	13.5	13.5	13.6	13.6	13.7	13.8	14.0	14.2	14.4	+260
C:S:T	The system CaO-SnO_2-TiO_2													
1:3:1	CT-SnO_2	39.5	37.8	37.1	36.0	35.9	35.2	34.8	34.5	34.0	33.8	33.6	33.4	−550
1:9:1 [c]	do	24.9	25.3	25.4	[a]	----	----	----	----	----	----	----	----	----
3:1:2	CT-CS	91	86	84	81	79	77	76	74	72	71	70	69	−920
2:1:1	do	----	----	60.8	59.1	57.6	56.3	55.3	54.4	53.4	52.7	51.9	51.4	−750
3:2:1	do	----	----	37.8	37.3	36.8	36.3	35.9	35.5	35.3	34.9	34.7	34.4	−420
5:4:1	do	24.6	24.4	24.3	24.2	24.1	24.0	24.0	23.9	23.9	23.8	23.8	23.8	−110
4:1:2 [c]	C_3T_2-CS	46.1	45.3	44.9	44.4	44.2	44.1	43.8	43.7	43.6	[a]	----	----	−250
6:3:2 [c]	do	38.6	37.9	37.6	37.1	36.9	36.7	36.5	36.5	36.4	36.4	[a]	----	−240
8:1:4 [c]	C_3T_2-C_2S	42.2	41.8	41.7	41.5	41.4	41.4	41.3	41.3	[a]	----	----	----	−110
7:2:2 [c]	do	35.0	34.9	34.9	[a]	----	----	----	----	----	----	----	----	----
19:8:2 [c]	do	17.6	17.7	17.7	17.8	17.9	18.1	18.3	[a]	----	----	----	----	+220
1:3:9	CT-SnO_2-TiO_2	82	78	76	74	72	71	69	68	67	65	64	[a]	−900
2:2:3	do	----	----	81.2	78.6	76.5	74.3	72.7	71.2	69.3	68.0	66.7	65.2	−970
2:1:4	do	----	----	110	107	103	99.5	97.1	94.7	92.0	90.0	88.4	86.0	−1,090
3:2:2 [c]	CT-CS-SnO_2	71.5	68.5	67.0	65.1	63.6	62.5	61.4	60.3	59.3	58.5	57.8	57.2	−740
3:3:2	do	56.0	54.0	52.0	50.0	49.5	48.5	47.5	47.0	46.5	46.0	46.6	[a]	−670
27:18:2 [c]	C_3T_2-CS-C_2S	17.2	17.3	17.3	17.4	17.4	17.6	17.7	17.8	18.0	18.1	18.4	18.6	+260
6:3:1 [c]	do	23.8	23.6	23.5	23.5	23.5	23.4	23.6	23.7	23.8	23.9	24.1	24.5	------
M:C:S:T	The system MgO-CaO-SnO_2-TiO_2													
8:1:4:1 [b]	M_2S-CT	15.0	14.8	14.7	14.6	14.5	14.4	14.4	14.3	14.3	14.3	14.3	14.2	−180
4:1:2:1 [b]	do	18.0	17.5	17.4	17.3	17.1	16.9	16.8	16.8	16.7	16.6	16.5	16.5	−290
2:1:1:1	do	32.0	30.4	29.6	29.1	28.4	27.9	27.5	27.0	26.6	26.3	26.0	25.8	−710
2:2:1:2	do	50	55	53	52	50	49	48	47	46	45	44	43	−1,050
2:5:1:5 [b]	do	116	106	102	99	96	93	90	88	84	83	82	81	−1,190
2:9:1:9 [b]	do	135	124	118	113	110	106	103	101	98	96	94	92	−1,260
2:1:1:2	M_2ST-CT	35.0	33.2	32.6	32.1	31.5	30.9	30.4	30.0	29.7	29.4	29.1	29.0	−625
2:2:1:3	do	62	58	56	54	53	52	51	50	49	48	48	47	−925
2:9:1:10 [b]	do	124	114	109	105	102	99	96	94	92	90	88	87	−1,210
1:3:1:2 [b]	MgO-CT-CS	80	75	73	71	69	68	66	65	64	63	62	61	−890
2:2:1:1 [c]	do	35.3	34.2	33.7	33.6	32.8	32.4	32.1	31.7	31.5	31.2	31.1	30.9	−445
3:4:3:1	do	22.5	22.2	22.1	22.0	21.8	21.8	21.7	21.6	21.6	21.5	21.5	21.4	−200
2:5:4:1	do	22.6	22.4	22.3	22.2	22.2	22.1	22.0	21.9	21.9	21.9	21.8	21.8	−110
2:2:2:1	M_2S-CT-CS	29.1	28.1	27.6	27.2	26.8	26.4	26.1	25.8	25.6	25.4	25.3	24.9	−500
3:1:1:2	M_2S-MT-CT	29.0	27.9	27.4	26.9	26.5	26.2	25.9	25.6	25.4	25.2	24.9	24.8	−620
5:1:2:3	MT-M_2S-M_2ST-CT	24.6	24.2	23.9	23.6	23.4	23.2	23.1	22.9	22.8	22.7	22.6	22.5	−310
5:1:1:3	MT-M_2T-M_2S-CT	25.2	24.3	23.9	23.6	23.3	23.1	22.9	22.6	22.5	22.3	22.2	22.0	−450
5:1:1:2	MgO-M_2S-M_2T-CT	28.6	27.4	27.1	26.5	26.2	25.9	25.6	25.4	25.2	25.0	24.9	24.7	−500
4:3:2:2	MgO-M_2S-CS-CT	45	42	41	40	39	38	38	37	37	36	36	35	−830
1:5:1:3	MgO-CS-CT-C_3T_2	47.4	46.3	45.8	45.4	45.1	44.8	[a]	----	----	----	----	----	−370
1:6:2:2	MgO-C_2S-CS-C_3T_2	35.1	34.5	34.2	33.9	33.7	33.5	33.4	33.3	33.3	33.2	33.2	33.3	−180
1:6:1:2	MgO-CaO-C_2S-C_3T_2	38.7	37.9	37.3	36.8	36.5	36.2	36.0	35.8	35.7	35.6	35.5	[a]	−340
1:15:4:4	do	30.4	30.1	30.0	29.9	29.8	29.8	29.7	29.5	29.3	28.9	28.4	28.3	−240

[a] At and above the temperature indicated, the specimen behaved as a semiconductor.
[b] A commercial grade of CaO-TiO_2 was used in the preparation of the specimen.
[c] One percent of Fe_2O_3 was added to the specimen.

TABLE 15. *Variation of Q value with temperature*

Mole ratio	Binary join, ternary field, or quaternary volume	Value of Q at 1 Mc and—											
		−50° C	0° C	25° C	50° C	75° C	100° C	125° C	150° C	175° C	200° C	225° C	250° C
M:C:T		The system MgO-CaO-TiO_2											
9:1:10	MT-CT	5,000	5,000	3,000	5,000	5,000	3,500	3,000	2,400	1,300	650	320	155
4:1:5	do	10,000	10,000	10,000	7,000	7,000	7,000	7,000	4,000	3,000	2,000	900	500
2:1:3	do	10,000	10,000	10,000	10,000	10,000	10,000	10,000	5,000	3,000	1,300	700	340
1:1:2	do	10,000	10,000	10,000	10,000	10,000	10,000	4,000	4,000	3,000	1,200	600	270
38:1:20	M_2T-CT			8,000	10,000	8,000	8,000	8,000	6,000	4,500	2,500	1,600	820
6:1:4	do	10,000	10,000	10,000	10,000	7,000	5,000	4,000	3,000	1,650	850	440	210
2:1:2	do	10,000	10,000	10,000	10,000	6,000	4,000	3,000	2,200	1,200	530	250	100
2:2:3	do	10,000	10,000	7,000	5,000	3,000	2,500	1,800	1,050	530	230	115	100
2:7:8	do	10,000	10,000	9,000	5,000	4,000	3,000	1,700	1,100	550	250	120	50
4:1:1	MgO-CT	10,000	10,000	10,000	6,000	3,000	2,300	1,300	700	330	160	75	30
2:1:1	do	6,000	6,000	6,000	4,000	3,000	1,700	1,000	500	260	110	60	(a)
2:1:1 [b]	do	2,300	2,600	4,000	2,000	1,900	1,900	1,800	980	590	400	190	100
1:1:1	do	7,000	7,000	7,000	4,000	3,000	1,700	900	500	230	104	55	(a)
2:3:3 [b]	do	910	2,500	2,300	2,300	2,200	2,200	2,100	1,030	1,000	400	160	90
1:2:2	do	7,000	7,000	7,000	3,000	2,400	1,400	800	420	230	103	48	(a)
1:3:3 [b]	do	1,800	1,800	2,300	2,200	2,200	2,100	2,000	990	550	380	160	80
18:3:2	MgO-C_3T_2	3,000	3,000	2,070	1,670	1,120	510	420	260	150	90	51	(a)
2:3:2	do	2,000	2,000	1,470	880	520	310	150	100	60	30	(a)	
1:3:9	MT_2-CT-TiO_2	2,200	1,300	900	700	800	1,150	1,400	1,500	1,700	1,650	1,600	1,400
4:1:4	MT-M_2T-CT	10,000	10,000	9,000	6,500	5,000	4,000	3,000	2,500	1,700	1,000	530	230
3:2:3	M_2T-MgO-CT	10,000	10,000	10,000	10,000	7,000	5,000	3,000	1,600	800	370	180	90
2:3:1	MgO-C_3T_2-CaO	2,000	2,000	1,300	870	500	370	190	160	70	40	(a)	
1:4:1	do	2,000	1,350	790	510	300	190	105	59	34	(a)		
M:C:S		The system MgO-CaO-SnO_2											
2:6:7	M_2S-CS	1,500	550	150	55	60	65	75	95	110	130	190	190
4:1:1	MgO-CS	7,000	4,000	4,000	7,000	7,000	7,000	7,000	7,000	7,000	7,000	7,000	7,000
2:1:1	do	10,000	10,000	4,000	5,000	5,000	4,000	4,000	2,500	2,400	2,300	2,200	2,200
1:1:1	do	3,000	6,000	10,000	10,000	7,000	5,000	5,000	5,000	5,000	5,000	5,000	5,000
1:1:1 [c]	do	2,000	1,500	2,000	2,000	1,500	1,500	1,200	800	690	480	370	260
1:2:2	do	3,000	6,000	10,000	10,000	7,000	7,000	5,000	5,000	4,000	4,000	4,000	4,000
4:2:1 [c]	MgO-C_2S	440	260	240	230	240	240	230	220	180	150	110	80
2:2:1	do	1,400	1,400	1,000	950	820	780	780	750	720	720	720	640
1:2:1 [c]	do	1,500	1,000	800	500	330	200	130	95	65	45	35	25
C:S:T		The system CaO-SnO_2-TiO_2											
1:3:1	CT-SnO_2	2,000	2,000	620	680	880	870	700	570	370	240	150	80
1:9:1 [c]	do	20	30	30	(a)								
3:1:2	CT-CS	3,500	3,500	6,000	5,000	4,000	3,500	2,500	1,650	1,300	870	400	200
2:1:1	do			5,600		5,300	3,900	1,900	1,380	590	280	140	60
3:2:1	do			10,000	10,000	10,000	10,000	6,000	6,000	3,000	1,620	1,210	740
5:4:1	do	9,000	9,000	7,000	7,000	7,000	7,000	5,000	4,000	4,000	4,000	2,500	2,000
4:1:2 [c]	C_3T_2-CS	700	500	400	270	220	170	130	100	70	(a)		
6:3:2 [c]	do	1,450	860	620	380	290	200	150	110	85	55	(a)	
8:1:4 [c]	C_3T_2-C_2S	1,400	700	450	270	190	140	90	70	(a)			
7:2:2 [c]	do	140	90	70	70								
19:8:2 [c]	do	860	370	230	150	100	70	45	(a)				
1:3:9	CT-SnO_2-TiO_2	10,000	9,000	2,000	1,900	750	640	580	390	350	200	110	70
2:2:3	do			2,400	1,900	1,400	1,400	1,300	1,300	1,300	810	650	350
2:1:4	do			2,600	2,500	1,900	1,800	2,200	1,700	980	440	220	100
3:2:2 [c]	CT-CS-SnO_2	1,200	1,750	1,530	1,430	1,460	1,140	890	660	370	220	140	80
3:3:2	do	4,000	4,000	1,300	900	620	390	230	130	70	40	30	(a)
27:18:2 [c]	C_3T_2-CS-C_2S	850	450	360	210	180	120	90	70	50	35	25	20
6:3:1 [c]	do	1,000	610	460	250	220	160	110	75	50	40	25	20
M:C:S:T		The system MgO-CaO-SnO_2-TiO_2											
8:1:4:1 [b]	M_2S-CT	6,000	2,000	1,200	1,100	1,000	900	700	600	560	500	400	280
4:1:2:1 [b]	do	4,000	1,600	900	800	800	1,000	1,000	1,000	1,000	1,000	800	500
2:1:1:1	do	5,000	5,000	5,000	5,000	5,000	5,000	4,500	2,000	1,500	870	390	200
2:2:1:2	do	3,500	3,500	3,500	2,000	4,500	4,000	3,000	1,400	1,000	620	380	190
2:5:1:5 [b]	do	4,000	4,000	4,000	3,000	3,000	3,000	2,000	1,500	990	560	220	120
2:9:1:9 [b]	do	2,500	2,500	2,500	1,400	1,300	1,300	1,200	910	590	380	200	110
2:1:1:2	M_2ST-CT	2,000	1,500	2,000	1,900	1,800	1,400	1,100	870	650	400	230	160
2:2:1:3	do	780	860	1,100	1,300	1,250	950	760	750	540	400	250	160
2:9:1:10 [b]	do	2,000	2,000	3,000	3,000	2,000	990	970	400	280	180	110	70
1:3:1:2 [b]	MgO-CT-CS	2,000	2,000	3,000	3,000	2,000	2,000	2,000	1,600	1,300	800	410	200
2:2:1:1 [c]	do	3,000	3,000	3,000	2,700	1,800	1,300	860	570	360	240	160	90
3:4:3:1	do	6,000	6,000	4,000	3,000	2,900	2,300	1,600	1,400	1,300	1,100	700	500
2:5:4:1	do	5,000	5,000	5,000	2,000	1,500	1,300	1,000	1,200	1,100	820	660	450
2:2:2:1	M_2S-CT-CS	1,800	570	1,390	2,750	2,700	2,670	2,630	1,740	1,410	1,280	1,270	1,080
3:1:1:2	M_2S-MT-CT	6,000	6,000	6,000	6,000	6,000	3,000	2,500	1,900	1,100	550	340	230
5:1:2:3	MT-M_2S-M_2ST-CT	1,400	1,400	1,400	1,900	1,900	1,900	1,300	950	630	340	210	130
5:1:1:3	MT-M_2T-M_2S-CT	5,000	5,000	5,000	500	5,000	2,500	2,500	1,600	930	660	330	210
5:1:1:2	MgO-M_2S-M_2T-CT	1,600	2,400	930	910	810	760	720	680	560	400	270	170
4:3:2:2	MgO-M_2S-CS-CT	2,300	2,200	1,900	3,000	2,100	2,000	1,530	1,030	690	350	200	100
1:5:1:3	MgO-CS-CT-C_3T_2	590	350	260	100	70	60	(a)					
1:6:2:2	MgO-C_2S-CS-C_3T_2	760	560	440	250	210	170	150	120	95	65	40	25
1:6:1:2	MgO-CaO-C_2S-C_3T_2	1,100	880	830	580	400	380	260	170	100	70	30	(a)
1:15:4:4	do	240	80	60	36	33	31	31	31	33	34	35	24

[a] See footnote a at end of table 14. [b] See footnote b at end of table 14. [c] See footnote c at end of table 14.

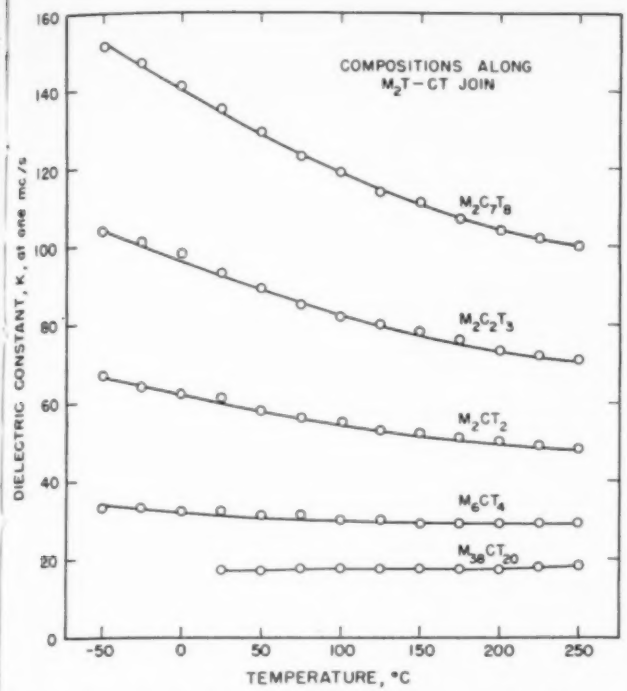

FIGURE 9. *Effect of temperature variations on the dielectric constant of specimens along the* M_2T-CT *join.*

especially along the MgO-CT join, when high-purity batch materials were used. Three specimens on the MgO-CT join were prepared with a commercial-grade perovskite, replacing the high-purity components usually used. Their maturing temperature was lowered more than 200° C by this change in components.

The dielectric properties of specimens on the binary joins were found to undergo a regular change with variations in the proportions of the end members. This change is illustrated in figure 9 for the dielectric constant, which varied from about 15 to about 165, depending on the compositions. The use of commercial-grade components caused a slight decrease in these values, together with the lowered maturing temperatures. The Q-values were good in all parts of the system, being, with a few exceptions, between 500 and 10,000.

Along the MT-CT, M_2T-CT, and MgO-CT joins, the temperature coefficient of dielectric constant (*TCK*) varied in a regular fashion as the composition was changed along the join (see fig. 9, in which this behavior is illustrated). It was found to be strongly negative near the CT end of the joins, and to approach zero or positive values as the percentage of CT in the specimen approached zero.

For specimens along the MgO-C_3T_2 join, the *TCK* values were irregular, showing shallow minima, and the values were numerically small.

4.2. The System MgO-CaO-SnO_2

The results of the dielectric tests on specimens from this system are listed in tables 13, 14, and 15. Specimens of these compositions are characterized by low K-values, high Q-values, and by a positive

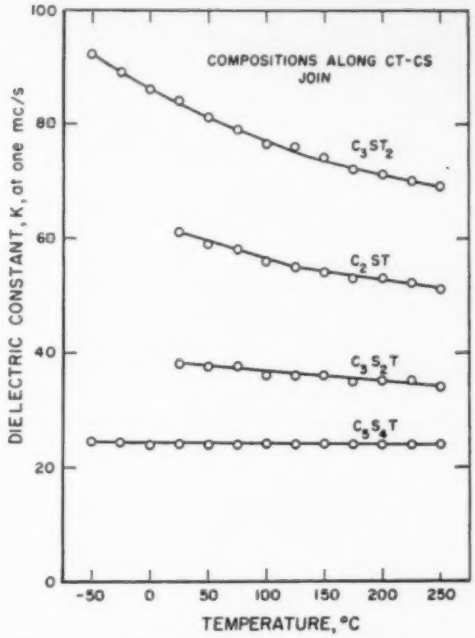

FIGURE 10. *Effect of temperature variations on the dielectric constant of specimens along the* CT-CS *join.*

temperature coefficient of K throughout the system.

Specimens along the MgO-CS join are noteworthy for the fact that they maintain a Q-value of several thousand, at temperatures as high as 250° C.

In some cases 1 percent of Fe_2O_3 was added as an aid in securing matured specimens. This additive was found to have the undesirable effect of lowering the Q-value, particularly at the higher temperatures.

4.3. The System CaO-SnO_2-TiO_2

The dielectric properties of specimens from this system are given in tables 13, 14, and 15. Maturing temperatures varied from 1,400° to 1,550° C, depending on the composition. In a number of cases the use of a 1-percent addition of Fe_2O_3 as a flux or mineralizer was required in order to obtain matured specimens. The same effect probably could have been achieved by using less pure components.

Table 13 shows that the value of K changes regularly along the binary joins as the specimen composition changes from that of one end member to the other. The highest value of K noted was about 165 for the compound CaO·TiO_2. The lowest values noted were 12 and 14 for the compounds C_2S and CS, respectively. No regular variation was noted in the Q-values. It may be observed, however, that these values were generally higher on joins having CT as an end member than they were on joins having C_3T_2 as an end member. This difference was probably due to the presence of Fe_2O_3 in the specimens on the latter joins.

Data concerning the variation of K and Q with temperature are listed in tables 14 and 15. On the binary joins, there was a regular variation of the temperature coefficient of K with composition. For example, see figure 10. A few specimens showed a

small negative *TCK*, and two specimens had a positive value. It is thought that not too much significance should be attached to the positive values and the smaller negative ones, as the specimens were semiconductors at the higher temperatures. This lower value may be caused by the Fe_2O_3 additive in these specimens.

4.4. The System MgO-CaO-SnO_2-TiO_2

The dielectric properties of the specimens in the quaternary system are about as would be expected from a knowledge of the ternary subsystems and from the knowledge that there are no quaternary compounds formed. The solid-solution development seems to result in an averaging of the properties of the compounds existing in the system. The results of the tests are listed in tables 13, 14, and 15.

The structure of the compound C_3T_2 seems to be very sensitive to small quantities of impurities. It was observed that the introduction of small amounts of MgO and C_2S into the C_3T_2 lattice caused very pronounced changes in the diffraction pattern of the material. The structural change seemed to be from a probable monoclinic symmetry to a very close approach to a cubic-perovskite symmetry, without, however, appreciable changes in the dielectric properties of the material.

5. Summary

A study of solid-state reactions in the system MgO-CaO-SnO_2-TiO_2 and its subsystems has been conducted. The results have either substantiated or shown that there exist in the system eight binary compounds, one ternary compound, and no quaternary compounds. Compatibility relations have been established for each of the four ternary subsystems and for the quaternary system. Extensive solid-solution formation was noted.

Dielectric-test samples were prepared and tested in each system except the system MgO-SnO_2-TiO_2, from which matured specimens were not obtained. Maturing temperatures were, in general, higher than 1,500° C. Values of the dielectric constant varied between 12 and 165, depending upon the composition of the specimen. For most samples tested, the temperature coefficient of K was negative, although the system MgO-CaO-SnO_2 is characterized by positive values. Values for Q of several thousand were found for most of the specimens studied. A number of test pieces maintained high Q-values at temperatures as high as 250° C.

6. References

[1] R. Rieke and A. Ungewiss, Ber. deut. keram. Ges. **17,** 237 (1936).
[2] George R. Shelton, Ansel S. Creamer, and Elmer N. Bunting, J. Research NBS **41,** 17 (1948) RP1899.
[3] Elmer N. Bunting, George R. Shelton, and Ansel S. Creamer, J. Research NBS **43,** 237 (1949) RP2025.
[4] C. Schusterius, Z. tech. Phys. **16,** 640 (1935).
[5] E. J. W. Verwey and J. M. Stevels, U. S. Patent 2,534,390 (December 1950).
[6] Eugene Wainer, U. S. Patents 2,402,515 (June, 1946), 2,399,082 (April, 1946), 2,402,518 (June, 1946), and 2,452,532 (October, 1948).
[7] William W. Coffeen, J. Am. Ceram. Soc. **36,** 207 (1953).
[8] Wilfrid R. Foster, Bull. Am. Ceram. Soc. **30,** 291 (1951).
[9] S. M. Lang and R. F. Geller, J. Am. Ceram. Soc. **34,** 193 (1951).
[10] L. W. Coughanour and V. A. DeProsse, J. Research NBS **51,** 85 (1953) RP2435.
[11] L. W. Coughanour, R. S. Roth, and V. A. DeProsse, J. Research NBS **52,** 37 (1954) RP2470.
[12] H. D. Megaw, Acta Cryst. **7,** 187 (1954).
[13] G. A. Rankin and H. E. Merwin, J. Am. Chem. Soc. **38,** 571 (1916).
[14] Y. Tanaka, J. Chem. Soc. Japan **61,** 1023 (1940).
[15] Y. Tanaka, J. Chem. Soc. Japan **62,** 199 (1941).

WASHINGTON, July 21, 1954.

Journal of Research of the National Bureau of Standards Vol. 54, No. 3, March 1955 Research Paper 2577

Chromatographic Method for the Fractionation of Asphalt Into Distinctive Groups of Components

Lawrence R. Kleinschmidt

A chromatographic method for the separation of asphalt into four distinct groups of components is described. The method utilizes fuller's earth as the adsorbent, and *n*-pentane, methylene chloride, and methyl ethyl ketone as selective solvents. The fractionation of asphalts into components in this manner facilitates the study of the degradation of asphalts in service. Although the method, in general, is not limited by the size of the specimen, it is particularly suited to samples of 3 to 6 grams, in which case it requires from 6 to 8 hours, depending upon the nature of the asphalt, for a complete fractionation. The time required to fractionate the *n*-pentane soluble components is about 3 hours.

1. Introduction

Asphalts, when exposed to various atmospheric conditions or to accelerated durability tests, undergo changes that have been determined mainly by physical methods. Studies of the chemical changes that occur in blown petroleum asphalts during the weathering process are greatly facilitated by the separation of the asphalts into groups of similar components.

Marcusson [1][1] was one of the first investigators to separate asphalt into three groups of components. By his procedure, asphalt was digested with 88° Bé naphtha.[2] The insoluble portion was designated as "asphaltenes", that adsorbed by certain clays from the soluble portion as "asphaltic resins", and the remainder as "total oily constituents". Strieter [2] improved the method by substituting *n*-pentane for the 88° Bé naphtha, and effected a nearly complete recovery of all components by using ethyl ether as a desorbent for the asphaltic resins, Hubbard and Stanfield [3] used anhydrous aluminum oxide as the adsorbent for their asphaltic resins. O'Donnell [4] used isopentane for the separation of the asphaltenes, and silica gel as the adsorbent for the asphaltic resins. Various other modifications of these methods are described by Abraham [5]. Grant and Hoiberg [6] and Traxler and Schweyer [7] employed solvents alone in their separations. Rostler and Sternberg [8] used dry hydrogen chloride gas and varying strengths of sulfuric acid for a separation of the *n*-pentane soluble portion of the asphalt.

The conventional specimen of asphalt for both outdoor and accelerated durability tests is usually a 2¼- by 5¼-in. film of asphalt on a 2¾-by 6-in. aluminum panel. When such a film is prepared in a thickness of about 0.01 cm (25 mils), approximately 5 g of asphalt is available for examination. The primary purpose of this investigation was to develop a rapid and reproducible method for fractionating such small samples (3 to 6 g) of asphalt into distinct groups of components. This is the preliminary phase of the study of the chemical changes that take place during the degradation of asphalts in service.

[1] Figures in brackets indicate the literature references at the end of this paper.
[2] Petroleum mixture of *n*-pentane, isopentane, and cyclopentane (d^{15}_4 about 0.642).

2. Procedure

A schematic diagram of the method of fractionation is given in figure 1. Specimens of asphalt for fractionation (about 5 g) were prepared in the same manner as those used for outdoor and accelerated durability tests, that is, by uniformly leveling the asphalt on a 2¾- by 6-in. aluminum panel, using the hydraulic-press method proposed by Greenfeld [9], or by uniformly distributing hot asphalt around the periphery of a 4-in. aluminum disk. The weight of the specimen was readily obtained by weighing the panel or disk before and after applying the asphalt. The large ratio of surface to volume obtained with such specimens facilitated the digestion with *n*-pentane.

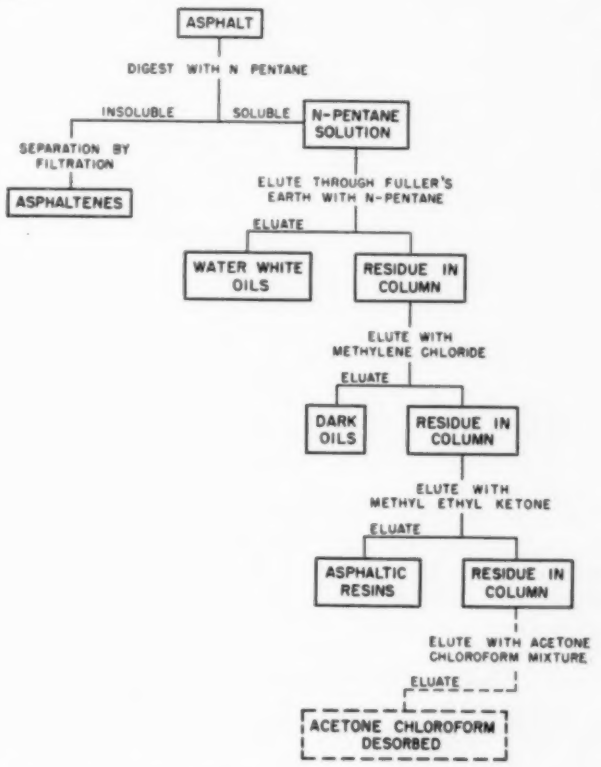

FIGURE 1. *Schematic diagram of method of fractionation.*

2.1. Separation of the *n*-Pentane Soluble and Insoluble Fractions

Specimens prepared by either method described above were digested with *n*-pentane (40 ml for each gram of asphalt) until the undissolved asphalt could be removed readily from the aluminum base with a rubber policeman. The aluminum base was washed free from any adhering material with *n*-pentane and removed from the beaker. The digestion with *n*-pentane was continued for 2 hr. The separation of the insoluble material was made by filtering the solution through a porcelain bitumen crucible with an asbestos mat. When the insoluble material was to be used for further study, the asbestos mat was topped with a tightly fitting filter-paper disk. It was found desirable to keep the insoluble matter covered with *n*-pentane throughout the filtration, using a rubber policeman to concentrate the insoluble portion, the bulk of which was readily transferred to the crucible with a spatula. This procedure was desirable because the insoluble portion from some asphalts was quite gelatinous and ahdered tenaciously to the beaker. The *n*-pentane insoluble fraction was washed with *n*-pentane until the filtrate was practically colorless. It was air-dried until free from *n*-pentane, then heated for 30 min at 105° C, and weighed. This fraction of the asphalt was designated as asphaltenes.

2.2. Fractionation of the *n*-Pentane Soluble Components

The amount of the *n*-pentane soluble portion of the asphalt was taken as the difference between the weight of the original specimen and that of the insoluble asphaltenes. This *n*-pentane soluble portion was fractionated by eluting it through a chromatographic column containing fuller's earth. Three groups of components were obtained from this solution by eluting successively with technical grades of *n*-pentane, methylene chloride, and methyl ethyl ketone. A ratio of 15 to 1 for the weight of the fuller's earth placed in the chromatographic column to that of the *n*-pentane soluble material was found to be convenient. However, the method, in general, is not limited to this ratio, as the procedure in fractionating the *n*-pentane soluble material is the same for any ratio of these two materials.

The chromatographic column (see fig. 2) was prepared by sealing a 3-cm length of 6-mm-diameter Pyrex tubing to a 30-cm length of standard-wall Pyrex tubing, approximately 30 mm in diameter.[3] A plug of glass wool was tamped into the bottom of the column before adding the fuller's earth [4] in a continuous stream while tapping the column to compact the adsorbent.

After adding the fuller's earth to the column, a plug of glass-wool was placed over the adsorbent to aid in an even distribution of the eluents and to prevent disturbing the column of fuller's earth during the successive elutions. In general, the ratio of the length of the column of fuller's earth to its diameter was approximately 5 to 1. This permitted a ready flow of all eluents through the column with only the force of gravity. A reservoir consisting of at least one-fourth the volume of the tube was available above the fuller's earth as storage space for the eluents.

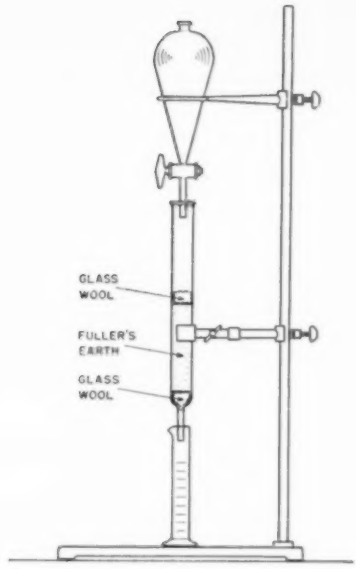

FIGURE 2. *Fractionation assembly.*

The *n*-pentane solution before being fractionated was concentrated to approximately 50 ml by heating on a steam bath. The fuller's earth in the chromatographic column was wetted with *n*-pentane to a depth of approximately 2 in. before adding the *n*-pentane solution. After the solution was placed in the column, *n*-pentane was added in 20-ml portions until the glass-wool plug on top of the fuller's earth was washed free of *n*-pentane soluble components. Sufficient *n*-pentane was then added to the reservoir to maintain a rate of flow of about 5 ml/min of the eluate. When 2 to 3 g of *n*-pentane soluble material was to be fractionated, 50 ml portions of the *n*-pentane eluate were collected consecutively, and the amount of nonvolatile material in each was determined.

Rapid evaporation of the *n*-pentane was accomplished without troublesome creepage by placing the beakers, not more than two-thirds full, approximately 15 in. from a 250-w infrared lamp (uncolored glass, reflector type) arranged so that the center line of the rays was parallel to and slightly above the level of the solution. (The red-colored infrared lamp was found to be unsatisfactory for this purpose in that the entire beaker was heated, which resulted in creepage of the nonvolatile constituents.) The sample was then heated at 105° C for about 15 min to remove last traces of pentane before weighing. When the nonvolatile material in these fractions had

[3] Columns prepared from 28-, 30-, and 32-mm-diameter tubing will accommodate sufficient fuller's earth for the fractionation of from 1.5- to 3.5-g quantities of the *n*-pentane soluble material.

[4] The bulk of material passing a 200-mesh sieve was removed by passing the fuller's earth through a centrifugal air separator. The fuller's earth was heated at 150° C for 18 hr prior to use.

reached a constant value (in the order of 0.025 g, when 5 g of asphalt was being processed), all previous fractions up to this point were combined. This fraction of the asphalt was designated "water-white oils."

After the *n*-pentane elution, methylene chloride was passed through the column until the eluate was practically colorless and the glass-wool plug at the bottom of the column was free from stain. The *n*-pentane holdup in the column was collected with this fraction. The eluents were evaporated from this solution on a steam bath. Water and traces of the eluents, if present, were removed by heating at 105° C for about 10 min before weighing. This fraction of the asphalt was designated as "dark oils."

Following the elution with methylene chloride, methyl ethyl ketone was passed through the column until the eluate was colorless. The methylene chloride holdup was collected with this fraction. This fraction, designated as asphaltic resins, was treated in the same manner as the previous one before weighing.

During the latter part of the investigation, R. W. Faid and D. C. McLean [5] suggested the use of a mixture of 10 percent of water and 90 percent of acetone,[6] followed by chloroform [7] for the removal of the major portion of the materials not removed by the *n*-pentane, methylene chloride, and methyl ethyl ketone. When this step was taken, the acetone-water mixture and chloroform eluates were collected together and freed from solvents in the same manner as that used for methylene chloride before weighing. This small fraction of the asphalt was designated "acetone-chloroform desorbed."

3. Description and Distribution of Fractionated Components

The four principal components obtained in the fractionation had distinctly different physical characteristics. The asphaltenes were black, brittle, hard solids, which intumesce rather than melt when heated. The water-white oils were colorless when freshly prepared and had about the same viscosity as a heavy lubricating oil at room temperature. The dark oils were reddish-orange in color and had a very high viscosity at room temperature. The asphaltic resins were glossy, brownish-black solids at room temperature. The small fractions of acetone-chloroform desorbed material obtained in the later experiments were black solids slightly harder than the asphaltic resins.

The results shown in table 1 are typical of those obtained in repeated determinations of the percentage of each fractionated component in specimens of the same asphalt. In this case a blown petroleum asphalt with a softening point[8] of approximately 95° C was fractionated, using 15 parts of fuller's earth to each part of *n*-pentane soluble material. After the methyl ethyl ketone desorption in these analyses, the fuller's earth at the top of the column was darkened slightly (evidence of nondesorbed material). Very little, if any of this strongly adsorbed material was removed by successive washing with ethyl ether, ethyl and methyl alcohols, acetone, benzol, chloroform, and carbon tetrachloride. Water alone caused swelling of the fuller's earth, which obstructed the flow by gravity. When external pressure was applied above the water, the fuller's earth swelled to the extent of breaking the glass tubing.

TABLE 1. *Repeatability of determinations [a] with specimens from the same asphalt*

Determination Number	1	2	3	Average
Asphaltenes, %	39.8	39.2	38.4	39.1
Water-white oils, %	24.5	24.7	24.0	24.4
Dark oils, %	22.9	23.8	23.3	23.3
Asphaltic resins, %	9.6	10.1	10.2	10.0
Total recovered, %	96.8	97.8	95.9	96.8

[a] Fifteen parts of fuller's earth used for each part of the *n*-pentane soluble material.

TABLE 2. *Distribution of the fractionated components of six shingle coating asphalts from different geographical sources [a]*

Asphalt	A	B	C	D	E	F
Softening point (R&B method), °C	...	104	108	111	96	102
Asphaltenes, %	43.6	42.2	39.1	40.5	37.5	37.4
Water-white oils, %	20.2	20.0	28.3	27.3	26.0	21.0
Dark oils, %	25.3	25.2	22.8	20.0	21.8	24.6
Asphaltic resins, %	6.9	9.1	8.0	9.5	11.0	12.8
Acetone[b]-chloroform desorbed, %	1.1	1.3	0.9	2.0	1.9	2.5
Total recovered, %	97.1	97.8	99.1	99.3	98.2	98.3

[a] Fifteen parts of fuller's earth was used for each part of the *n*-pentane soluble material.
[b] Acetone plus 10 percent of water.

Table 2 shows the distribution of the fractionated components obtained from six blown petroleum asphalts produced from fluxes of different geographical origin. The percentages of material recovered by the acetone-water mixture and chloroform wash are also reported in this table.

Although this method of fractionating asphalts was developed primarily for the study of changes occurring in the various components during the weathering of blown asphalts, it also facilitates the examination of vacuum-reduced asphalts and fluxes used in the preparation of the blown asphalts.

Table 3 shows the distribution of the fractionated components obtained from three blown petroleum asphalts and from the fluxes from which they were prepared.

Table 4 shows how the distribution of the *n*-pentane soluble components was effected by varying the ratio of the amount of fuller's earth to that of

[5] Chemists, Mexican Petroleum Corporation, Baltimore, Md.
[6] Technical grade. It was found later that the acetone-water mixture used in deactivating the fuller's earth could be eliminated if water-saturated methyl ethyl ketone was used instead of the technical grade.
[7] United States Pharmacopoeia grade.

[8] Tentative method of test for softening point, ball and shouldered ring apparatus, ASTM Designation E28-42T.

TABLE 3. *Distribution of fractionated components in three blown shingle coating asphalts and in the fluxes from which they were produced* [a]

Asphalt	G		H		I	
Type	Flux	Coating	Flux	Coating	Flux	Coating
Asphaltenes, %	19.4	37.8	13.1	39.1	13.2	41.8
Water-white oils, %	20.8	19.5	28.0	24.4	32.4	27.4
Dark oils, %	42.0	28.0	38.4	23.3	29.6	18.2
Asphaltic resins, %	14.1	11.9	14.9	9.9	16.8	10.3
Acetone [b]-chloroform desorbed, %	2.0	1.3	2.0		3.8	
Total recovered, %	98.3	98.5	96.4	96.7	95.8	97.7

[a] Fifteen parts of fuller's earth was used for each part of the *n*-pentane soluble material.
[b] Acetone plus 10 percent of water.

TABLE 4. *Influence of the ratio of the amount of fuller's earth to that of the n-pentane soluble material on the distribution of the water-white oils, dark oils, and asphaltic resins*

Ratio of amount of fuller's earth to that of *n*-pentane soluble material	10:1	15:1	20:1	25:1
Asphaltenes, %	38.4	38.1	38.6	37.5
Water-white oils, %	33.2	29.0	24.4	22.2
Dark oils, %	13.7	17.8	18.7	20.6
Asphaltic resins, %	11.7	13.0	13.8	15.1
Total recovered, %	97.0	97.9	95.5	95.4

the *n*-pentane soluble material of a blown petroleum asphalt having a softening point of approximately 85° C (R&B method). In changing this ratio from 10:1 to 25:1, the percentage of water-white oils decreased by a factor of 3 to 2, whereas the percentages of the dark oils and asphaltic resins increased by about the same factor.

4. Conclusion

The procedure described provides a rapid and reproducible method of fractionating asphalts into four distinct groups of components. The fractionation of asphalts in this manner facilitates chemical studies of the degradation of asphalts under service conditions. The method is well suited for samples as small as those (about 5 g) used in conventional weathering and accelerated durability tests.

5. References

[1] J. Marcusson, Die Naturlicken und Kunstlicken Asphalts, 2d ed. (Leipzig, Verlag Von Wilhelm Engleman, 1931).
[2] O. G. Strieter, J. Research NBS **26,** 415 (1941) RP1387.
[3] Rethel L. Hubbard and K. E. Stanfield, Anal. Chem. **20,** 460 (1948).
[4] Gordon O'Donnell, Anal. Chem. **23,** 894 (1951).
[5] Herbert Abraham, Asphalts and allied substances, 5th ed., vol. 2, P. 1224 (D. Van Nostrand Co., Inc., New York, N. Y., 1945).
[6] F. R. Grant and A. J. Hoiberg, Proc. Assoc. Asphalt Paving Technol. **12,** 87 (1940).
[7] R. N. Traxler and H. E. Schweyer, Oil Gas J. (Aug. 31, 1953).
[8] Fritz S. Rostler and Heinz W. Sternberg, Ind. Eng. Chem. **41,** 598 (1949).
[9] Sidney H. Greenfield, Bull. No. 193, ASTM (Oct. 1953).

WASHINGTON, November 15, 1954.

Journal of Research of the National Bureau of Standards Vol. 54, No. 3, March 1955 Research Paper 2578

Nature of Stark Rubber[1]

Donald E. Roberts and Leo Mandelkern

The melting behavior and X-ray diffraction patterns of four different samples of "stark rubber" have been investigated. The melting temperatures, 39° to 45.5° C, are substantially higher than that observed for natural rubber crystallized by cooling. The X-ray diffraction patterns indicate that the crystallites in stark rubber are oriented. This observation can explain the higher melting temperatures. Thus, the previous assignment of an equilibrium melting temperature, 28° ±1° C, to unoriented crystalline natural rubber is shown to be appropriate. Several different methods that have been used successfully in preparing stark rubber under controlled conditions in the laboratory are outlined.

1. Introduction

Long-chain molecules that possess a sufficient amount of chain regularity are capable of crystallizing under favorable conditions. The crystallization and the subsequent melting are similar to the processes that occur in monomeric materials of low molecular weight. The existence of an equilibrium melting temperature in polymers has been demonstrated [1];[2] it has also been shown that this temperature is systematically depressed by low molecular weight diluents in a manner quantitatively describable by the application of the thermodynamics of phase equilibria [1,2]. Similarly, the kinetics of crystallization of polymers can be satisfactorily accounted for by the assumption of the concurrence of nucleation and growth, with the magnitude of the nucleation rate dependent mainly on the difference between the equilibrium melting temperature and the temperature of the crystallization [3]. The success achieved in describing both the melting process and the crystallization kinetics gives additional evidence for the existence of an equilibrium melting temperature, and adds to its significance in the understanding of the crystallization behavior of polymers. This temperature is defined as the one at which the most perfect crystallites are unstable relative to the undeformed, unoriented liquid state.

For many polymers, including natural rubber, it has been observed that the melting temperature, T_m, depends on the crystallization temperature when the heating rate is relatively rapid [4,5,6,7]. However, for polyesters [5], polyamides [6], and more recently for natural rubber [8], it has been demonstrated that when slow heating rates are employed the melting temperature observed is independent of previous thermal history and then the equilibrium melting temperature is approached. This heating schedule is presumably conducive to the formation of more perfect crystallites, which are stable at higher temperatures. For natural rubber the equilibrium melting temperature has been found to be 28° ±1° C [7]. Melting temperatures appreciably higher than 28° C have also been reported for natural rubber. Considerable confusion has arisen due to the apparent variability of its melting point. Since the melting temperatures below 28° C have been demonstrated to be solely a result of the heating rates used in their determinations, the occurrence of melting temperatures above 28° C also requires explanation.

The natural rubber samples that have been observed to be high melting can be divided into two types, "racked" rubber and "stark" rubber. If unvulcanized natural rubber is repeatedly extended at an elevated temperature and then cooled, it can be given a rather enormous pseudopermanent extension without any applied force being maintained [9]. Extensions as great as 10,000 percent have been reported. Rubber thus treated has been termed "racked" rubber, and its mechanical properties are similar to those of a hard inelastic material. The racking process is accompanied by increase in density of the rubber, and its X-ray diffraction pattern gives a very intense fiber-type diagram, indicating not only that crystallization is occurring, but that the crystallites thus formed are highly oriented in the direction of the stretching. On heating, racked rubber retracts and the X-ray pattern disappears, indicating that fusion is occurring. The melting temperature, which depends on the extent of racking, occurs in the range 35° to 50° C, substantially higher than the equilibrium melting temperature assigned to natural rubber. However, as the crystallites are highly oriented in racked rubber, the connecting amorphous regions must be deformed from their statistically more probable configuration, and so the crystallites will be expected to be stable at higher temperatures than crystallites in an undeformed system.

When natural rubber is stored in temperate climates it is occasionally found to be hard and inelastic, because of the development of appreciable amounts of crystallinity. Many of these samples also exhibit high melting points on initial heating and this type of rubber has been designated as "stark" rubber because it is hard and rather rigid at room temperature. Stark rubber has not heretofore been prepared

[1] A portion of this work was supported by the Office of Naval Research.
[2] Figures in brackets indicate the literature references at the end of this paper.

330526—55——4

under controlled conditions, and the reasons for its higher melting temperature cannot be ascertained from existing information, as in the case of racked rubber.

In an effort to understand the nature of stark rubber and the reasons for its high melting temperature, the melting behavior and X-ray diffraction patterns of four stark rubber samples, from widely different sources, have been investigated. As a result of this study some conclusions have been reached both as to the reasons for its high melting temperature and as to how it is formed. As a further consequence of these studies, methods have been devised for the laboratory preparation of stark rubber under controlled conditions.

2. Experimental Procedure

The specific volume-temperature relations and the melting temperatures were determined, using dilatometric techniques. Descriptions of the volume dilatometers employed and the procedures followed have been published [6, 10]. The dilatometers were immersed in constant-temperature baths controlled within ± 0.1 deg C. The thermal histories of the samples and the times held at the various temperatures are detailed below. The absolute densities of the stark rubber specimens were determined at 25° C by the method of hydrostatic weighings [11].

The samples for the X-ray diffraction studies were cut from the sheets of stark rubber into rectangular strips about 1 mm thick. The X-ray diffraction photographs were taken in a flat plate camera, using copper radiation ($K\alpha$) and operating at 40 kv and 20 ma. The sample-to-film distance was 10 cm, the aperture of the sample holder was 0.025 in., and the exposure time was 5½ hours. The variation in intensity of the diffraction around the circumference of a ring was determined by the manual use of a densitometer.

3. Samples

Sample I was received from G. S. Whitby about 1936. It was a sample of smoked sheet, identified by the year of its preparation, 1913, and appeared to be similar to a specimen referred to in the literature [9, p. 105]. Sample II was also a smoked sheet and had been highly milled, with the intention of using it as a rubber cement. It was stored in the basement of the Geophysical Laboratory of the Carnegie Institution of Washington from 1936 until 1951, when it was discovered to have become stark. Sample III was received in 1929. It had been tapped and smoked on the Upper Amazon River and washed and dried at Belem (Para). The sample was firm when received but not so stiff as it had become by 1952, when it was reexamined. Sample IV was from a bale of smoked sheet that had been stored in the NBS Rubber Section for several years; a portion of this bale was found to be stark, whereas other portions, including regions contiguous to the stark portion, were completely amorphous.

4. Results

4.1. Chemical Analyses

The results of chemical analyses for major constituents, which were performed on three of the stark rubber samples, are given in table 1.[3] The amounts of the major constituents found are typical of the composition of unpurified raw rubber. Hence the behavior of stark rubber cannot be attributed to any major chemical differences from the usual, or normal, raw rubber.

TABLE 1. *Chemical analyses of stark rubbers*

Major constituent	Sample		
	I	II	III
	%	%	%
Rubber hydrocarbon [a]	94.1	94.7	94.8
Acetone extract	3.3	3.5	2.6
Benzene insolubles	1.2	0.9	1.1
Protein [b]	2.1	2.3	2.5

[a] Chromic acid oxidation method.
[b] Boric acid method.

4.2. Melting Behavior

The melting behavior of the four stark rubber samples was investigated. Because of time effects above 35° C, a revision was required in the heating schedule that has been used with ordinary natural rubber [8] and other polymers [2, 6, 10]. The observations were initiated at about 15° C, and the temperature was raised at the rate of 1 deg each 12 to 24 hours. Up to temperatures of about 35° C, volume equilibrium appeared to be attained simultaneously with temperature equilibrium, and the specific volume varied linearly with temperature. This is in marked contrast to other polymers [2, 6, 8, 10], in which partial melting and recrystallization always occur in the temperature range below the equilibrium melting temperature. At a given temperature above 35° C the volume of the stark rubber samples no longer remained invariant with time, but was observed to increase slowly. These slow increases in the volume of stark rubber in this temperature region have also been observed by Whitby [9, p. 165]. Although the rate of volume increase was slow, the total volume change at a given temperature was significant. A typical example of this phenomenon is that for sample I after 500 hours at 37° C the specific volume had increased 0.0135 cm^3/g. After the temperature was raised to 38° C and held there for 240 hours, the specific volume had increased 0.00318 cm^3/g. Similarly, after 600 hours at 39° C it had increased 0.0030 cm^3/g, and after 500 hours at 39.5° C it had increased 0.0008 cm^3/g. These observations are also in marked contrast to the behavior of other polymers for which, in the vicinity of T_m, only very slight increases in volume with time are observed. These observations for stark

[3] The authors are indebted to Mrs. R. J. Fanning for performing the chemical analyses.

rubber necessitated that the samples be held for exceptionally long periods of time in the temperature interval between 35° C and T_m. In this interval the temperature was raised in 1-deg increments, and the sample was held at a given temperature until there was no perceptible increase in volume for about 5 to 7 days. Thus, the total heating process for a typical determination of T_m was of the order of 50 to 100 days. The melting temperature was then taken as the temperature at which the last trace of crystallinity disappeared, following the typical heating schedule just described.

Possible reasons for this rather unusual melting behavior will be discussed in more detail in connection with the X-ray diffraction analysis of the structure of stark rubber. It is apparent that the value observed for T_m will depend on the over-all rate of heating and on the total time held at specified temperatures just below T_m. For example, sample II was initially held in the temperature range of 37° to 41° C for 26 days; T_m was found to be 41° C, and the total volume change in melting was 0.0250 cm^3/g. Another specimen of sample II was brought from 30° to 38° C in 7 days, and up to the present has been held at 38° C for a little over a year. A steady increase of the volume has been observed, and 60 percent of the total volume change occurring on melting the first specimen has already occurred. There is thus the distinct likelihood that if a sample of stark rubber is held at a temperature below the reported T_m for a sufficiently long time, a lower melting temperature will be observed [9, p. 105].

Plots of the relative volume as a function of temperature are given in figure 1 for samples I and II.

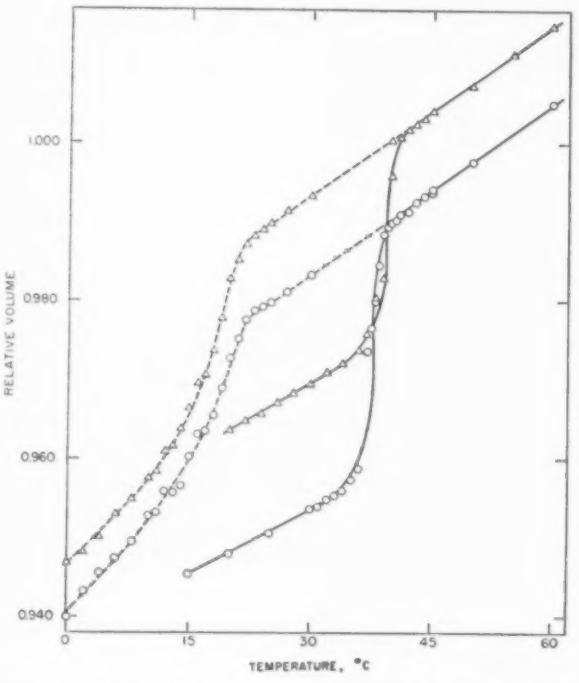

FIGURE 1. *Relative volume-temperature plot for stark rubber.*

Solid lines, original heating; dashed lines, heating after initial melting and then crystallizing at 0° C; ○, sample I; △, sample II.

This figure also shows the curves that are obtained for the same samples after they were first melted and then recrystallized at 0° C. For the latter case the melting behavior is similar in all respects to that usually observed for natural rubber. If stark rubber is first dissolved, and the solvent is sublimed or evaporated off, and if the sample is recrystallized at 0° C and slowly heated, the usual type of behavior is also found [8]. Thus, if the crystallites originally present in stark rubber once disappear, subsequent crystallization induced by cooling is identical with that which occurs in ordinary amorphous natural rubber.

4.3. Melting Temperatures and Densities

In table 2 the densities of the semicrystalline rubber, ρ_{sc}; the completely amorphous rubber after melting the same samples, ρ_a; and their differences at 25° C are given, as well as their respective melting temperatures, T_m, which were determined from the specific volume–temperature studies. As the stark rubber samples are almost identical in chemical composition, the variations in the density differences must reflect variations in the degree of crystallinity. The fact that the samples, when arranged in order of decreasing density differences, as in table 2, are also in order of increasing melting temperatures may be regarded as fortuitous because the range of melting temperatures is only a little larger than the precision of determination. Therefore, the authors are of the opinion that the melting temperature does not depend on the amount of crystallinity.

TABLE 2. *Densities at 25° C and melting temperatures of stark rubbers*

Sample	ρ_{sc}	ρ_a	$\Delta\rho$	T_m
				° C
I	0.9405	0.9129	0.0276	39.5 to 40
II	.9302	.9094	.0208	41
IV	.9270	.9092	.0178	42.0
III	.9114	.8945	.0169	45.5

4.4. X-Ray Diffraction

Typical X-ray diffraction patterns are illustrated in figures 2 and 3. The positions of the four most intense rings correspond to the *d*-spacings given in table 3 and confirm the values given by Barnes [12] for stark rubber and that given by Clark, Wolthuis, and Smith [13] for rubber crystallized by either stretching or cooling. Thus, the crystalline form present in stark rubber is the same as that obtained on cooling amorphous natural rubber.

TABLE 3. *Spacings for stark rubber*

d-spacing	Indices [a]
6.30	200
5.00	201
4.24	120
3.77	121
	121

[a] For a unit cell of dimensions *a*, *b*, and *c*, the direction of the chains (the fiber axis) is the *c* axis in the above.

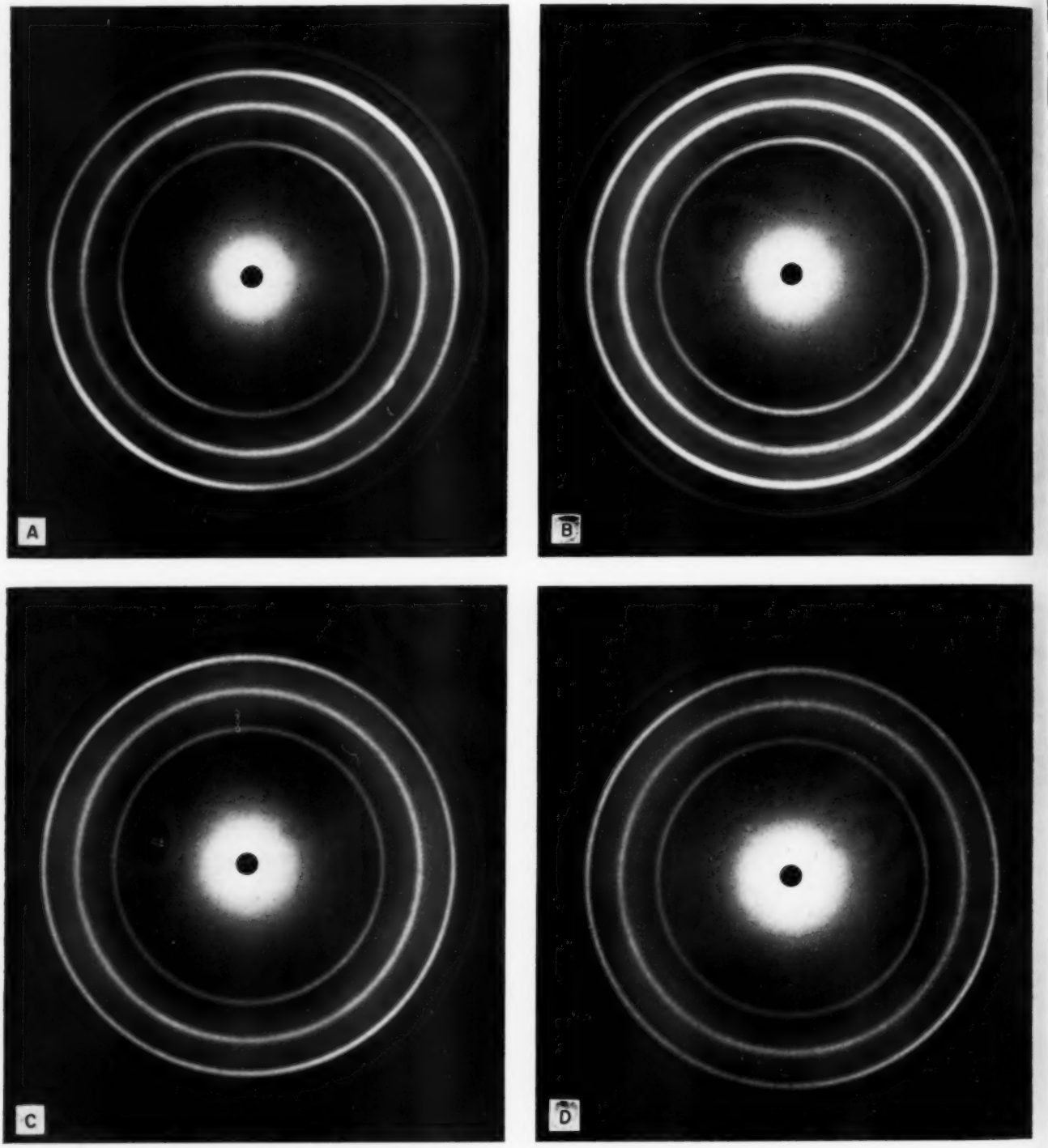

FIGURE 2. *X-ray diffraction photographs of stark rubber.*

A and B, Sample I, with position of X-ray beam parallel and normal, respectively, to plane of rubber sheet; C and D, sample II, with position of X-ray beam parallel and normal, respectively, to plane of rubber sheet.

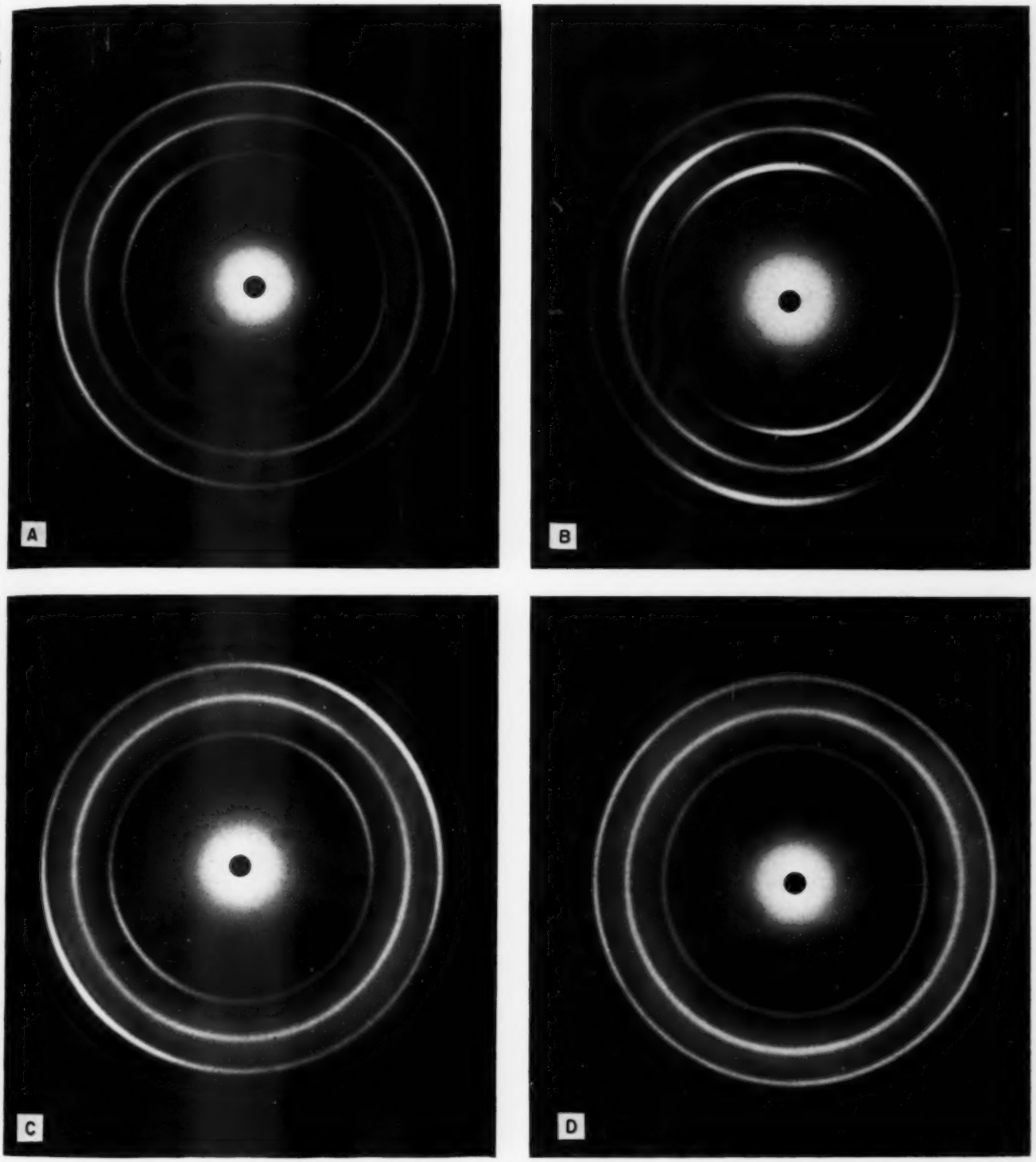

FIGURE 3. *X-ray diffraction photographs of stark rubber.*

A and B, Sample III, with position of X-ray beam parallel and normal, respectively, to plane of rubber sheet; C and D, sample IV, with position of X-ray beam parallel and normal, respectively, to plane of rubber sheet.

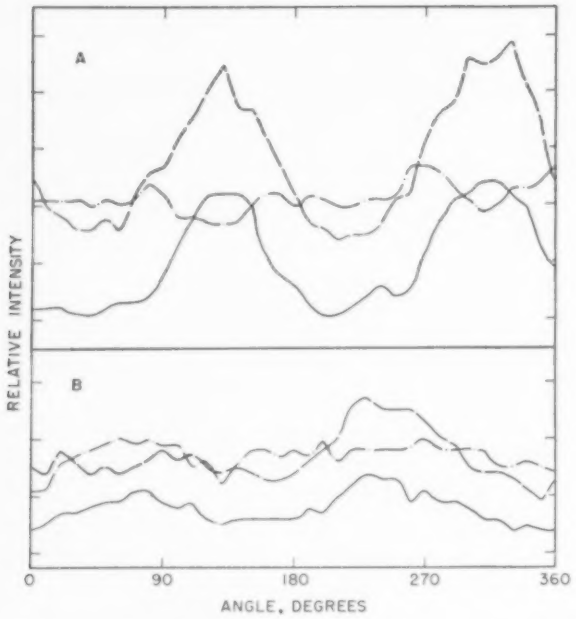

FIGURE 4. *Relative intensity of diffraction around circumference of rings.*

A, Sample I, X-ray beam parallel to plane of rubber sheet; B, sample II, X-ray beam normal to plane of rubber sheet.
Curves correspond to the following *d*-spacings:——, 6.30; ·—·, 5.00; — —, 4.24. The unit of relative intensity is 0.1.

An inspection of the X-ray patterns indicates that around certain of the rings the intensity of the diffracted X-ray is not uniform. This is seen most clearly in the patterns for samples III and IV (fig. 3). If the crystallites were randomly oriented with respect to a fixed direction in the sample, then the intensity of the diffraction should be uniform around the circumference of any given ring. The nonuniformity of the rings indicates that the crystallites have a preferred orientation in the sample. To further confirm the reality of the orientation, a direction in the sample was fixed as reference, and the diffraction photographs were taken with the X-ray beam successively normal to and parallel to this direction. The results shown in figures 2 and 3 indicate that the diffraction patterns depend on the position of the beam relative to the sample, and hence the nonuniformity of the rings is caused by diffraction from oriented crystalline planes.

To further illustrate these observations, the variations of the relative intensity around the circumferences of the diffraction rings of interest are plotted in figures 4, 5, and 6. For all the samples the major variation in intensity occurs in the rings corresponding to reflections from the 200 and 120 planes which are the only diffracting planes parallel to the direction of the chain axis. In sample II the effect is smaller than in the other samples, but the results are reproducible and well within the experimental limits of the photometering procedure. Figures 5 and 6 indicate quite clearly the nonuniformity of the rings and the changes in intensity that occur when the position of the X-ray beam

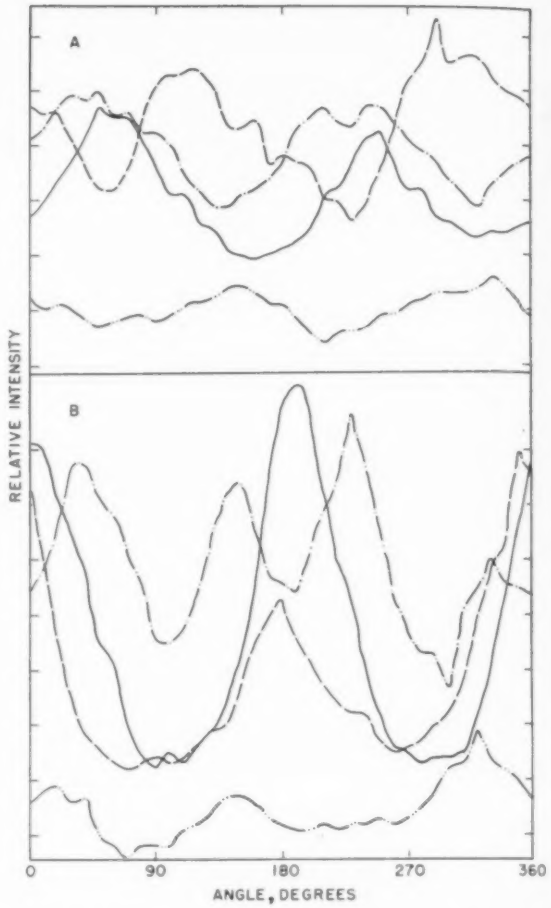

FIGURE 5. *Relative intensity of diffraction around circumference of rings for sample III.*

A, X-ray beam parallel to plane of rubber sheet; B, X-ray beam normal to plane of rubber sheet.
Curves correspond to the following *d*-spacings: ——, 6.30; ·—·, 5.00; — —, 4.24; ·· —, 3.77. The unit of relative intensity is 0.1.

relative to the sample is altered. More than two diffraction photographs for each sample are required to establish the detailed nature of the orientation. It is hoped that an analysis of the more detailed X-ray work now in progress will lead to a more quantitative description of the orientation. For present purposes, the establishment of the fact that the crystallites in stark rubber are oriented suffices.

5. Discussion

It has been suggested that there are two forms of crystalline natural rubber and that one of these forms is the higher-melting stark rubber [14,15]. However, the X-ray analyses of a sample of stark rubber by Barnes [12], the results of which are corroborated by the present work, indicate that the structure of the crystals in stark rubber is identical in all major respects with the structure of crystals induced by either stretching or cooling the amorphous rubber. Hence, polymorphism does not appear to be an explanation of the nature of stark rubber.

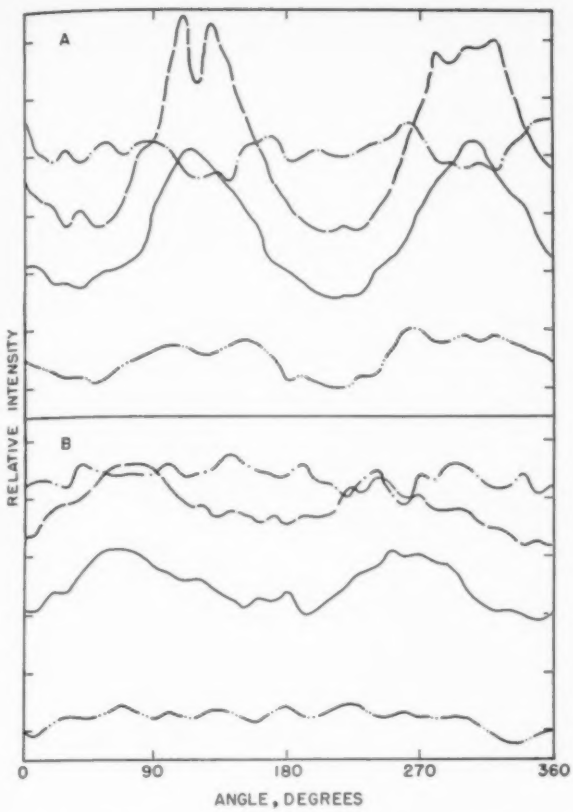

FIGURE 6. *Relative intensity of diffraction around circumference of rings for sample IV.*

A, X-ray beam parallel to plane sheet; B, X-ray beam normal to plane of sheet. Curves correspond to the following *d*-spacings: —, 6.30; ·—·, 5.00; — —, 4.24; ·· —, 3.77. The unit of relative intensity is 0.1.

Wood and Bekkedahl [4] observed that when natural rubber is crystallized by cooling, the melting temperature depends very markedly on the temperature of crystallization if rapid heating rates are employed. This led them to make the suggestion that the melting temperature observed in stark rubber is caused by a relatively high crystallization temperature. The validity of this suggestion is difficult to establish directly from experiment. Natural rubber crystallized at 14° C has a melting temperature of 28° C; to accomplish the crystallization at this temperature requires about 200 days. Crystallization at any higher temperature takes such an unduly long time as to make the necessary experiments a practical impossibility. However, in this temperature range the crystallization rate is governed mainly by the steady-state nucleation rate [3]. The extreme slowness of the rate of production of stable nuclei indicates that the difference between the crystallization temperature and the equilibrium melting temperature must be small, so that the equilibrium melting temperature is being approached. From studies of the crystallization rates of other polymers in this region [3], it is thought unlikely that the assigned value of the equilibrium melting temperature of undeformed natural rubber can be raised more than a few degrees. Thus the possibility that the high melting temperature of stark rubber results solely from a high temperature of crystallization seems somewhat remote.

Pickles [16] noted some years ago that under the same conditions of storage certain bales of natural rubber seemed more prone to become hard than others. This led him to believe that some factor in the previous history of the material, particularly the plantation processing, might be causing the observed effect. The X-ray diffraction patterns indicate quite clearly that a characteristic of stark rubber is the orientation of its crystallites. It is not difficult to envisage how the plantation processing might eventually cause the presence of oriented crystallites. After coagulation of the latex, the amorphous rubber is rolled into sheets, and the sheets are then stacked one upon another in an irregular manner. The bale of rubber is then subjected to a rather large simple compressional stress, which is eventually removed. It is likely that this process can cause the amorphous segments to be preferentially oriented, and because of the high viscosity of natural rubber, this orientation can persist for long periods of time at the usual storage temperatures when the external stresses are removed. Orientation of the chain segments will facilitate the rate of crystallization at temperatures where the crystallization rate is prohibitively slow for undeformed rubber.

Because the crystallites are oriented, the amorphous regions that connect them can also be oriented to some extent. If this orientation were maintained during the fusion process, then a crystalline segment would gain less entropy on melting than in the case where the amorphous region was completely random. Then for an oriented system the fusion would have to occur at a higher temperature than in an unoriented system. If the orientation were maintained, this could explain the higher melting temperatures observed for both stark and racked rubber. However, it does not explain the observed peculiarities of the melting process nor the fact that all the stark rubbers have melting temperatures in approximately the same range. Furthermore, if unvulcanized natural rubber is crystallized by stretching and the external force maintained during the subsequent heating (thus maintaining the orientation during the fusion), much higher melting points are observed [17].

After stark rubber has been melted and then recrystallized by cooling, the melting temperatures that one subsequently observes are the same as for normal natural rubber. Thus the initial heating of the stark rubber samples to temperatures slightly above the tabulated T_m causes the orientation to disappear. During the heating process, and within the time scale of the experiments, a temperature may be reached where the segmental motions of the amorphous rubber become sufficiently great to cause a return to their more probable configurations. If this temperature is greater than the equilibrium melting temperature of the unoriented semicrystalline polymer, T_m°, then crystallites that were thermodynamically stable above T_m° due to the orientation will now become unstable and will melt. Because

the fusion process causes an increase of the specific volume, the uniqueness of the melting behavior of stark rubber can be explained by the fact that at a temperature several degrees below the assigned T_m, but above T_m°, the relatively large volume changes with time are a manifestation of the slow rearrangement of the amorphous regions. Because the increases of the volume with time occur at all temperatures between 35° C and T_m, the rearrangement process is extremely temperature sensitive. It would then be expected that as long as no external forces are maintained, melting will occur in approximately the same temperature interval, irrespective of the amount and type of orientation.

It is interesting to note that in their study of the dimensional changes of unvulcanized natural rubber, using interferometric techniques, Wood, Bekkedahl, and Peters [18] observed that plastic flow occurred in the vicinity of 40° C. Similarly, Smith and Saylor [19] noted that the birefringence in natural rubber caused by induced strains (not crystallites) disappeared in the range 40° to 55° C. With the observation that the crystallites in stark rubber are oriented and with the above explanation for the melting behavior, it is clear that the assigned values of T_m are not thermodynamically significant. The assignment of an equilibrium melting temperature to the unoriented semicrystalline natural rubber would thus appear to be justified [8].

In principle, other crystalline polymers should display this behavior. Its common observation in natural rubber is due to a combination of circumstances. The high viscosity of amorphous natural rubber allows the orientation of the chain segments to be maintained for relatively long periods of time in the temperature range of interest. The lower limit of this temperature range is set by T_m°. As long as T_m° is sufficiently low, as in the case of natural rubber, for the rate of amorphous segmental rearrangement to be slow, this phenomenon should be observed.

6. Stark Rubber Prepared in a Laboratory

As stark rubber has not been prepared heretofore under controlled conditions, it is now thought possible to prepare it in the laboratory. One should seek conditions such that the crystallization occurs while the rubber is being deformed, and that when the external stresses causing the deformation are removed, the orientation will persist at temperatures above T_m°. Carson [20] was able to produce stark rubber by deforming a sample in a rubber-cutting machine and storing under slight pressure for nearly a year at temperatures between 5° and 35° C.

Early attempts in this direction were made by Smith and Saylor [19], who compressed a sample of amorphous natural rubber between aluminum plates for 6 months at −25° C. The resulting crystallites displayed definite orientation, but the melting point was only 10° to 11° C. A further experiment was performed wherein the rubber was compressed in a steel block at a pressure of 1,000 atmospheres and held at −25° C for 2 weeks. Upon removal of the sample and on subsequent heating to room temperature, the rubber remained crystalline, and its melting point was found to be about 33° to 34° C.

About 1934 A. T. McPherson and W. L. Hol then in the NBS Rubber Section, pressed some smoked sheet between aluminum-faced boards and then wrapped it very tightly with strips of stretched vulcanized rubber. Although the details of th thermal history of the sample are not precisel known, the sample was kept most of the time in th temperature range 0° to 14° C. The sample w examined in May 1954, and found to possess an appreciable amount of crystallinity at 25° C. Dila tometric observations indicate that its meltin temperature is greater than 35° C. In figure 7,A the X-ray diffraction photograph of this sampl indicates very marked orientation.

A portion of a bale of sprayed latex, which con tained about 95 percent of rubber hydrocarbon and whose X-ray diffraction pattern indicated it to be completely amorphous, was passed through a mill several times and rolled into a tight cylinder. Afte storage at 25° C for 2 years, it was reexamined an found to have lost some of its rubberlike elasticity. Its X-ray diffraction pattern is given in figure 7,B. Although the intensity of the diffraction pattern i not great, it is evident that the crystallites are oriented. Because of the small amount of crystal linity developed, the melting point could not be determined precisely, but it is in the range 35° t 40° C. A portion of the roll was placed in a vacuum press at 28° C and subjected to a compressive loa of 50 tons. The result of this treatment, as illus trated in figure 7,C, was to further increase the amount of both crystallinity and orientation. The melting temperature of this specimen is 42° ±2° C.

A small section of cast-iron pipe, which was closed at the lower end and threaded at the upper end, was completely filled with the amorphous sprayed latex. The upper end of the pipe was closed with a threaded cap and tightened completely, thus subjecting the rubber to a compressive stress with orientation of certain regions brought about in the process of tightening the cap. After storage at 14° C for 18 months, portions of the rubber had crystallized. They maintained their crystallinity after warming to room temperature. The X-ray diffraction pattern is illustrated in figure 7, D, and its high orientation is apparent. The melting temperature was difficult to determine accurately, but it is in the vicinity of 35° C.

Stark rubber can thus be prepared in the laboratory by a variety of methods. Those discussed above are certainly not exhaustive, and other methods should be equally successful. The essential requirement seems to be orientation during the crystallization. This is a necessary, but not a sufficient, condition. In the course of this study several methods that were attempted have not as yet yielded stark rubber. For example, holding samples at 14° C in simple extension at various extension ratios caused crystallization. However, when the tensile

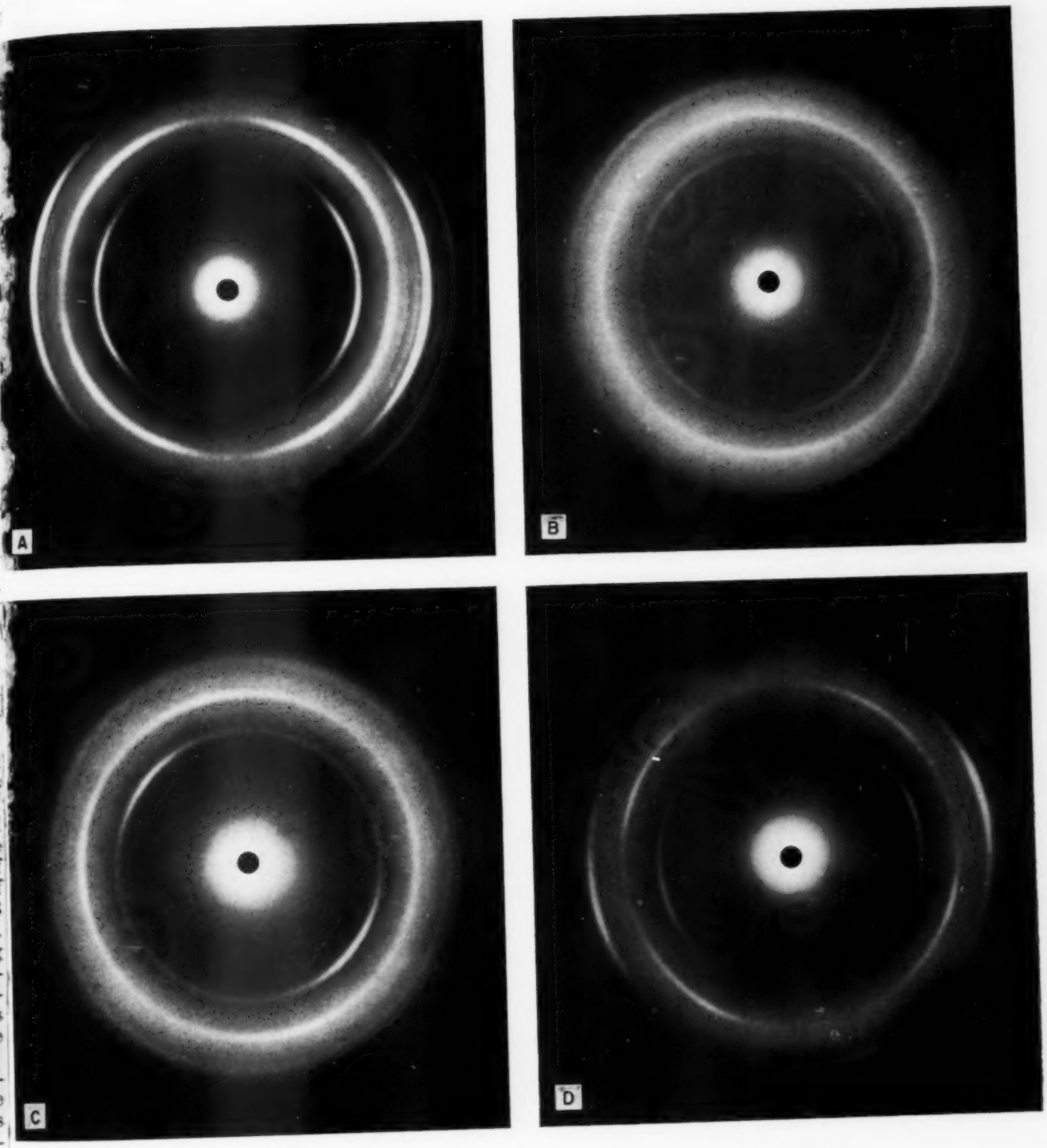

FIGURE 7. *X-ray diffraction photographs of laboratory-prepared stark rubber.*

A, Prepared by McPherson and Holt; B, sprayed latex milled and rolled; C, cold-molding of sample B; D, prepared in cast-iron pipe.

force was removed and the sample heated to 28° C, the crystallinity completely disappeared. Similarly, it is known from the work of Goppel and Van Rossem [21], that calendering rubber causes the crystallites that are formed on cooling to be oriented. However, when these experiments were repeated at the National Bureau of Standards a completely amorphous X-ray diffraction pattern was obtained at 25° C. The difference between these results and those of Goppel and Van Rossem can be attributed to the fact that the diffraction photographs of the latter investigators were taken in the temperature range 17° to 20° C [22]. The apparent failure of the methods just described cannot be taken as final. It is possible that after longer times, when greater amounts of crystallinity have developed, the rubber may become stark by the methods outlined.

Some additional samples of stark rubber are being studied, and other laboratory methods of preparation are being explored. The melting behavior of some of the stark-rubber samples reported in the present paper is being reexamined, using much slower heating rates.

The authors gratefully acknowledge the assistance of G. Ugrinic and H. E. Swanson of the NBS Mineral Products Division for undertaking and accomplishing the X-ray diffraction work. Very helpful and interesting discussions of the problem were held with W. O. Baker and W. P. Slichter of the Bell Telephone Laboratories, and H. S. Kaufman of the M. W. Kellogg Co. L. A. Wood and N. Bekkedahl participated in many interesting discussions with the authors.

WASHINGTON, November 4, 1954.

7. References

[1] P. J. Flory, Principles of Polymer Chemistry, p. 563 (Cornell University Press, 1953).
[2] P. J. Flory, R. R. Garrett, S. Newman, and L. Mandelkern, J. Polymer Sci. **12,** 97 (1954).
[3] L. Mandelkern, F. A. Quinn, Jr., and P. J. Flory, J. Appl. Phys. **25,** 830 (1954).
[4] L. A. Wood and N. Bekkedahl, J. Appl. Phys. **17,** 362 (1946); J. Research NBS **36,** 489 (1946) RP1718; Rubber Chem. and Technol. **19,** 1145 (1946).
[5] R. E. Evans, H. Mighton, and P. J. Flory, J. Am. Chem. Soc. **72,** 2018 (1950).
[6] P. J. Flory, H. K. Hall, and L. Mandelkern, J. Am. Chem. Soc. **73,** 2532 (1951).
[7] J. T. Maynard and W. E. Mochel, J. Polymer Sci. **13,** 235 (1954); Rubber Chem. and Technol. **27,** 634 (1954).
[8] D. E. Roberts and L. Mandelkern, J. Am. Chem. Soc. **77,** 781 (1955).
[9] G. S. Whitby, Chapter in Davis and Blake's "Chemistry and Technology of Rubber," pp. 69, 78 (Reinhold Publishing Corp., New York, N. Y., 1937).
[10] L. Mandelkern and P. J. Flory, J. Am. Chem. Soc. **73,** 3206 (1951).
[11] L. A. Wood, N. Bekkedahl, and F. L. Roth, J. Research NBS **29,** 391 (1942) RP1507; Ind. Eng. Chem. **34,** 1291 (1942); Rubber Chem. and Technol. **16,** 244 (1943).
[12] W. H. Barnes, Can. J. Research **15,** 156 (1937); Rubber Chem. and Technol. **10,** 462 (1937).
[13] G. L. Clark, E. Wolthuis, and W. H. Smith, J. Research NBS **19,** 479 (1937) RP1039; Rubber Age (N. Y.) **42,** 35 (1937); Rubber Chem. and Technol. **11,** 32 (1938).
[14] N. Bekkedahl, J. Research NBS **13,** 411 (1934) RP717; Rubber Chem. and Technol. **8,** 5 (1935).
[15] F. H. Cotton, Trans. Inst. Rubber Ind. **16,** 303 (1941); Rubber Chem. and Technol. **14,** 762 (1941).
[16] S. S. Pickles, India-Rubber J. **67,** 69 (1924).
[17] J. E. Field, J. Appl. Phys. **12,** 23 (1941); Rubber Chem. and Technol. **14,** 555 (1941).
[18] L. A. Wood, N. Bekkedahl, and C. G. Peters, J. Research NBS **23,** 571 (1939) RP1253; Rubber Chem. and Technol. **13,** 290 (1940).
[19] W. H. Smith and C. P. Saylor, J. Research NBS **21,** 257 (1938) RP1129; Rubber Chem. and Technol. **12,** 18 (1939).
[20] C. M. Carson, Ind. Eng. Chem. **23,** 691 (1931); Rubber Chem. and Technol. **4,** 417 (1931).
[21] J. M. Goppel and A. Van Rossem, Physica **9,** 213 (1942); Rubber Chem. and Technol. **19,** 403 (1946).
[22] J. M. Goppel (private communication).

U. S. DEPARTMENT OF COMMERCE
Sinclair Weeks, Secretary
NATIONAL BUREAU OF STANDARDS
A. V. Astin, Director

APRIL • 195
VOLUME • 5
NUMBER •

JOURNAL OF RESEARCH

of the

NATIONAL BUREAU OF STANDARDS

PERIODICALS OF THE NATIONAL BUREAU OF STANDARDS

(Published monthly)

The National Bureau of Standards is engaged in fundamental and applied research in physics, chemistry, mathematics, and engineering. Projects are conducted in fifteen fields: electricity and electronics, optics and metrology, heat and power, atomic and radiation physics, chemistry, mechanics, organic and fibrous materials, metallurgy, mineral products, building technology, applied mathematics, data processing systems, cryogenic engineering, radio propagation, and radio standards. The Bureau has custody of the national standards of measurement and conducts research leading to the improvement of scientific and engineering standards and of techniques and methods of measurement. Testing methods and instruments are developed, physical constants and properties of materials are determined; and technical processes are investigated.

JOURNAL OF RESEARCH

The Journal presents research papers by authorities in the specialized fields of physics, mathematics, chemistry, and engineering. Complete details of the work are presented, including laboratory data, experimental procedures, and theoretical and mathematical analyses. Annual subscription: domestic, $4.00; foreign, $5.25.

TECHNICAL NEWS BULLETIN

Summaries of current research at the National Bureau of Standards are published each month in the Technical News Bulletin. The articles are brief, with emphasis on the results of research, chosen on the basis of their scientific or technologic importance. Lists of all Bureau publications during the preceding month are given, including Research Papers, Handbooks, Applied Mathematics Series, Building Materials and Structures Reports, Miscellaneous Publications, and Circulars. Each issue contains 12 or more two-column pages; illustrated. Annual subscription: domestic, $1.00; foreign, $1.35.

BASIC RADIO PROPAGATION PREDICTIONS

The Predictions provide the information necessary for calculating the best frequencies for communication between any two points in the world at any time during the given month. The data are important to all users of long-range radio communications and navigation, including broadcasting, airline, steamship, and wireless services, as well as to investigators of radio propagation and ionosphere. Each issue, covering a period of one month, is released three months in advance and contains 16 large pages, including pertinent charts, drawings, and tables. Annual subscription: domestic, $1.00; foreign, $1.25.

Order all publications from the Superintendent of Documents
U. S. Government Printing Office, Washington 25, D. C.

The printing of this publication has been approved by the Director of the Bureau of the Budget, May 12, 1953.